PIEZOELECTRIC BISMUTH TITANATE CERAMICS FOR HIGH TEMPERATURE APPLICATIONS

THÈSE N° 1646 (1997)

PRÉSENTÉE AU DÉPARTEMENT DES MATÉRIAUX

ÉCOLE POLYTECHNIQUE FÉDÉRALE DE LAUSANNE

POUR L'OBTENTION DU GRADE DE DOCTEUR ÈS SCIENCES TECHNIQUES

PAR

Holly Sue SHULMAN

Master of Science in Materials Science and Engineering, University of Pittsburgh, USA

de nationalité américaine

acceptée sur proposition du jury:

Prof. N. Setter, directeur de thèse
Dr C. Cavalloni, corapporteur
Dr D. Damjanovic, corapporteur
Prof. H. Hofmann, corapporteur
Dr M. Kosec, corapporteur

Lausanne, EPFL
1997

This Ph.D. thesis is dedicated with love
to my Grandpa Charlie (Israel Shulman).

Abstract

Bismuth titanate ($Bi_4Ti_3O_{12}$) shows promise in piezoelectric applications in a temperature range (300-600 °C) which is not well served by standard piezoelectric ceramics. The proposal to use bismuth titanate ceramics for these applications has a major flaw, namely that the high electrical conductivity precludes the efficient polarization of these materials in an electric field. The degree of polarization is critical since it is directly related to the piezoelectric response. In addition, once bismuth titanate ceramics are successfully polarized, they must have a sufficiently low conductivity for use at temperatures above 300 °C. The premise of this study was that control of the conductivity in bismuth titanate ceramics would allow useful piezoelectric properties to be realized. The approach taken was to investigate the origins of the electrical conductivity and examine the impact of microstructure, starting materials, and dopants on the conductivity. The effects of these parameters on the piezoelectric coefficient in the longitudinal mode (d_{33}) were examined.

Results presented in this thesis show that the conductivity in undoped $Bi_4Ti_3O_{12}$ ceramics is p-type and electronic. The conductivity was decreased by adding niobium, a donor dopant. The conductivity as a function of Nb concentration reached a minimum which corresponds to the condition for complete compensation of the ionized holes. Further increases in Nb concentration produced n-type behavior.

A study of the frequency and temperature dependence of the dielectric properties revealed behavior characteristic of ionic motion in undoped bismuth titanate. It appears that oxygen vacancy migration promotes an ion jump relaxation at relatively low temperatures and frequencies (e.g. 200 °C, 20 Hz). Any contribution of this ionic motion to the conductivity was masked by the high p-type conduction. The addition of Nb suppressed the dielectric relaxation which suggests that donor dopants restrict the diffusion of oxygen in bismuth titanate.

The initial premise was proven, in that by decreasing the p-type conductivity in bismuth titanate, the piezoelectric coefficient was quadrupled from ~5 pC/N to ~20 pC/N. An unforeseen result was that bismuth titanate ceramics with the lowest conductivity did not possess the highest piezoelectric coefficient.

An analysis of the phase lag between the applied sinusoidal force and resulting charge provided deeper insight into the effect of Nb doping on the piezoelectric response. An undesirable hysteretic behavior was observed between the force and charge for undoped (p-type) and lightly Nb doped bismuth titanate (fully compensated), but was absent in the highly Nb doped (n-type) compositions. The origins of the hysteresis in the piezoelectric coefficient was discussed in terms of extrinsic contributions from domain wall motion.

It has been established that decreasing the conductivity in bismuth titanate is a necessary but not sufficient condition for achieving a useful piezoelectric response. Donor doping into the n-type region provides a bismuth titanate composition with stable and reproducible piezoelectric properties. This material can be produced via standard ceramic processing methods and is a candidate for high temperature piezoelectric applications.

Version Abrégée

Les céramiques de titanate de bismuth ($Bi_4Ti_3O_{12}$) montrent des propriétés prometteuses pour des applications dans une gamme de température (300-600 °C) qui n'est pas bien couverte par les céramiques piézoélectriques conventionnelles. L'utilisation de céramiques de titanate de bismuth pour ces applications présente une difficulté majeure, à savoir que la conductivité électrique élevée de ces matériaux ne permet pas une polarisation efficace sous champ électrique. Le degré de polarisation est un paramètre critique puisque la réponse piézoélectrique en dépend directement. De plus, une fois la polarisation achevée, ces matériaux doivent avoir une conductivité suffisamment faible pour permettre leur utilisation au dessus de 300 °C. Cette étude est basée sur l'hypothèse qu'un contrôle de la conductivité du titanate de bismuth devrait permettre d'obtenir des propriétés piézo-électriques utilisables. L'approche choisie consiste à rechercher les causes de la conductivité électrique et à évaluer l'influence de la microstructure, des réactifs et des dopants sur la conductivité. Les effets de ces paramètres sur le coefficient piézo-électrique en mode longitudinal (d_{33}) ont été examinés.

Les résultats présentés dans ce travail indiquent que la conductivité dans le $Bi_4Ti_3O_{12}$ non dopé est électronique et de type-p. L'ajout de Nb comme dopant donneur a permis de diminuer la conductivité. La conductivité en fonction de la concentration de Nb passe par un minimum correspondant à une compensation complète des trous ionisés. Des concentrations supérieures en Nb résultent en une conductivité de type-n.

Une étude de la dépendance en fréquence et en température des propriétés diélectriques révèle un comportement caractéristique de migration ionique pour le titanate de bismuth non dopé. Il apparaît que la migration de lacunes d'oxygène favorise une relaxation par saut ionique à relativement basse température et basse fréquence (ex. 200 °C, 20 Hz). Toute contribution à la conductivité de ces déplacements ioniques est masquée par la conduction de type-p élevée. L'ajout de Nb supprime la relaxation diélectrique, ce qui suggère que les dopants donneurs limitent la diffusion d'oxygène dans le titanate de bismuth.

L'hypothèse de base est vérifiée par le fait qu'une diminution de la conductivité de type-p permet de quadrupler le coefficient piézo-électrique qui passe de ~5 pC/N à ~20 pC/N. De manière imprévisible, on constate que les céramiques de titanate de bismuth possédant la conductivité la plus faible ne sont pas celles qui présentent les coefficients piézo-électriques les plus élevés.

Une analyse du déphasage entre la force sinusoïdale appliquée et la charge développée permet de détailler l'effet du dopant Nb sur la réponse piézo-électrique. Un comportement hystérétique indésirable est observé entre la force et la charge pour le titanate de bismuth non dopé (p-type) et faiblement dopé (compensé) par contre on n'observe aucune hysterèse dans le cas des compositions à forte teneur en Nb (n-type). Les origines de cette hystérèse piézo-électrique sont discutées en termes de contributions extrinsèques des mouvements des parois de domaines ferroélectriques.

Ce travail montre que la diminution de conductivité du titanate de bismuth est une condition nécessaire, mais pas suffisante pour l'obtention d'une réponse piézo-électrique utile. Le dopage par un donneur dans la zone de conductivité de type-n crée une composition de titanate de bismuth aux propriétés piézo-électriques stables et reproductibles. Ce matériau peut être produit par des méthodes d'élaboration conventionnelles et est un bon candidat pour des applications piézo-électriques à haute température.

Acknowledgments

I would like to express my appreciation to Professor Nava Setter for giving me the opportunity to carry out this thesis work. I owe a great deal of thanks to Dr. Dragan Damjanovic who has advised me throughout this work.

I am indebted to Dr. Ian Brown, manager of the Ceramics Team at Industrial Research, Ltd., for providing ideal working conditions which helped me to finish this thesis.

I must warmly thank my colleagues for many useful and interesting discussions. Thanks especially to Chu Fan, Marlyse Demartin, and Pascal Streit.

I would like to express my gratitude to my husband, Dr. Marc Daglish for his patience and sacrifice. Thanks also to Marc for his incredible encouragement, support, and command of the English language. A great big hug and kiss to our son Daniel Bruce Daglish. Thank you for respecting my work and not touching my computer.

Thank you Tina Albertini and Viv Wahren for taking care of my precious boy while I was working on this thesis. I will never forget all the coffee and sympathy you poured out to help me keep going.

I also would like to mention my parents, Joy Robins and Frank Shulman, because I love them...and you too Rachie, Mikki, and Gigi. A big thank you to Marc's wonderful family for their love and support during somewhat trying years.

This acknowledgment wouldn't be complete without saying how much I appreciate my girlfriends, Leaky Lori, Cactus, Little Ann, Anna B, Debi Cakes, Pattio, Lana, and Donna.

Chapter 1. Introduction and Objectives 1
1.1 General Introduction 1
1.2 Thesis Objectives 3

Chapter 2. Processing and Properties of Bismuth Titanate 6
2.1 Historical Perspective 6
2.2 Materials with High Ferroelectric Transition Temperatures 9
2.3 Crystal Structure and Symmetry 10
2.3.1 Perovskite crystal structure 10
2.3.2 Aurivillius crystal structures 12
2.3.3 Symmetry of Aurivillius phases 15
2.4 Origins of Ferroelectricity in Bismuth Titanate 16
2.4.1 Domain structure 17
2.5 Bismuth Titanate Ceramics 19
2.5.1 Bismuth titanate phase formation 19
2.5.2 Microstructural evolution 20
2.6 Defect Chemistry and Conductivity in Bismuth Titanate 21
2.6.1 Single crystals 21
2.6.2 Grain oriented bismuth titanate ceramics 23
2.6.3 X-ray Photoelectron Spectroscopy 23
2.6.4 Ionic substitution 23
2.7 Piezoelectricity in Bismuth Titanate Ceramics 25
2.8 Summary 27

Chapter 3. Ceramics Development 28
3.1 Introduction 28
3.2 Experimental Procedures 29
3.2.1 X-ray diffraction 29
3.2.2 Particle size analysis 29
3.2.3 Electron microscopy and energy dispersive spectroscopy 29
3.3 Powder Preparation and Characterization 30
3.3.1 Analysis of raw materials 30
3.3.2. Process description 33
3.3.3 Dopant additions to bismuth titanate 35
3.3.4 Bismuth titanate powder characterization 36
3.4 Phase Formation 37
3.4.1 Reaction route 37
3.4.2 Reaction kinetics 41
3.4.3 Raw materials and reaction rate 44
3.5 Densification and Microstructural Investigations 46
3.5.1 Densification and grain growth in bismuth titanate 47
3.5.2 Densification and grain growth in doped bismuth titanate 51
3.5.3 Solubility limit of Nb in bismuth titanate 53
3.5.4 Grain growth in Nb doped bismuth titanate 55
3.5.5 Hot forged bismuth titanate 57
3.6 Chapter Summary and Conclusions 59

Chapter 4. Electrical Conductivity in Bismuth Titanate 60
4.1 Introduction 60
4.2 Experiment Procedures 62
4.2.1 Sample preparation for electrical measurements 62
4.2.2 AC measurement method 62
4.2.3 Charge-discharge method 63
4.3 Discussion of Band Structure, Defects , and Conductivity 65
4.4 Conductivity in Undoped Bismuth Titanate 69
4.4.1 The conductive layer in bismuth titanate 69
4.4.2 Comparison of single crystals and oriented ceramics 72
4.4.3 Reducing and oxidizing atmosphere 75
4.4.4 Quenching study 81
4.4.5 Raw materials 83
4.5. Analysis of Acceptor and Isovalent Dopants in Bismuth Titanate 85
4.6. Analysis of a Donor Dopant in Bismuth Titanate 87
4.6.1 Niobium concentration 87
4.6.2 The impact of raw materials on donor doping 91
4.7 Grain Size Effect in Undoped and Nb doped Bismuth Titanate 94
4.8 Binding Energy in Undoped and Nb doped Bismuth Titanate 99
4.9 Summary of Defect Chemistry in Bismuth Titanate 105
4.10 Chapter Summary and Conclusions 106

Chapter 5. Dielectric Properties and Piezoelectricity in Bismuth Titanate Ceramics 108
5.1 Introduction 108
5.2 Ferroelectric to Non-Ferroelectric Phase Transition 109
5.3 Additional Dielectric Anomalies 113
5.3.1 Relative permittivity 113
5.3.2 Dielectric relaxation 116
5.3.3 Niobium doping and dielectric relaxation 124
5.4 Poling Conditions for Bismuth Titanate Ceramics 126
5.4.1 Poling procedure 126
5.4.2 Poling regime 127
5.5 Analysis of the Complex Piezoelectric Coefficient 128
5.5.1 Description of the complex piezoelectric coefficient 129
5.5.2 Piezoelectric measurements 131
5.5.3 Niobium concentration 131
5.5.4 Sample variation 133
5.5.5 Frequency dependence 137
5.5.6 Alternating pressure 140
5.5.7 The effect of grain size, conductivity, and partial polarization 142
5.5.8 Discussion of possible piezoelectric relaxation mechanisms 145
5.6 Chapter Summary 149

Chapter 6. Summary 151
6.1 Conclusions 151
6.2 Suggestions for Future Work 153

List of Figures

Figure 2.1 Schematic illustration of the perovskite unit cell 11
Figure 2.2 Schematic illustration of the bismuth titanate unit cell. 14
Figure 2.3 The crystallographic axes for Aurivillius phases. 16
Figure 2.4 Possible domain configurations in monoclinic bismuth titanate. 18

Figure 3.1 SEM of TiO_2 and Bi_2O_3 powders 32
Figure 3.2 Processing flow chart for preparing bismuth titanate ceramics. 34
Figure 3.3 Phase diagrams for TiO_2-Bi_2O_3. 38
Figure 3.4 Portion of the XRD traces showing phases in TiO_2-Bi_2O_3 mixture 40
Figure 3.5 Dependence of volume fraction of bismuth titanate on calcination time 44
Figure 3.6 XRD trace comparing the $Bi_{12}TiO_{20}$ 100% peak for different combinations of Bi_2O_3 and TiO_2 powders 45
Figure 3.7 Densification of bismuth titanate as a function of sintering temperature 48
Figure 3.8 SEM of AC bismuth titanate ceramics 48
Figure 3.9 SEM comparing AC, TC, and TF bismuth titanate sintered at 1100 °C for 1 hour and 10 hours 50
Figure 3.10 SEM and density of bismuth titanate with various dopants 52
Figure 3.11 TEM and EDS comparing the grains and a triple point from 0.74 at% Nb doped bismuth titanate. 54
Figure 3.12 SEM of Nb doped bismuth titanate ceramics 56
Figure 3.13 SEM of hot forged bismuth titanate parallel to and perpendicular to the hot forging axis 58

Figure 4.1 Dielectric loss as a function of reciprocal angular frequency. 63
Figure 4.2 Example of charging and discharging currents as a function of time 64
Figure 4.3 Example of Ohmic behavior 65
Figure 4.4 Schematic illustration of the band structure in alkaline earth perovskites 66
Figure 4.5 Schematic illustration of band structure in lead based perovskite titanate 68
Figure 4.6 Comparison of conductivity in ceramics of Bi_2O_3, $Bi_4Ti_3O_{12}$ and PZT. 70
Figure 4.7 Schematic illustration of the change in electronic charge between the layers in the bismuth titanate unit cell 71
Figure 4.8 Comparison of single crystal conductivity and randomly oriented bismuth titanate 73
Figure 4.9 Comparison of the conductivity in randomly oriented and hot forged bismuth titanate ceramics. 74
Figure 4.10 The effect of oxidizing and reducing treatments on the conductivity in AC bismuth titanate 76
Figure 4.11 Conductivity as a function of approximate annealing atmosphere in AC bismuth titanate showing p-type trend. 77
Figure 4.12 Conductivity as a function of approximate annealing atmosphere in TF bismuth titanate showing p-type trend. 77
Figure 4.13 Conductivity measured at 200 °C as a function of quenching temperature (TF bismuth titanate). 81
Figure 4.14 Comparison of conductivity as a function of reciprocal temperature in AC, TC, and TF bismuth titanate 84
Figure 4.15 The effect of acceptor and isovalent dopants which replace Bi in bismuth titanate on the conductivity 86
Figure 4.16 The effect of acceptor dopants which replace Ti in bismuth titanate on the conductivity 86
Figure 4.17 The effect of Nb concentration on the conductivity in bismuth titanate 88
Figure 4.18 The effect of Nb doping on the conductivity (at 200 °C) in bismuth titanate 89

Figure 4.19 A comparison of the effect of oxygen annealing on the conductivity in 0.05 at% Nb doped and 0.53 at% Nb doped bismuth titanate. 89
Figure 4.20 Arrhenius relationship for conductivity in 0.21 at% Nb doped bismuth titanate illustrating the changes in the activation energy. 90
Figure 4.21 Comparison of the conductivity for undoped and 0.05 at% Nb doped TF and TC bismuth titanate. 92
Figure 4.22 Comparison of the conductivity in a 0.5 at% Nb doped bismuth titanate composition with 0.2 at% Nb doped TF bismuth titanate. 93
Figure 4.23 The effect of grain size on the conductivity in AC bismuth titanate 94
Figure 4.24 Conductivity measured at 200 °C in undoped and 0.05 at% Nb doped bismuth titanate as a function of sintering time. 96
Figure 4.25. The effect on the conductivity of annealing small and large grain 0.05 at% Nb doped bismuth titanate in oxygen. 97
Figure 4.26 Survey spectrum by XPS showing the energy due to bonding of Bi, Ti, and O in undoped TF bismuth titanate 100
Figure 4.27 The effect of 0.74 at% Nb doping on the binding energy of Ti in bismuth titanate. 101
Figure 4.28 The effect of 0.74 at% Nb doping on the binding energy of Bi in bismuth titanate. 101
Figure 4.29 One half of the bismuth titanate unit cell projected down the b-axis showing the position of the atoms 104
Figure 4.30 Suggested defect band model for bismuth titanate. 106

Figure 5.1 a) The reciprocal of the susceptibility as a function of temperature in undoped and 0.05 at% Nb doped bismuth titanate b) Theoretical Curie-Weiss behavior
for a first order phase transition 111
Figure 5.2 Curie temperature in bismuth titanate as a function of Nb dopant. 112
Figure 5.3 Relative permittivity as a function of temperature showing the effect of 0.05 at% Nb on an anomalous peak at 500 °C 114
Figure 5.4 Relative permittivity of undoped bismuth titanate as a function of temperature for six frequencies 114
Figure 5.5 Relative permittivity as a function of temperature and frequency showing the frequency dependence with 0.05 at% Nb 115
Figure 5.6 Relative permittivity as a function of temperature and frequency showing the frequency dependence with 0.74 at% Nb. 116
Figure 5.7 Frequency dependence of the polarization mechanisms in dielectrics 117
Figure 5.8 Dielectric loss in bismuth titanate as a function of temperature and frequency showing frequency dependent peaks. 119
Figure 5.9 Details of the dielectric loss tangent as a function of temperature 120
Figure 5.10 Arrhenius relationship for dielectric relaxation in undoped bismuth titanate 120
Figure 5.11 Dielectric loss tangent versus temperature in hot forged bismuth titanate for six frequencies. 122
Figure 5.12 Dielectric loss tangent as a function of temperature and frequency in highly Nb doped bismuth titanate showing very low loss 125
Figure 5.13 Dielectric loss tangent as a function of temperature and frequency for highly
Nb doped bismuth titanate after annealing in a reducing atmosphere 125
Figure 5.14 Comparison of the poling regime for undoped and Nb doped bismuth titanate. 127
Figure 5.15 An example of the hysteresis between the force and charge in an undoped bismuth titanate ceramic. 130
Figure 5.16 a) piezoelectric coefficient and b) piezoelectric tangent as a function of Nb concentration. 132
Figure 5.17 Analysis of the sample reproducibility for a low Nb dopant level. 134

Figure 5.18 Analysis of the sample reproducibility for a high Nb dopant level. 135
Figure 5.19 a) piezoelectric coefficient and b) piezoelectric tangent in bismuth titanate as a function of Nb dopant at four frequencies 138
Figure 5.20 Frequency dependence of a) piezoelectric coefficient and b) piezoelectric tangent for undoped and Nb doped bismuth titanate 139
Figure 5.21 Dependence of the a) piezoelectric coefficient and b) piezoelectric tangent on the amplitude of the alternating pressure in undoped and Nb doped bismuth titanate 141
Figure 5.22 Comparison of a) piezoelectric coefficient and b) piezoelectric tangent as a function of sintering time for undoped and 0.05 at% Nb doped bismuth titanate. 143
Figure 5.23 Bismuth titanate doped with 0.05 at% Nb showing an inverse relationship between piezoelectric coefficient and piezoelectric tangent with poling temperature. 144
Figure 5.24 Regions of 90° domains in large grain 0.05 at% Nb doped bismuth titanate 146

List of Tables

Table 2.1 Ferroelectric Oxides with high Curie temperatures (> 400 °C). 9
Table 2.2 Reported values of piezoelectric coefficient (d_{33}) in bismuth titanate ceramics. 25
Table 3.1 Abbreviations for TiO_2-Bi_2O_3 combinations. 31
Table 3.2 Analysis of TiO_2 and Bi_2O_3 starting powders. 31
Table 3.3. Type and quantity of dopant added to the mixed oxides to form doped bismuth titanate powder. 35
Table 3.4 Particle size analysis of bismuth titanate powders prepared from different sources of raw material 36
Table 3.5 Integrated peak intensities used to calculate the approximate volume fraction of bismuth titanate 43
Table 3.6 Semi-quantitative elemental analysis by EDS comparing the grain composition of highly Nb doped bismuth titanate with a triple point 55
Table 4.1. Calculated valences for ions in the parent orthorhombic and monoclinic structure of bismuth titanate 103

Chapter 1. Introduction and Objectives

1.1 General Introduction

A search for piezoelectric materials which can be utilized at elevated temperatures (> 300 °C) has stimulated recent interest[1] in the family of bismuth layer structure perovskites. This family was first described by Aurivillius[2,3] in 1949 and consists of interleaved layers of perovskite units $[(ABO_3)^{2-}]$ with bismuth oxide $[(Bi_2O_2)^{2+}]$ layers. Many of the compositions from the Aurivillius family remain ferroelectric up to significantly higher temperatures than the well known group of ferroelectric perovskites. For example, bismuth titanate ($Bi_4Ti_3O_{12}$ abbreviated BIT) is ferroelectric up to 675 °C[4] compared to ~380 °C for lead zirconate titanate (PZT)[5]*. The ferroelectric phase allows the alignment of dipoles (known as poling), and is essential for piezoelectricity in ceramics. The transition temperature (Curie temperature or T_c) at which ferroelectricity is lost, is therefore a critical selection parameter for high temperature piezoelectric ceramics.

The best known composition in the Aurivillius family, bismuth titanate, was originally of interest in the early 1970's for optical displays and information storage.[5,6] Bismuth titanate is an unusual ferroelectric in that it has two components of the polarization vector, one of which can be switched at low fields.[4,5] Attempts have been made to make use of the change in the angle of the optical indicatrix when the polarization in the direction of the **c**-axis is reversed.[5] Research in optical applications for single crystal bismuth titanate has met with limited success due to the difficulties in preparing crystals with an extended dimension in the **c**-direction. The crystal structure favors growth of plate-like grains in the **ab** plane with slow growth in the **c**-direction. Thin film technologies[7] are now being investigated to obtain bismuth titanate which is suitable for electro-optic devices.

In the 1980's, a growing industrial need for high temperature piezoelectric ceramics stimulated new interest in the Aurivillius phases.[8] Several commercial materials are now available which provide Curie temperatures up to 600 °C and piezoelectric coefficients up to 18 pC/N.[9,10] Although bismuth titanate offers a high Curie temperature (675 °C), the low

---

* The lead zirconate titanate system provides the most widely used piezoelectric ceramic compositions.

resistivity interferes with the poling process and degrades the piezoelectric properties at elevated temperatures. These problems have prevented the use of bismuth titanate in piezoelectric applications.

Much of the published work on bismuth titanate ceramics has focused on developing oriented microstructures to maximize the piezoelectric response. A complication arises in that the maximum piezoelectric response is observed in the direction with the maximum conductivity. The problem of poling has been overcome by applying a pulse poling technique[11], however, the high conductivity still interferes with the intended use of these materials. It is evident that the conductivity in bismuth titanate must be controlled before elaborate processing or poling schemes can be beneficial.

Since the focus changed from single crystals in the 1970's to oriented bismuth titanate ceramics in the 1980's, a gap appears in the literature concerning the standard ceramic processing techniques. It is rather an unusual twist that bismuth titanate has been studied in various forms for nearly half a century, and yet very little has been published on subjects such as the reaction kinetics of the mixed oxide method or microstructural development during pressureless sintering. In addition, various workers have noted the effect of impurities[12,13] and dopants[14,15] on the conductivity, however, the defect structure remains largely unexplored.

Bismuth titanate has one of the least complicated chemical compositions of the bismuth layer structure perovskites and therefore is an ideal member to study the relationship between the defect structure and conductivity. Conflicting reports exist on the type of dopant, acceptor[14] or donor[15], which must be added to decrease the conductivity in bismuth titanate. This demonstrates the lack of understanding of the defect structure in bismuth titanate. According to a study in 1988[15], the conductivity in bismuth titanate was sufficiently decreased by donor doping to polarize the ceramics and achieve a piezoelectric coefficient (d_{33}) of 21 pC/N. The use of dopants to control the conductivity in bismuth titanate is a promising direction which requires further investigation.

In summary, necessary information is lacking for the successful application of piezoelectric bismuth titanate ceramics. From the materials perspective, a standard processing

route, which entails mixed oxide powder production and consolidation by sintering, has not been well defined. The microstructural development of bismuth titanate ceramics during pressureless sintering has never been reported in detail. In addition, the impact of the processing factors on the conductivity and piezoelectric properties is almost completely unknown. Lastly, the limited studies on dopant additions which decrease the conductivity in bismuth titanate are very promising. It has thus been established that a better understanding of the effects of processing and dopants on the electrical properties of bismuth titanate will be of scientific and technological significance.

1.2 Thesis Objectives

The practical aspect of this research is that of developing bismuth titanate ceramics with sufficiently high resistivity to be utilized in piezoelectric applications at elevated temperatures (300-600 °C). In order to evaluate the piezoelectric properties of interest, a target application was selected. This is a force or pressure sensor[1] which utilizes the direct piezoelectric effect in terms of the piezoelectric coefficient in the longitudinal mode, (d_{33}).

The main objectives of this study are to determine and understand the effect of raw materials, dopants, and microstructure on the dielectric and piezoelectric properties, to lower the conductivity with the use of dopants and/or microstructural control, and to obtain well polarized bismuth titanate ceramics with stable piezoelectric properties. To meet these goals the reaction kinetics and grain growth during sintering will be examined, and a tentative model for the defect structure will be developed by considering the effect of dopants, impurities, and partial pressure of oxygen on the conductivity. In addition, the piezoelectric response in the longitudinal mode will be critically analyzed.

The specific objectives of this investigation are defined as follows.

1. Ceramic Materials Development

a) It is known that the choice of raw materials can affect the reaction kinetics.[16] The formation of bismuth titanate from the mixed oxide method will be analyzed and the effect of raw materials will be discussed.

b) It is believed that the frequent ambiguity in the measurement of electrical properties originates to some extent from the use of different purity powders.[17] Bismuth titanate ceramics will be prepared from different sources of powders to determine the significance of this variable on the electrical properties.

c) It has been noted that bismuth titanate undergoes anisotropic grain growth.[18] The evolution of the microstructure and the effect of raw materials and dopants on grain growth will be examined. The impact of microstructural variations on the electrical properties will be determined.

2. Conductivity

a) A high conductivity interferes with the polarization of bismuth titanate.[15,19] Conflicting studies[14,15] exist on the origins and type of conducting species. The conduction type will be determined from the effect of partial pressure of oxygen on the conductivity. An appropriate dopant will be selected to decrease the conductivity.

b) A simple model of the defect structure in bismuth titanate will be proposed from the effect of dopants and partial pressure of oxygen. Comparisons of the band structure in transition metal oxides will be made to better understand the electronic properties of bismuth titanate.

c) The conductivity in bismuth titanate single crystals and grain oriented ceramics is highly anisotropic.[20] A model will be developed to describe this anisotropy and evidence will be presented for a conducting perovskite layer.

3. Dielectric Behavior and Piezoelectricity

a) From previous work,[15,21] it is expected that the conductivity can be decreased adequately with dopants so that bismuth titanate ceramics can be poled. The effect of dopant concentration on the piezoelectric properties will be studied in detail.

b) An undesirable hysteresis between force and charge in piezoelectrics has been described in the literature.[22,23] The effect of Nb doping on this aspect of the piezoelectric behavior will be investigated.

c) An anomalous peak in the dielectric response in bismuth titanate has been reported by several authors.[19,20,24,25] Analysis of the dielectric properties will be conducted in order to understand the origins of this behavior. It will be shown that Nb suppresses the anomaly, which is attributed to an ion jump relaxation.

Chapter 2. Processing and Properties of Bismuth Titanate

In order to clearly establish the goals of this thesis in a historical context, the important literature will be reviewed. The scope of this work is quite broad as it encompasses ceramics development, defect chemistry, conductivity, dielectric properties, and piezoelectricity. The common theme is how these factors are interrelated to produce useful piezoelectric bismuth titanate ceramics. Where the scientific knowledge is well established, the reader will be referred to well known texts on the subjects.

2.1 Historical Perspective

A brief historical account of piezoelectricity, pyroelectricity, and ferroelectricity is given in this section. Several classic texts on these subjects are identified as references.

Piezoelectricity is based on the existence of dipoles which cause a coupling between the electrical and mechanical responses.[26] A charge is produced on the surface of piezoelectric crystals when placed under stress (the direct effect) and a change in dimension is produced under an applied electric field (the converse effect). Piezoelectricity is discussed in classic texts by Cady[27,28], Mason[29], and von Hippel.[26]

The direct piezoelectric effect was first discovered by Pierre and Jacques Curie in 1890.[30] The Curies reasoned that due to the asymmetry of the $(SiO_4)^{4-}$ tetrahedra, a charge would be collected on the surfaces of a quartz crystal when pressure was applied (the direct effect) in a direction which forced the oxygen base of the tetrahedra to change its distance from the Si^{4+} ion. The converse effect was predicted by Lippmann[31] from thermodynamic reasoning and was demonstrated soon after by the Curies.

Pierre and Jacque Curie showed that the quantity of electric charge (or polarization) is proportional to the magnitude of the applied stress. The proportionality constant between the polarization vector (P_i) and stress (X_{ij}) is a third rank tensor known as the piezoelectric modulus (d_{ijk}). Due to symmetry considerations, a concise matrix notation can be used. This subject is described in detail by Nye.[32] In matrix notation, the piezoelectric modulus reduces

to d_{im} where the first suffix refers to the direction of the polarization and the second suffix indicates the direction of applied stress.

Polarization implies the existence of dipoles. It can be reasoned intuitively that a form without a center of symmetry, such as a tetrahedron, provides the environment for charge displacement or dipoles. Dipole formation is essential for piezoelectricity and occurs only in non-centrosymetric crystal structures. There are thirty two crystal classes, twenty one* of which are non-centrosymetric, and twenty of which can contain piezoelectric crystals. A non-centrosymetric structure permits piezoelectricity but does not guarantee it. Von Hippel [26] pointed out that an analysis of the point charges and their arrangement in a crystal can aid in predicting piezoelectricity.

The absence of a charge symmetry does not imply that piezoelectric crystals have a polar axis. Polar axes will exist in piezoelectric crystals only when the individual momentum vectors in the unit cell add up to a permanent resultant moment, instead of mutually canceling. Crystals in ten of the twenty possible piezoelectric crystal classes can have one or more polar axes. The magnitude of the resultant moment depends on the lattice dimensions so that uniform heating or cooling of a spontaneously polarized crystal will change its inherent polarization due to expansion and contraction of the lattice. As a result, piezoelectric crystals which have polar axes develop a voltage across the crystal as the temperature is changed. The polarity reverses between heating and cooling. This phenomenon is termed pyroelectricity.[26]

Pyroelectricity was described by Theophrastus in 315 BC.[27] An atomic understanding of the origins of pyroelectricity was not developed until the discovery of piezoelectricity by the Curies, the dipole moment being an essential element in explaining pyroelectric phenomena. Pyroelectricity was reviewed in 1981 by Lang.[33,34] Other sources which discuss pyroelectric materials and applications include Lang[35], Whatmore[36] and Herbert.[5]

Ferroelectrics are pyroelectrics which have dipole moments whose orientation can be changed between two or more distinct crystallographic directions by the application of an electric field. Ferroelectricity was first recognized by Valasek[37] in 1921 while studying a

* One of the non-centrosymetric crystal classes has holoaxial symmetry which reduces the piezoelectric coefficients to zero.[26]

single crystal of Rochelle salt ($KNaC_4H_4O_64H_20$). He observed a hysteresis in the relationship between polarization and applied electrical field and concluded that the dipoles switched direction with the applied field. The presence of this hysteresis loop is part of the definition of a ferroelectric material.

Until 1940, ferroelectric oxides were not known and polar hydrogen oxygen bonds were considered to be essential for ferroelectricity. During World War II, the high dielectric constant of barium titanate ($BaTiO_3$) was discovered simultaneously in different parts of the world.[38] In 1946, von Hippel and co-workers at MIT* realized that the high dielectric constant (~6000 at 20 °C) in $BaTiO_3$ ceramics was due to ferroelectricity.[38] Previously the highest dielectric constant (~80) was found in TiO_2.[38] The search for ferroelectric oxides ensued, and hundreds of ferroelectrics have been found which belong to structure types including perovskite, pseudo-pyrochlore, illminite, and tungsten bronze.[5]

Many compounds from the structural family described by Aurivillius in 1949[2,3], the bismuth layer structure perovskites, were shown to be ferroelectric by Subbarao[39-41] in 1961-1962. To date, more than seventy compounds have been reported in the Aurivillius family and more than fifty of them are ferroelectric.[42,43]

A significant result of ferroelectricity is that it is possible to align the dipoles of randomly oriented ferroelectric grains and observe the piezoelectric effect in a ceramic.[38] Prior to the understanding of the switching of dipole moments in a ferroelectric, the phrase "piezoelectric ceramic" seemed a contradiction. Piezoelectric ceramics, such as lead zirconate titanate (PZT) are now well known materials and are incorporated into thousands of products including watches, ultrasonic equipment, and hydrophones. There are many books on the subject of ferroelectric and piezoelectric ceramics which provide details on processing, properties, and applications.[38,44,45]

The most widely used piezoelectric ceramics (i.e. PZT) cannot be used at temperatures greater than 250 °C due to depoling and finally the loss of ferroelectricity at the Curie temperature.[5] Many of the Aurivillius phases have high transition temperatures (> 400 °C) and therefore are of interest for high temperature piezoelectric applications.[1]

---

* Massachusetts Institute of Technology

2.2 Materials with High Ferroelectric Transition Temperatures

The Curie temperature gives an upper limit for the ferroelectric phase and is therefore an important criterion in the search for high temperature ferroelectrics for piezoelectric applications. A survey of the materials which show the highest Curie temperatures is given in Table 2.1.

Table 2.1 Ferroelectric Oxides with high Curie temperatures (> 400 °C).
(note: The values in this table are representative. They appear to be affected by the processing, poling, and measurement techniques.)

Material	T_c (°C)	d_{33} (pC/N)	ρ 20 °C (Ωm)	ref
Perovskite layer structure				
$La_2Ti_2O_7$ (single x-tal)	1500	16		[46]
$Sr_2Nb_2O_7$ (single x-tal)	1300	18		[47]
Illminite				
$LiNbO_3$ (single x-tal)	1200	d_{22}=21	10^{10}	[1,48]
$LiTaO_3$ (single x-tal)	665	6		[48]
Bismuth layer structure perovskite				
$Bi_4Ti_3O_{12}$ (grain oriented ceramic)	675	25	10^9	[19]
$Na_{0.5}Bi_{4.5}Ti_4O_{15}$ (ceramic)	660	16-19	10^{12}	[49-51]
$SrBi_4Ti_4O_{15}$ (ceramic)	530	15-18	10^{12}	[41,51]
$CaBi_4Ti_4O_{15}$ (ceramic)	790	8	10^{11}	[51,52]
$PbBi_4Ti_4O_{15}$ (ceramic)	560	12	10^{12}	[53]
Bi_3TiNbO_9 (ceramic)	940	5	10^9	[54]
Tungsten Bronze				
$PbNb_2O_6$ (ceramic)	560	85		[1,38]
Perovskite				
$PbTiO_3$ (ceramic)	470	51	10^{12}	[55]

Several layer structure perovskites*, for example, $La_2Ti_2O_7$ and $Sr_2Nb_2O_7$ remain ferroelectric to temperatures in excess of 1300 °C, however, the high coercive field§ has proved a major obstacle in poling the ceramics.[56] $LiNbO_3$ has a similar problem, as well as high conductivity and oxygen loss at elevated temperatures. Single crystal $LiNbO_3$ is used as a piezoelectric in the high temperature range.[1]

Lead metaniobate ($PbNb_2O_6$) from the tungsten-bronze family has a Curie temperature of 560 °C and a d_{33} of 85 pC/N. Dopants are necessary to decrease the conductivity which also decreases the Curie temperature. These piezoelectric ceramics are generally not recommended for use above 300 °C.[1]

Several of the bismuth layer structure perovskites offer an intermediate range of Curie temperatures (T_c~500-900 °C) and piezoelectric responses (d_{33}~4-30 pC/N). The compositions $Bi_4Ti_3O_{12}$ (T_c=675 °C), $CaBi_4Ti_4O_{15}$ (T_c=790 °C), and Bi_3TiNbO_9 (T_c=910 °C) show the highest Curie temperatures from this group, however, the low resistivities make them difficult to pole. It can be anticipated that as the understanding of these materials improves, solutions will be found to control the conductivity.

In summary, many of the bismuth layer structure perovskites are of interest for piezoelectric applications in the temperature range 300-600 °C. Lead metaniobate based ceramics have a higher piezoelectric coefficient and can be used up to 300 °C. For very high temperatures (e.g. ~600 °C), $LiNbO_3$ single crystals are available, however, these are expensive to fabricate and prone to oxygen loss. The bismuth layer structure perovskites provide reasonably high piezoelectric coefficients and can be prepared via an inexpensive ceramic processing route. In order for this potential to be realized, the conductivity must be controlled in the Aurivillius phases with the highest Curie temperatures.

2.3 Crystal Structure and Symmetry

2.3.1 Perovskite crystal structure

The perovskite crystal structure is described here so that a comparison can be made with the perovskite-like layers in Aurivillius phases.

---

* ...not to be confused with bismuth layer structure perovskites as discussed later.

§ Coercive field, E_c, is related to the electric field necessary to switch the orientation of dipoles.

The mineral perovskite, $CaTiO_3$, actually occurs in a defective form of what is known as the perovskite structure, ABO_3. This structure is illustrated in Figure 2.1 and can be viewed as a close packed cubic cell of large cations at the cube corners and oxygen ions at the faces with small highly charged cations occupying octahedral interstices. The A-site cations are in 12-fold coordination with oxygens and the small B-site cations are in 6-fold coordination. The terms "A" and "B"-site are used frequently in describing perovskites and perovskite-like structures.

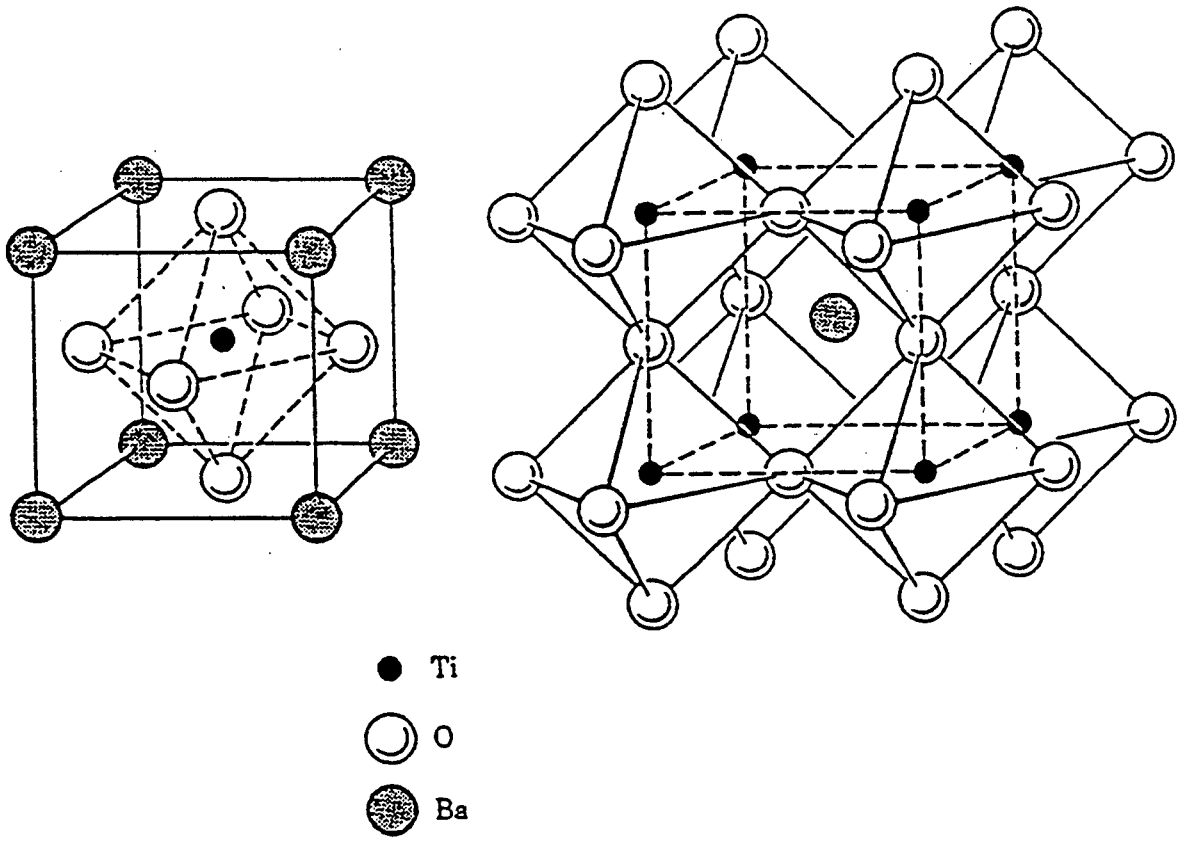

Figure 2.1 Schematic illustration of the perovskite unit cell ($BaTiO_3$ as an example).

The A-site can accommodate large cations such as Ba^{2+}, Pb^{2+}, and Sr^{2+}, while the B-site accepts smaller cations such Ti^{4+}, Nb^{5+}, and Zr^{4+}. More specifically, the size of the A-site cation is controlled by the space available and the electrostatic charge. Goldschmidt[57] determined the size of the cations that can be accommodated by the perovskite structure

according to Pauling's Rules. The A-site can contain ions with ionic radii* between 1.34 (Ca^{2+}) and 1.61 Å (Ba^{2+}) while the B-site can accommodate ions from 0.535 Å (Al^{3+}) to 0.87 Å (Ce^{4+}).

2.3.2 Aurivillius crystal structures

The terminology has not been standardized for the Aurivillius or bismuth layer structure perovskites. In the literature they are referred to as "layered bismuth compounds", "perovskite-like layered structures", "bismuth containing laminated perovskite-like compounds", and other combinations of these words. These structures consist of different numbers of perovskite units separated by layers of bismuth oxide. To add to the confusion the term "perovskite layer structure" has been used for the $A_2B_2O_7$ compounds characterized by stacked perovskite-type slabs containing corner-shared BO_6 octahedra.[61] The phases described by Aurivillius[2,3] are defined in this work as "Aurivillius phases" or "bismuth layer structure perovskites".

The bismuth layer structure perovskites are described by the formula ($Bi_2A_{m-1}B_mO_{3m+3}$) where "m" is an integer from 1 to 5 representing the number of perovskite groups separated by $(Bi_2O_2)^{2+}$ layers.[43] "A" is a cation in 12-fold coordination and "B" is an octahedrally coordinated cation in the perovskite-like units. For example, $SrBi_4Ti_4O_{15}$ is an Aurivillius phase with m = 4, B = Ti, and A = (Sr + 2Bi). The Aurivillius structures are sometimes described[62] by an equivalent formula $(Bi_2O_2)^{2+}(A_{m-1}B_mO_{3m+1})^{2-}$. The subscript "m" can be viewed as the number of perovskite units, or more precisely, two dimensional sheets of corner-sharing octahedra forming the perovskite-like slabs. The $(Bi_2O_2)^{2+}$ layer consists of double sided sheets made up of square pyramidal BiO_4 groups sharing their basal edges. These sheets have their oxygen ions in common with the perovskite slabs.

Ordered intergrowths or Aurivillius phases with "mixed layers" were first suggested by Kikuchi[63] in 1977. These ordered intergrowths have the general formula $Bi_4A_{m+n-2}B_{m+n}O_{3(m+n)+6}$, where m is the number of perovskite units in one half of the unit

---

* It should be noted that values for ionic radii differ depending on the source.[58-60]

cell and n is the number of perovskite units in the other half. Since it is more probable that a structure will form with the difference between layers being only one perovskite group (n = m+1) the general formula is often reduced to $Bi_4A_{2m-1}B_{2m+1}O_{6m+9}$.

$Bi_4Ti_3O_{12}$ is a bismuth layer structure perovskite having an "m" value of 3 in the formula ($Bi_2A_{m-1}B_mO_{3m+3}$) where A = Bi and B = Ti. This structure is shown schematically in Figure 2.2. Each perovskite layer contains three perovskite units* with Ti at the centers. Two of the perovskite units in the unit cell are completed by oxygens which bond to Bi in the $(Bi_2O_2)^{2+}$ layer. The Bi ions occupy two distinct positions, that of the 12-fold coordinated site in the perovskite layer, and the 4-fold site in the $(Bi_2O_2)^{2+}$ layer. It can be noted that the perovskite layers are offset with a translation in the **a**- and **b**-directions.

The "A"-site in bismuth layer structure perovskites and the ordered intergrowths can accommodate cations from 1.34 to 1.61 Å [43] such as Na^+, K^+, Ca^{2+}, Sr^{2+}, Pb^{2+}, Ba^{2+}, La^{3+}, Bi^{3+}, Y^{3+}, U^{4+}, and Th^{4+}, which is equivalent to the A-site in normal perovskites. The "B"-site can accept cations from 0.59 Å (W^{6+}) to 0.65 Å (Fe^{3+}). This is a narrower range of ionic sizes than in perovskites. The lower limit of the ionic radii is determined by the stability of the perovskite layer and the upper limit by the mismatch between the $(Bi_2O_2)^{2+}$ and perovskite layers.[43,64]

In summary, the Aurivillius phases and the related ordered intergrowths can be described as a combination of different numbers of perovskite units sandwiched between $(Bi_2O_2)^{2+}$ layers. The A-site, with 12-fold coordination, accepts ions of the same size range as perovskites. The B-site, with 6-fold coordination, has a smaller size range than the perovskite B-site. Bismuth titanate is an Aurivillius compound, $(Bi_2O_2)^{2+}(A_{m-1}B_mO_{3m+1})^{2-}$, with m = 3.

---

* Some authors (e.g. [62]) refer to two complete perovskite units, considering the Bi as the central ion. This is more difficult to imagine since one loses the perspective of the oxygen octahedra.

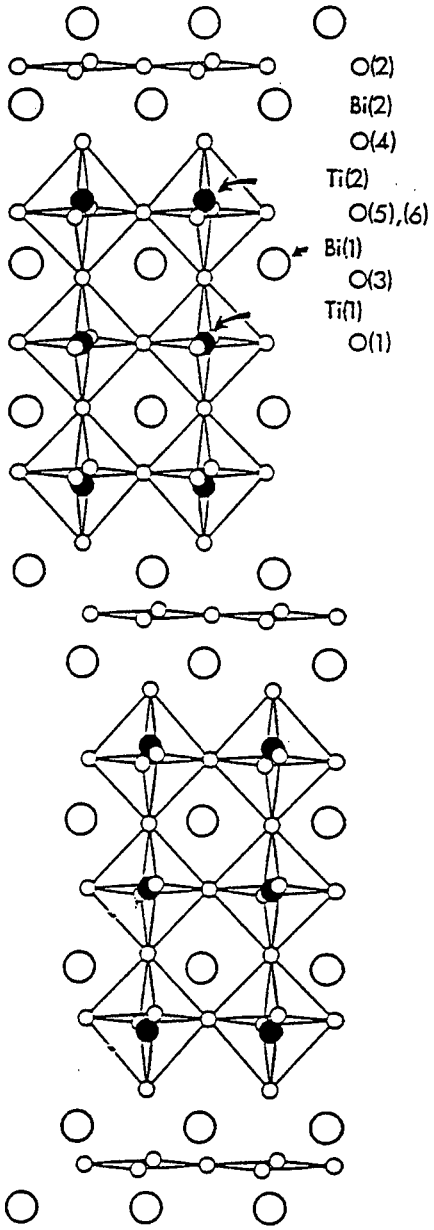

Figure 2.2 Schematic illustration of the $Bi_4Ti_3O_{12}$ unit cell.

2.3.3 Symmetry of Aurivillius phases

Initially Aurivillius assigned the symmetry of bismuth layer structure perovskites to tetragonal or pseudo-tetragonal.[2,3] Further investigations[41] have shown that most of the Aurivillius compounds are orthorhombic in the ferroelectric phase due to slight distortions from the high symmetry tetragonal (I4/mmm) parent structure.

Bismuth titanate unlike the other Aurivillius phases, is monoclinic with space group B1a1[65] in the ferroelectric phase. The dimensions of the monoclinic bismuth titanate unit cell are **a** = 5.450 Å, **b** = 5.4059 Å, and **c** = 32.832 Å. The angles between the axes are given by Rae, et al.[65]

The ferroelectric Aurivillius phases, including $Bi_4Ti_3O_{12}$, are usually described on the basis of a doubled orthorhombic diagonal cell which transforms the tetragonal I4/mmm prototype structure to an orthorhombic Fmmm underlying, non-polar, parent structure. The relationship between the tetragonal, orthorhombic, and monoclinic crystal directions in bismuth titanate is shown in Figure 2.3. Crystallographically, this choice of axes does not follow the convention, **c** < **a** < **b**, assumed in orthorhombic systems, however, it is suitable for the Aurivillius phases, since the **a**-direction can be viewed as the polar axis. The **c**-axis, which is the longest axis, is perpendicular to the $(Bi_2O_2)^{2+}$ layers.

In summary, most of the ferroelectric Aurivillius phases are orthorhombic below the Curie temperature. Bismuth titanate is an exception, showing monoclinic symmetry below T_c. The axes used to represent the Aurivillius phases are based on the orthorhombic Fmmm symmetry so that the **a**-direction contains the major component of the polarization vector and the **c**-direction is perpendicular to the layers.

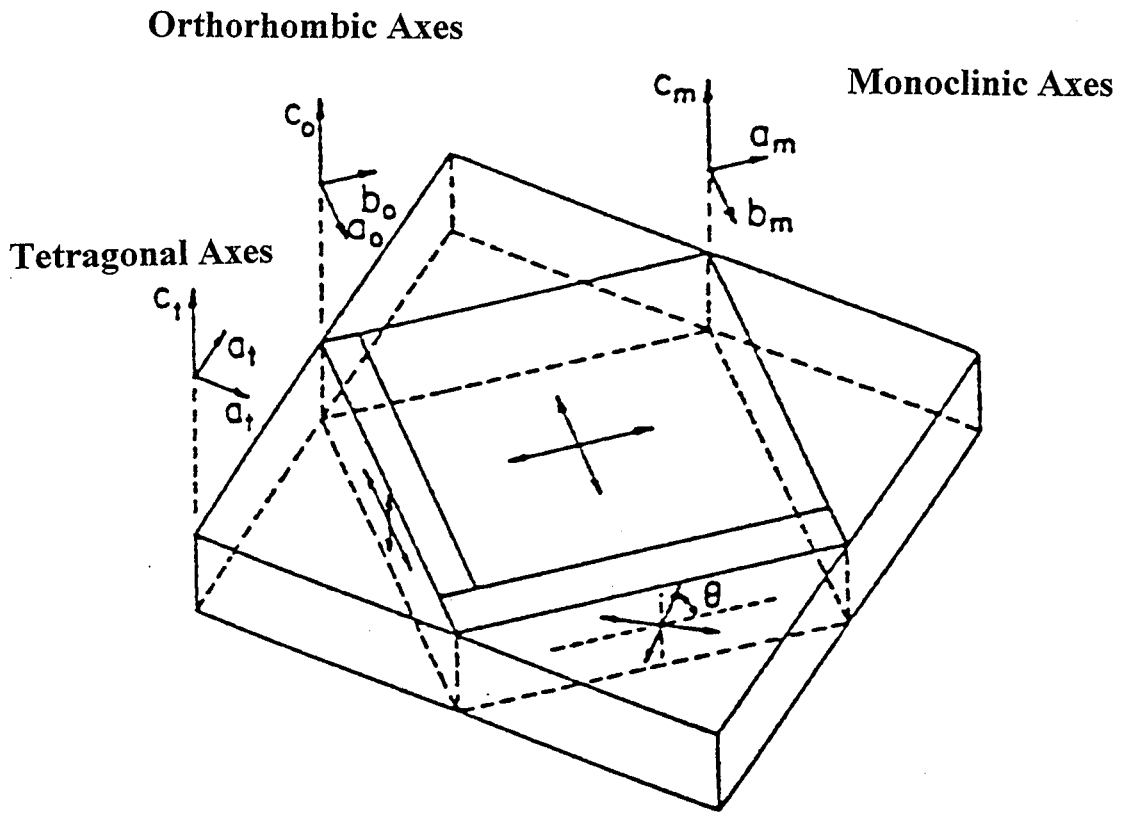

Figure 2.3 Illustration of the three sets of crystallographic axes (tetragonal, orthorhombic, and monoclinic) **which are used in discussing Aurivillius phases.**

2.4 Origins of Ferroelectricity in Bismuth Titanate

Newnham, et al.[42], identified the major contributors to the spontaneous polarization in bismuth layer structure perovskites as the octahedral cations (Ti^{4+}) moving towards the octahedral edges*. More recent refinements of the crystal structures of $Bi_2W\ O_6$,[66] Bi_3TiNbO_9[65], and $Bi_4Ti_3O_{12}$[67] have shown that the main structural cause of ferroelectricity in these compounds is the **a**-axis displacement of Bi atoms in the perovskite A-sites with respect to the chains of TiO_6 octahedra.

In $Bi_4Ti_3O_{12}$, a dipole moment of 36.3 $\mu C/cm^2$ was calculated in the **a**-direction and 2.4 $\mu C/cm^2$ in the **c**-direction.[65] The resultant polarization is 4.5° off of the **a**-axis in the **ac** plane. These dipole moments are slightly smaller than the values reported by Cross and Pohanka.[68]

* This is fairly accurate in perovskites.

The **c**-direction polarization component in bismuth titanate can be switched independently of the **a**-direction component.[4] The small polarization in the **c**-direction can be switched at low fields (≤ 4 kV/cm) while the **a**-direction polarization has a high coercive field (≤ 60 kV/cm). The values given for the coercive field in both directions vary widely.[4,12,13,69,70] Although a systematic investigation has never been reported, the differences in coercive field are believed to lie in the purity of the crystals.[13] Lower coercive fields are generally measured in higher purity crystals.

Discontinuous changes in the optical properties and the conductivity at the phase transition temperature indicate that the transition to the ferroelectric state is first order.[4,20,71] Although first order transitions are known to occur in ferroelectrics, the direct change from a low symmetry monoclinic phase to tetragonal symmetry is rather uncommon.[20,42] Recent work by Reaney, et al.[72] suggests that bismuth titanate undergoes two separate phase transitions, from monoclinic to orthorhombic to tetragonal, with increasing temperature.

In summary, the origin of ferroelectricity in bismuth titanate is related to the displacement of the Bi ions in the **a**-direction in the perovskite layer. A small polarization vector which lies in the **c**-direction can be switched independently from the major polarization in the **a**-direction.

2.4.1 Domain structure

A number of different twinning and domain structures exist in bismuth titanate. This is the result of the high degree of crystallographic symmetry at temperatures above the Curie transition, and the relatively low degree of symmetry below the transition. Fousek and Janovec[73] have shown that it is possible to derive the orientations of domain walls in any ferroelectric crystal if the point symmetry of the paraelectric phase and the orientation of the possible polarization vectors in the ferroelectric phase are known. The possible domain configurations in bismuth titanate[73] are illustrated in Figure 2.4. Cummins and Cross[4] found good agreement between the observed structures and those predicted.

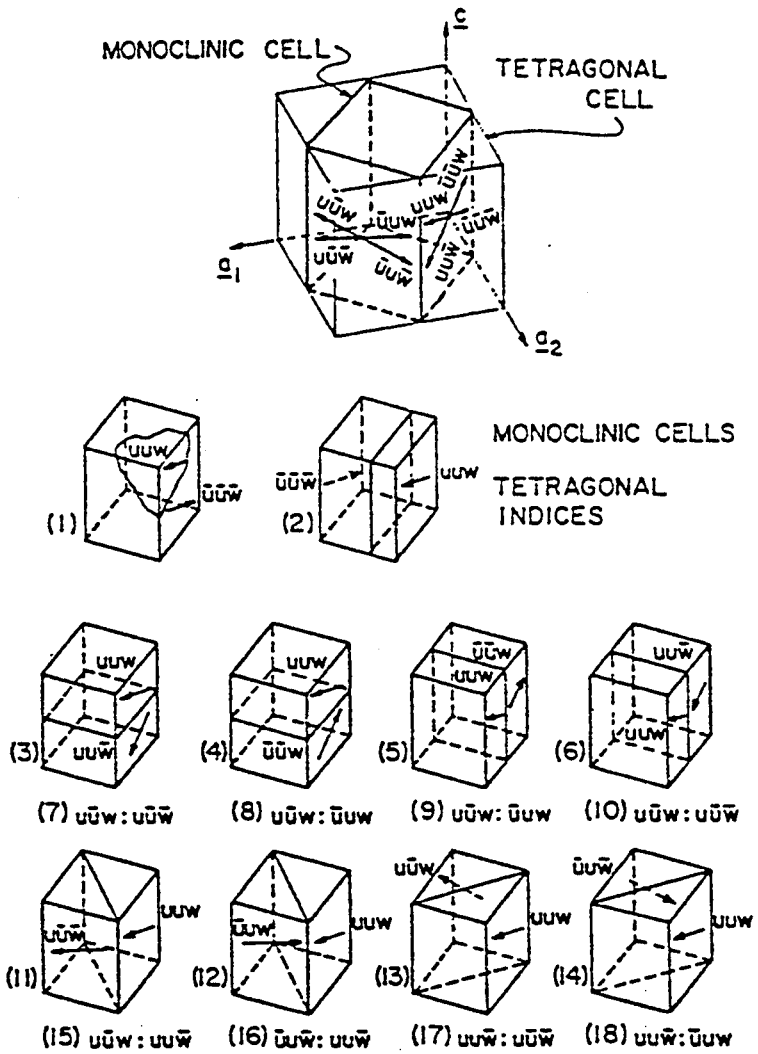

Figure 2.4 Schematic representation of the possible domain configurations in monoclinic $Bi_4Ti_3O_{12}$.

It was shown[4] that 90° twinning in an electric field involved the interchange of the **a**- and **b**-axis direction. With a high field (approximately 60 kV/cm) applied along the **b**-direction, a hysteresis loop appeared. This is not expected to occur with a polarization vector, $\mathbf{P_s}$, in the **ac** plane. The crystal showed 90° twinning on the faces perpendicular to **c**. These results indicate that electric switching of $\mathbf{P_s}$ by 90° (**b**-axis switches to **a**-axis) is possible with sufficiently high fields.

Hopkins and Miller[11] prepared twin free crystals of $Bi_4Ti_3O_{12}$ by slowly cooling through T_c. They observed that cooling bismuth titanate crystals under stress free conditions greatly reduced the number of 90° domains. Applying this to ceramics, the stress state on the grains will affect the domain formation. Factors such as the grain size and grain boundary phase may have a significant impact on the stabilization of 90° domain walls.

In summary, most of the possible domain configurations which were predicted, have been observed experimentally. Twinning associated with 90° domains was eliminated in single crystals by cooling slowly through the Curie temperature in an unclamped stress free environment. Non-180° domain walls are of particular interest because their motion contributes to the piezoelectric effect.[23,74-76] This subject will be discussed in Chapter 5.

2.5 Bismuth Titanate Ceramics

The research efforts in bismuth titanate ceramic processing have been aimed at developing oriented microstructures. Recently, the focus has shifted towards inexpensive ceramic processing which utilizes a mixed oxide method and pressureless sintering.[15,18,77] The limited work which has been published on these subjects will be discussed in the following sections.

2.5.1 Bismuth titanate phase formation

Many techniques have been employed to form $Bi_4Ti_3O_{12}$ powders. These include molten salt synthesis,[78,79] co-precipitation,[80] reactive calcination,[81] and sol-gel synthesis.[82,83] It is one of the goals in this work to enhance the understanding of the formation of $Bi_4Ti_3O_{12}$ via the mixed oxide method. The reaction kinetics and the effect of raw materials have not been studied in ceramics, however, the presence of an intermediate phase, $Bi_{12}TiO_{20}$, has been reported.[84]

Several references[8,15,85] report a calcination temperature of 800 °C for the reaction of bismuth titanate from the mixed oxides. Others have applied calcination temperatures up to 1100 °C.[64,86] A two stage calcination was recommended by Galasso[87] whereby pressed pellets were calcined at 700 °C, ground, pressed, and calcined again at 920 °C.

The approach taken by Jovalekic, et al.[77] was to study the reaction between Bi_2O_3 and TiO_2 indirectly by measuring the density of the mixture as a function of time and temperature. The authors concluded that the formation of $Bi_4Ti_3O_{12}$ from Bi_2O_3 and TiO_2 at temperatures above 825 °C proceeded in two steps. First Bi_2O_3 melts which allows solution and reprecipitation of $Bi_4Ti_3O_{12}$ and intermediate (unspecified) bismuth titanate phases. The intermediate phases then react with the liquid phase and also form $Bi_4Ti_3O_{12}$. Although this reaction scenario is feasible, it was not supported by an analysis of the phases present (e.g. by XRD). It can be noted that significant SiO_2 contamination must have been present by ball milling in agate. This would have an impact on the liquid phase formation, since there is a eutectic between Bi_2O_3 and SiO_2 at 800 °C.[88]

Shrout[81] reports a volume expansion of ~8% for a mixture of Bi_2O_3 and TiO_2 heated to temperatures between 750 °C and 900 °C and quenched. This is contrary to Jovalekics' report of an increase in density in this temperature range.[77] The contradiction may originate in the differences of impurities, particle sizes, and/or powder morphology.

In summary, the mixed oxide method can be used to form $Bi_4Ti_3O_{12}$, however, the impact of variables such as the purity, particle characteristics, calcination regime, and the reaction route have not been adequately explored.

2.5.2 Microstructural evolution

There are very few reports which characterize the microstructure in randomly oriented bismuth titanate ceramics. These are reviewed in this section.

Jovalekic, et al.[77] prepared $Bi_4Ti_3O_{12}$ by ball milling a mixture of Bi_2O_3 and TiO_2 in an agate mill for 24 hours, pressing samples and calcining at 1100 °C for ≤ 4 hours. The samples were re-ground, recompacted, and sintered at 1100 °C for 4 hours. Phase pure $Bi_4Ti_3O_{12}$ was reportedly obtained, however, a continuous grain boundary second phase was observed. No quantitative information was provided on the grain boundary phase.

The influence of thermal treatment on the microstructure was studied by the same authors.[89] Sintered ceramics were prepared as described above and then annealed at temperatures between 750 °C and 950 °C for 4 hours. The microstructures from the 750 °C

and 850 °C treatments were similar, while the sample annealed at 950 °C showed large abnormal anisotropic grains (~100 μm long and 20 μm wide). The rate of abnormal grain growth* became significant at 950 °C. A mechanism of liquid phase assisted grain growth was suggested.

Abnormal anisotropic grain growth has been observed in bismuth titanate for sintering temperatures ranging from 950 °C to 1100 °C.[18,89,90] On the other hand, starting with high purity raw materials, fine grained bismuth titanate microstructures have also been obtained after sintering at 1100 °C.[18] It is evident that the grain growth kinetics are affected by the impurities and processing parameters.

2.6 Defect Chemistry and Conductivity in Bismuth Titanate

One of the goals in this work is to develop an understanding of the role of impurities and dopants on the conductivity in bismuth titanate. This also provides an insight into the defect structure. The literature contains surprisingly few references to the defect structure of bismuth titanate or any of the bismuth layer structure perovskites. The current state of knowledge concerning the defect chemistry and conductivity in bismuth titanate will be discussed in the following sections.

2.6.1 Single crystals

Gurevich[91] determined that a bismuth titanate crystal (probably measured in the **c**-direction) was a p-type conductor at 700 °C as evidenced by the positive Seebeck coefficient. In addition, the ionic contribution was considered to be negligible in the temperature range from 300-500 °C by the verification of Faraday's law.

Fouskova and Cross[20] used an AC method to determine the conductivity from the dielectric loss tangent, tan δ, by the relationship:

equation 2.1 $$\tan\delta = \sigma/\omega\varepsilon$$

* Also known as exaggerated grain growth, discontinuous grain growth, and secondary recrystallization.

where σ represents the "quasi-static" conductivity, ω is frequency, and ε is the dielectric permittivity. This method was valid for temperatures greater than 500 °C where the contribution to tanδ from the conductivity was much higher than the other contributions (e.g. Debye type relaxation). They found that the conductivity in the **a**-and **b**-direction was approximately equal. Between 500 °C and 700 °C, the conductivity in the **c**-direction was ~30 times lower. The **c**-direction is perpendicular to the perovskite and bismuth oxide layers. Either of these layers may form a resistive barrier. This subject is discussed in Chapter 4.

Several interesting observations were made by Hopkins and Miller.[11] It was found that the purity of the bismuth titanate crystals was an important factor in determining the properties. Crystals grown from "semiconductor-grade" could be poled easily using their technique, while bismuth titanate crystals prepared from "ordinary reagent-grade" materials were impossible to pole due to a high conductivity. Impurities are believed to be responsible for the wide variation in values reported for the conductivity of single crystal bismuth titanate.[13]

Another point of interest is that high purity bismuth titanate crystals were colorless.[11]A brown coloration was observed after subjecting these crystals to electric fields at temperatures where the "conductivity was appreciable". The coloration was attributed to oxygen vacancies. The original state was re-gained by annealing in air at 600 °C. This suggests that oxygen vacancies are mobile defects in bismuth titanate at relatively low temperatures. The impact of oxygen diffusion on the dielectric properties is discussed in Chapter 5.

In summary, early measurements indicate that single crystal bismuth titanate is a p-type electronic conductor. The crystal direction and purity were not reported. The influence of impurities on the defect structure in single crystal bismuth titanate may explain the variation in reported values for conductivity, however, the mechanisms or defects responsible have not been identified.

2.6.2 Grain oriented bismuth titanate ceramics

Grain orientation provides samples with the **c**-direction mutually perpendicular to the randomly oriented **a**- and **b**- crystal direction. It was shown by Swartz, et al.[92] that the conductivity in 98% oriented tape cast bismuth titanate is an order of magnitude higher in the **ab** plane than in the **c**-direction (temperature range of 500-700 °C). This anisotropy in conductivity was slightly less than in single crystals[20] (10 times rather than 30 times), which can be expected from the imperfect orientation. An undesirable feature of oriented bismuth titanate ceramics is that the conductivity is maximized in the same direction as the major component of the polarization.

2.6.3 X-ray photoelectron spectroscopy

X-ray Photoelectron Spectroscopy (XPS) also known as electron spectrographic chemical analysis (ESCA) is a surface analysis technique (~300 Å) which gives the characteristic binding energy of electrons.[93] Jovalekic, et al.[77,89] determined that the valence state of the Bi ions was slightly lower than 3+. They concluded that oxygen vacancies caused the reduction of Bi^{3+}. This subjected is evaluated in Chapter 4 in the light of an XPS study on the effects of Nb doping on the valence state of Bi.

2.6.4 Ionic substitution

Charged defects resulting from ionic substitutions can have a significant impact on the conductivity in oxides.[38,94,95] In this section the possibilities for ionic substitutions in $Bi_4Ti_3O_{12}$ are explored.

Charged defects can result from aliovalent substitutions. The defect notation established by Kroger and Vink[96] is used extensively in the ceramic literature.[95,97] Cations which replace ions of greater valence are negatively charged with respect to the site. For example, in $Bi_4Ti_3O_{12}$, Mn^{3+} on a Ti^{4+} site, produces the defect Mn_{Ti}' which can be compensated by a free hole. This type of substitution is known as acceptor doping. Donor dopants replace cations of lesser charge, such as $Nb_{Ti}^{\bullet} + e'$. Anionic substitutions, such as $F_O^{\bullet} + e'$ are also possible, but are less well studied.

Armstrong and Newnham[64], Subbarao[40], and Dorrian, et al. [98] found that the A-site in the perovskite layer allowed substitution of alkaline earth, rare earth, and alkali ions, with higher solubility limits for the larger cations. It appears that the B-site has a lower tolerance for substitutions but can accept ions ranging in size from 0.58 to 0.65 Å (W^{6+} to Fe^{3+}).[64] The $(Bi_2O_2)^{2+}$ layer appeared to be "almost inviolate" to cation substitutions.[42,64] It has been suggested[43] that lone pair ions, such as Pb, can substitute for Bi in the bismuth oxide layer due to the suitable position (pyramidal coordination) for asymmetrical cations.

The earliest report of using aliovalent dopants to control the conductivity in $Bi_4Ti_3O_{12}$ comes from the former Soviet Union in 1975.[99] Vusevker, et al.[99,100] observed a decrease in the conductivity of bismuth titanate (by several orders of magnitude) over the temperature range 20-600 °C with the addition of niobium and tungsten oxide. The $Bi_4Ti_{2.967}W_{0.030}Nb_{0.003}O_{12}$ composition was identified as having the highest resistivity.

Continuing this work, in the late 1980's Lopatin, et al.[15] report the doping of bismuth titanate according to the formula $Bi_{4-x}(Ti_{1-x}M_x)_3O_{12}$ where M = Nb, Sb, Ta, W, V, or Mo. Several compositions with x ranging from 0 to 0.08 (0-1.3 at%) were prepared. The most effective dopant was Nb (x=0.03, ~0.5 at%) which decreased the conductivity by several orders of magnitude. Niobium is a donor dopant replacing Ti ($Nb_{Ti}^{\bullet} + e'$). A decrease in conductivity with donor dopants agrees with Gurevich's assessment of p-type conductivity in single crystal bismuth titanate.

Takenaka and Sakata[14] added Mn to bismuth titanate in the form of $MnCO_3$ also seeking to decrease the conductivity. In their conclusion, it is stated that "hot forged BIT + 0.2 wt% $MnCO_3$ (is) an attractive piezoceramic composition with high resistivity...". The resistivity values for doped and undoped bismuth titanate were not given. In perovskites, Mn is known to replace Ti as an acceptor dopant[38] ($Mn_{Ti}' + h^{\bullet}$). This is not consistent with Lopatin's report of donors decreasing the conductivity.

In summary, the conductivity of bismuth titanate was decreased with donor dopants indicating that it originally showed p-type conduction. A conflicting statement suggested that an acceptor dopant decreased the conductivity. More information must be made available

concerning the conductivity in undoped bismuth titanate and the effect of dopants in order to clarify this contradiction.

2.7 Piezoelectricity in Bismuth Titanate Ceramics

In this section the piezoelectricity will be discussed specifically in terms of the piezoelectric coefficient in the thickness mode, d_{33}. A summary of the highest reported values of d_{33} in $Bi_4Ti_3O_{12}$ is given in Table 2.2. Since most of the studies have been conducted on grain oriented ceramics, several of these are included. The percent alignment for grain oriented structures is according to the method of Lotgering.[101]

Table 2.2 Reported values of piezoelectric coefficient (d_{33}) in bismuth titanate ceramics.

Composition	d_{33} x10^{-12} (pC/N)	align-ment (%)	direction	poling conditions	ref
$Bi_4Ti_3O_{12}$	26.0	100	ab	*80 kV/cm 10 min, 20 °C	[19]
$Bi_4Ti_3O_{12}$	11.0	100	c	*55 kV/cm 10 min, 150 °C	[19]
$Bi_4Ti_3O_{12}$ +0.2 wt% $MnCO_3$	25.1	80	ab	30-60 kV/cm 1-30 min, 5-200 °C	[14]
$Bi_4Ti_3O_{12}$ +0.2 wt% $MnCO_3$	15.1	0	random	30-60 kV/cm 1-30 min, 5-200 °C	[14]
$Bi_{3.97}Ti_{2.91}Nb_{.09}O_{12}$	22.0	0	random	50 kV/cm 210 °C, 30 min	[15]
$Bi_{3.97}Ti_{2.91}Ta_{.09}O_{12}$	21.5	0	random	50 kV/cm 210 °C, 30 min	[15]
$Bi_{3.97}Ti_{2.91}Sb_{.09}O_{12}$	17.5	0	random	50 kV/cm 210 °C, 30 min	[15]
$Bi_{3.97}Ti_{2.955}W_{.045}O_{12}$	17.0	0	random	50 kV/cm 210 °C, 30 min	[15]

* pulse poling 2 msec wide and 10 msec apart

Seth and Schultz[19] used a pulse poling technique at room temperature to overcome the high conductivity in the **ab** plane. They obtained the highest reported value for d_{33} (26 pC/N) in undoped $Bi_4Ti_3O_{12}$. The d_{33} is lower in the **c**-direction than in the **ab** plane. This can be expected, since the **c** polarization vector is an order of magnitude lower than the **a** polarization. The ceramic was prepared via a process involving molten salt synthesis of powders, tape casting, and sintering.

Takenaka, et al.[14] reported a similar value, 25 pC/N in the **ab** plane, for Mn doped hot forged bismuth titanate. Poling was achieved in a DC field. Typically, undoped bismuth titanate cannot be poled in a DC field due to a combination of the high conductivity and the high coercive field.[90] The conductivity precludes poling at high temperatures, and the high coercive field demands it. Typical d_{33} values for undoped bismuth titanate poled in a DC field are 0-5 pC/N.[90,92]

The processing techniques utilized by Takenaka, et al.[14] and Seth and Schulze[19] to obtain d_{33} values ≈25 pC/N seem complex when one compares them with Lopatin's randomly oriented ceramics. Lopatin, et al.[15] prepared samples via a mixed oxide method and pressureless sintering to obtain a comparable d_{33} of 22 pC/N for a Nb doped bismuth titanate composition.

A randomly oriented material has several clear advantages. Firstly, samples can achieve a high d_{33} in any direction chosen for poling, compared to one direction in the grain oriented material. Secondly, the cost is lower to produce materials via a simple method than a complicated one. Thirdly, the shape restrictions from grain orientation methods are much greater. For the randomly oriented material one can envision using standard techniques such as extrusion, dry pressing, slip casting, or injection molding to form almost any shape of interest.*

In summary, a high d_{33} of ~25 pC/N was obtained in the **ab**-direction of grain oriented bismuth titanate ceramics. One of these contained an acceptor dopant (0.2 wt% $MnCO_3$) which appears to aid in the poling process, presumably through a decrease in the conductivity. A comparable d_{33} of 22 pC/N was obtained in a randomly oriented ceramic

* This assumes nearly isomorphic particles which is typical of bismuth titanate powder from the mixed oxide method (see section 3.3.4).

which was donor doped with 0.5 at% Nb. The high d_{33} in this material was also attributed to a decrease in conductivity. There seems to be an inconsistency in that a donor dopant in one case, and an acceptor dopant in another, decreased the conductivity and allowed polarization in a DC field.

2.8 Chapter Summary

Complicated methods have been implemented for preparing bismuth titanate powders and oriented ceramics. These methods do not provide a clear advantage over the mixed oxide method and pressureless sintering of bismuth titanate ceramics for high temperature piezoelectric applications. As complex technologies have grown, a gap has developed on the more standard forms of ceramic processing of bismuth titanate.

The mixed oxide method for producing bismuth titanate powder will be studied in detail in Chapter 3. The densification and microstructural evolution of bismuth titanate ceramics will be investigated to add to the knowledge of this material in the non-oriented form. The impact of microstructure, impurities, and dopants on the electrical properties will be discussed in Chapters 4 and 5.

This thesis is primarily concerned with understanding the relationship between the microstructure, dopants, impurities, electrical conductivity, and the piezoelectric response in randomly oriented bismuth titanate ceramics. It is proposed that this study will provide the basis for the future development of high temperature piezoelectric bismuth titanate sensors.

Chapter 3. Ceramics Development

3.1 Introduction

The electrical properties of ceramics are often influenced by the microstructure and defect structure.[38,95,102] The processing factors which affect these parameters must be understood and controlled in order to avoid ambiguity during the interpretation of the electrical properties.[17] In addition, the ceramic must be reproducible so that the measured properties are representative of the composition rather than of a specific sample.[103]

It is the goal of this chapter to investigate processing variables which influence bismuth titanate phase formation, densification, and grain growth. These variables include the raw materials, sintering conditions, and dopants. Ultimately, investigations are expected to allow the reproducible fabrication of ceramics with well defined microstructures. The electrical properties of the ceramics developed in this chapter will be analyzed in the following chapters.

The experimental realization of the goals includes the following steps:

1. Examine the reaction route to form $Bi_4Ti_3O_{12}$ from Bi_2O_3 and TiO_2 by using XRD to observe the phase formation at various stages in the calcination process.

2. Choose a suitable model to describe the kinetics of formation of $Bi_4Ti_3O_{12}$, and determine the effect of raw materials' selection on the reaction kinetics.

3. Evaluate grain growth in undoped $Bi_4Ti_3O_{12}$ ceramics using SEM to observe the microstructures as a function of sintering time.

4. Determine the effects of acceptor and donor dopants on densification and grain growth.

3.2 Experimental Procedures

The analysis methods for phase determination, particle size distribution, and microstructural features are described in the following sections.

3.2.1 X-ray diffraction

X-ray diffraction was used to determine the phases of the raw materials and of the calcined and sintered products. The X-ray diffraction (XRD Siemens Kristalloflex 805) measurements were performed with a step scan of 0.04 and a count time of 4 seconds. Profiles were collected from 5° to 65° 2θ using Cu Kα radiation. Integrated peak intensities were calculated using, Peak Locate, a Siemens Difrac 5000 version 2.32 program. Phases existing in quantities less than approximately 2 vol% could not be detected.

3.2.2 Particle size analysis

A Horiba particle size analyzer (CAPA7000) was used to measure the particle size distribution of powders. The Horiba works on the principle of light absorption to measure the equivalent spherical diameter of particles. The Horiba employs a centrifuge sedimentation technique which accelerates the experiment. Powders were dispersed in 90 vol% ethylene glycol with 0.2 g/l $Na_4P_2O_7$ and treated for 10 minutes in an ultrasonic bath. The viscosity of the solutions was 15.2 cP. Calcined powders were milled* before testing.

The particle size distribution can be expressed in terms of the D_{10}, D_{50}, and D_{90}. The D_{50} gives the diameter of the median particle size. The diameter at which 10% of the particles in the sample are smaller, is known as the D_{10}. The D_{90} is the particle size at which 90% of the particles in the sample are smaller.

3.2.3 Electron microscopy and energy dispersive spectroscopy

Scanning electron microscopy (SEM) (Cambridge S-100, S-250, S-360) was used to observe polished and etched microstructures and fracture surfaces. Transmission electron microscopy (TEM) (Phillips EM430 and CMK20) was necessary to examine grain

* Milling details are found in section 3.3.2.

boundaries. Elemental analysis was performed by energy dispersive spectroscopy (EDS) with a Tracor system.

Sintered samples were polished with 1000 μm grit SiC paper, 6 μm and 1 μm diamond paste, successively, so that a mirror finish was obtained. It was noted that polishing was fastest with isopropanol as the lubricant. Microstructures were observed after thermal etching of the grain boundaries. It was found that the temperature for effective thermal etching was 100 °C below the sintering temperature with a dwell time of 10 to 15 minutes.

Thin foils for TEM were prepared by grinding to ~30 μm thick and ion milling using a Gatan dual chamber ion mill (model 600) with an accelerating voltage of 5 kV and a combined gun current of 1 mA.

3.3 Powder Preparation and Characterization

In the following sections the raw materials and the reacted $Bi_4Ti_3O_{12}$ powders are characterized. In addition, the mixed oxide process to form $Bi_4Ti_3O_{12}$ from Bi_2O_3 and TiO_2 is described. Bismuth titanate phase formation is analyzed more critically in section 3.4.

3.3.1 Analysis of raw materials

The raw materials' characterization included an analysis of the particle sizes, particle morphologies, impurities, and phases of the Bi_2O_3 and TiO_2 powders.

Powders from two sources for TiO_2, and two sources for Bi_2O_3 were analyzed. The combinations of TiO_2 and Bi_2O_3 to form bismuth titanate ceramics are abbreviated as described in Table 3.1. The first letter designates the TiO_2 source and the second letter, the Bi_2O_3 source. For example **AC** BIT refers to $Bi_4Ti_3O_{12}$ formed from **A**lpha TiO_2 and **C**erac Bi_2O_3. Compositions corresponding to **AC**, **TC**, and **TF** bismuth titanate were prepared. This allows a comparison of material with the same Bi_2O_3 source but different TiO_2 (comparing AC and TC) and between the same TiO_2 but different Bi_2O_3 (TC and TF). A summary of the TiO_2 and Bi_2O_3 powder analysis is given in Table 3.2. The impurity analysis was performed by the companies from which they were obtained.

Table 3.1 Abbreviations for TiO_2-Bi_2O_3 combinations.

	Cerac[1] Bi_2O_3	Ferro[2] Bi_2O_3
Alfa[3] TiO_2	AC	---
Tioxide[4] TiO_2	TC	TF

Table 3.2 Analysis of TiO_2 and Bi_2O_3 starting powders.

	Alfa TiO_2	Tioxide TiO_2	Cerac Bi_2O_3	Ferro Bi_2O_3
type		HPT-3	B-1067	320-A
lot #		NP87/124	X13680	920585
SEM	equiaxed d~1-5 μm	2 μm agglomerate 0.3 μm particles	platelets typical ~4x 8x 20 μm some length ~200 μm	equiaxed d~1 μm
BET* **(m^2/g)**	--	4-6	--	1.2
D_{50} **D_{10}** **D_{90}**	4.5 μm 0.3 6.0	1.8 μm 1.0 2.5	--	1.1 μm 0.2 2.7
XRD	tetragonal rutile+anatase	tetragonal rutile	p-orthor§ bismite	p-orthor§ bismite
Purity (%)	99.8	99.95	99.9	99.9
Impurity (ppm)+	1000 Fe, 400 Ni 200 Si, 100 Mn 60 Cr, 60 Cu	200 Cl, 100 S 50 Sb, 50 Sn, 50 Si 20 Nb, 20 Na	100 Fe, 100 Ti 50 Ni	30 CaO

[1]Cerac, Inc Milwaukee, WI, USA lot # x13680
[2]Ferro Corp. Transalco Division, Penn Yan, NY, USA, 320-A lot #s 920585, 940190
[3]Alfa Products, Johnson Matthey GmbH, Karlsruhe, Germany
[4]Tioxide Specialties Ltd., Cleveland, UK. NP87/124
* from supplier: BET measures the specific surface area.[103]
§ pseudo-orthorhombic.
+ from supplier: listing only ≥ 20 ppm.

X-ray diffraction showed that Alpha TiO_2 contained two tetragonal phases, rutile and anatase*, while the Tioxide TiO_2 contained only anatase. The Bi_2O_3 from both sources was pseudo-orthorhombic.

The SEM micrographs of Tioxide TiO_2 and Cerac Bi_2O_3 starting powders are shown in Figure 3.1a and 3.1b. The other powders did not contain unusual morphologies and are described adequately in Table 3.2.

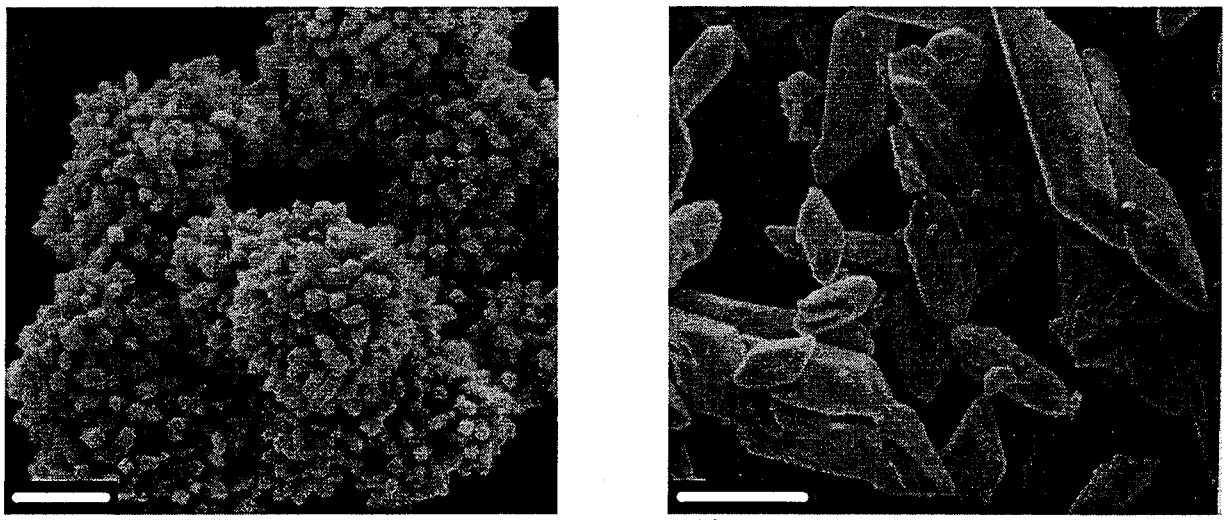

Figure 3.1 Scanning electron micrographs: a) Tioxide TiO_2 powder consists of agglomerates of small particles b) platelets of Cerac Bi_2O_3 powder.

The Tioxide TiO_2 powder (Figure 3.1a) showed ~2 μm agglomerates of small ~0.3 μm crystallites. The average particle size diameter was 2.0 μm by the Horiba measurement which indicates that the crystallites were bound together as hard agglomerates. Due to the morphology of the powder, Tioxide TiO_2 has a much higher specific surface area (4-6 m^2/g) than a powder containing 2.0 μm diameter spherical particles (~0.5 m^2/g).[103] The Alfa TiO_2

*Rutile is the low temperature phase of TiO_2 (<730°C) and anatase the high temperature form.

powder consisted of jagged particles, characteristic of ball milling, with an average particle diameter of ~4 μm.

The Cerac Bi_2O_3 (Figure 3.1b) was in the form of platelets which ranged from 2-10 μm in the smaller dimensions and in length from 20 μm to over 200 μm. The Ferro Bi_2O_3 contained a uniform fine powder with an average diameter of 1 μm.

In summary, four powders were analyzed, two of TiO_2 and two of Bi_2O_3. Differences in the purity, particle size, morphology, and phases were noted.

3.3.2. Process description

A mixed oxide method was used to prepare $Bi_4Ti_3O_{12}$ powder from Bi_2O_3 and TiO_2. The term "mixed oxide" refers to a high-temperature solid-state reaction between binary oxide powders (and carbonates) which are stable in air.[104] The mixed oxide route was chosen since it is a reproducible, inexpensive method and large batches* (> 10 g) are easily prepared. Other methods which have been utilized to prepare $Bi_4Ti_3O_{12}$ powders include sol-gel synthesis[83], molten salt[79] and co-precipitation.[80]

The processing route is described in the flow chart in Figure 3.2. Starting powders were dispersed in isopropanol in polyethylene jars and ball milled for 24 hours with cylindrical ZrO_2 media. A typical mill consisted of 50 g of powder, 150 ml isopropanol, and 150 g media in a 500 ml jar. The mills were less than one half full. After milling/mixing, the mixtures were stir dried in glass beakers at approximately 50 °C to increase the evaporation rate of the solvent.

Powders were calcined in a high density alumina crucible which was loosely covered with an alumina plate. A typical calcination schedule for undoped $Bi_4Ti_3O_{12}$ consisted of a ramp rate of 5 °C/min, a dwell for 1 hour at 600 °C, 5 °C/min to 800 °C for 4 hours and natural cooling of the furnace. The calcination schedule was developed to avoid liquid phases, promote reaction, and minimize particle coarsening. This subject is discussed in section 3.4. Calcined powders were milled in a similar manner to the mixing but with more ZrO_2 media

* Large batches are desired to decrease the weighing error as well as to have sufficient quantities of powder.

(~250 g) and less alcohol (125 ml), for better particle size (or agglomerate size) reduction. Powders were then dried and sieved through a 100 μm nylon sieve.

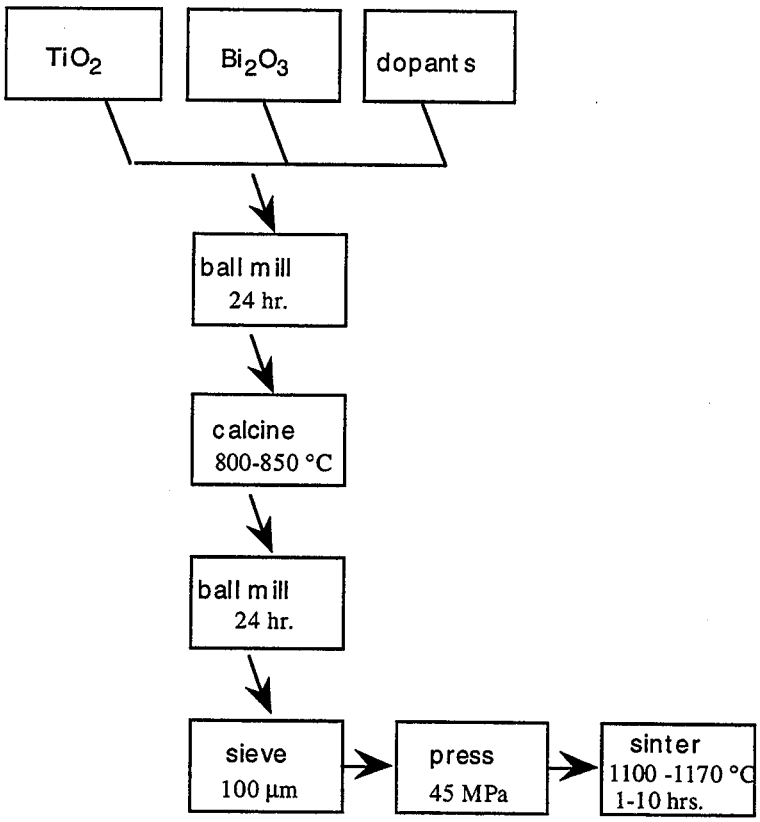

Figure 3.2 Processing flow chart for preparing bismuth titanate ceramics.

Samples were uniaxially pressed to 45 MPa in cylindrical stainless steel dies. The sample size before sintering was 10 mm in diameter and ~2 mm thick. Samples were placed on a platinum plate and covered with an alumina crucible for sintering. A typical sintering schedule for undoped bismuth titanate was a ramp rate of 5 °C/min to 1100 °C for one hour and natural cooling of the furnace. Higher sintering temperatures were required to densify bismuth titanate with dopants. For example, 0.2 at% Nb doped BIT was sintered at 1130 °C for one hour to achieve a density of 96% theoretical.

It was found that bismuth titanate, unlike lead containing compounds, was not prone to weight loss during calcination or sintering. This was supported by thermogravimetric analysis in which bismuth titanate was heated to 900 °C for 50 hours without measurable weight loss.

3.3.3 Dopant additions to bismuth titanate

Several acceptor dopants (Sr_{Bi}', Ca_{Bi}', Fe_{Ti}'), one donor ($Nb_{Ti}^{\bullet}$), and one isovalent ion (La_{Bi}), were chosen to study the effect of dopants on the microstructure and electrical properties of bismuth titanate.

Dopants were added in the first stage of the mixed oxide process. The dopant additions are described in Table 3.3.

Table 3.3 Type and quantity of dopant added to the mixed oxides to form doped bismuth titanate powder.

Formula	M (in formula)	x (in formula)	at. % (all atoms)	Dopant source
$Bi_{4-(x/3)}M_{x/2}Ti_3O_{12}$	Ca	0.02	0.05	$CaCO_3$[1]
	Ca	0.20	0.53	
$Bi_{4-(x/3)}M_{x/2}Ti_3O_{12}$	Sr	0.02	0.05	$SrCO_3$[2]
	Sr	0.20	0.53	
$Bi_{4-x}M_xTi_3O_{12}$	La	0.01	0.05	La_2O_3[3]
	La	0.10	0.53	
$Bi_4Ti_{3-(x/4)}M_{x/3}O_{12}$	Fe	0.02	0.08	Fe_2O_3[4]
	Fe	0.15	0.79	
$Bi_4Ti_{3-(x/4)}M_{x/5}O_{12}$	Nb	0.05	0.05	Nb_2O_5[5]
	Nb	0.20	0.21	
	Nb	0.50	0.53	
	Nb	0.70	0.74	
$Bi_4Ti_3O_{12}$ + 0.15 wt% MnO_2	Mn		0.15	MnO_2[6]

[1] Alfa Products, Johnson Matthey GmbH. Kalsruhe, Germany, 99.9% purity
[2] Alfa Products, 99.994% purity, # 46300801
[3] Alfa Products, 99.99% purity, # 76502802
[4] Cerac Inc., Milwaukee, WI, USA, 99.9% purity, # 3803
[5] Alfa Products, 99.95 % purity, # 31902004
[6] Alfa Products, 99.99% purity, #46301312

3.3.4 Bismuth titanate powder characterization

Calcined and milled bismuth titanate powders prepared from the different sources of TiO_2 and Bi_2O_3 are characterized in this section. The effect of doping with Nb on particle size is also discussed.

The reacted powders were observed by SEM prior to milling. The powders did not appear in the form of platelets.* Further characterization of the as-reacted powders was not attempted. It is assumed that the powder morphology and size distribution after milling has a more important impact on grain growth.

After milling, the particle size distribution and median particle diameter of the calcined powders was similar for the three compositions as shown in Table 3.4. All of the bismuth titanate particles, as observed by SEM, were isomorphic with somewhat jagged edges typical of milled powders.

Table 3.4 Particle size analysis of $Bi_4Ti_3O_{12}$ powders prepared from different sources of raw material.

	BIT D_{10} (μm)	BIT D_{50} (μm)	BIT D_{90} (μm)
AC BIT	0.6	1.7	4.7
TC BIT	0.8	2.0	3.2
TF BIT	0.6	2.4	4.3
TF BIT + 0.7 at% Nb	---	≈ 0.5 §	---

The average particle size (after milling) of bismuth titanate powder doped with Nb was ~0.5 μm (by SEM) which was significantly smaller than the undoped powder (D_{50} 2.4 μm). This suggests that 1) Nb prevents particle coarsening during calcination or 2) the

* BIT platelets can be prepared by the molten salt method.[78]
§ estimate from SEM.

calcined structures are more brittle and ball mill to a finer particle size. The particle size of the other doped powders was not examined.

3.4 Phase Formation

In the following sections, the reaction route to form $Bi_4Ti_3O_{12}$ from the mixed oxide method is discussed. A model is used to interpret the kinetics of $Bi_4Ti_3O_{12}$ formation. The effect of raw materials on the rate of phase formation agrees qualitatively with the kinetic model.

3.4.1 Reaction route

It is useful to develop a calcination schedule which avoids melting and allows a sufficiently rapid solid state reaction.[103] Phase diagrams provide information on the melting temperatures of the reactants, eutectic compositions, and intermediate phases which may occur during the reaction process. With the mixed oxide method, intermediate phases are often formed prior to the thermodynamically stable phase, due to the inhomogeneity which is inherent in powder mixtures.[103]

An early phase diagram of the Bi_2O_3-TiO_2 system[105] is given in Figure 3.3a. Additional phases $Bi_{12}TiO_{20}$[88], $Bi_2Ti_2O_7$[106], and $Bi_{20}TiO_{32}$[107] have since been identified. It can be seen in Figure 3.3a that Bi_2O_3 melts* at 840 °C[108] which must be avoided in the calcination profile.

A eutectic forms between Bi_2O_3 and $Bi_{12}TiO_{20}$ with a melting temperature of 795 °C as shown in Figure 3.3b. In order to determine if this eutectic composition is significant, a mixture of Bi_2O_3 and TiO_2 (to form stoichiometric $Bi_4Ti_3O_{12}$) was heated with a ramp of 5 °C/min to 800 °C. Melting occurred as evidenced by a glassy phase fused to the crucible. This indicates that Bi_2O_3 and $Bi_{12}TiO_{20}$ were both present at 795 °C which caused the "melt-down".

---

* A temperature of 860 °C is given in the CRC[60] for the melting point of Bi_2O_3.

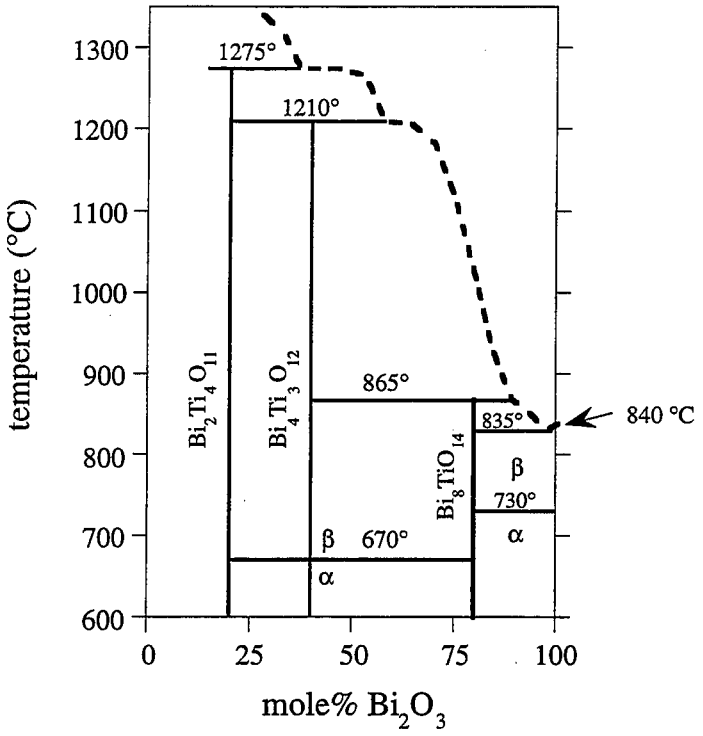

a) early phase diagram showing $Bi_4Ti_3O_{12}$.[105]

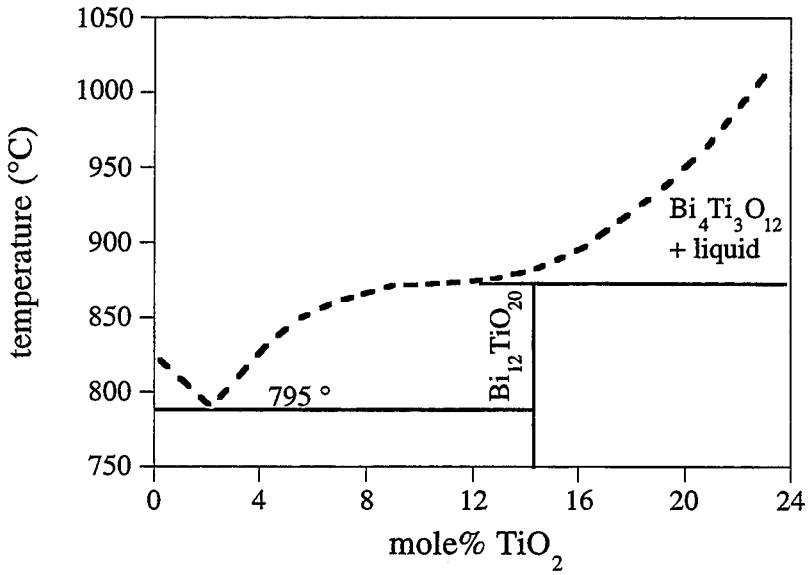

b) the 0-22 mole% TiO_2 range showing a eutectic between Bi_2O_3 and $Bi_{12}TiO_{20}$.[108]

Figure 3.3. Phase diagrams for TiO_2-Bi_2O_3.

Melting did not occur after heating to 600 °C for a dwell of one hour. The composition could then be heated to temperatures above the Bi_2O_3-$Bi_{12}TiO_{20}$ eutectic (790 °C) and above the melting point of Bi_2O_3 (840 °C) without the appearance of a glassy phase. This implies that Bi_2O_3 was not present as these temperatures were reached. This conclusion was supported with an analysis of the phases by XRD.

A portion of the XRD scan taken from powder calcined for one hour at 600 °C is given in Figure 3.4a. A similar scan is shown in Figure 3.4b of a powder calcined for one hour at 600 °C and heated to 800 °C (ramp rate 5 °C/min) for a one minute dwell. Bismuth oxide was not detected in either sample. All possible forms of Bi_2O_3 were considered in the analysis. In each sample, the $Bi_4Ti_3O_{12}$ phase and unreacted TiO_2 (rutile) were detected as well as the Bi rich phase $Bi_{12}TiO_{20}$. All of the peaks in the XRD traces from 2θ of 5° to 65° were accounted for by these three phases. There was no evidence of the Ti rich phases $Bi_2Ti_2O_7$ and $Bi_7Ti_4O_{11}$.

All of the peaks corresponding to 100% intensity for the identified phases occur in the region shown in Figure 3.4*. The 100 % intensity peaks are as follows: a) $Bi_4Ti_3O_{12}$ (171) reflection at 30.054° 2θ, b) TiO_2 (110) reflection at 27.446° 2θ, and c) $Bi_{12}TiO_{20}$ (310) reflection at 27.920° 2θ. It can be noted that there is an overlap of the major peaks (100% intensity) for TiO_2 and $Bi_{12}TiO_{20}$. The TiO_2 peak corresponding to the (101) reflection (50% intensity) at 2θ of 36.085° was also observed which supports the analysis.

* The full spectra were not shown because they contain more than 60 peaks which do not provide any added understanding of the system.

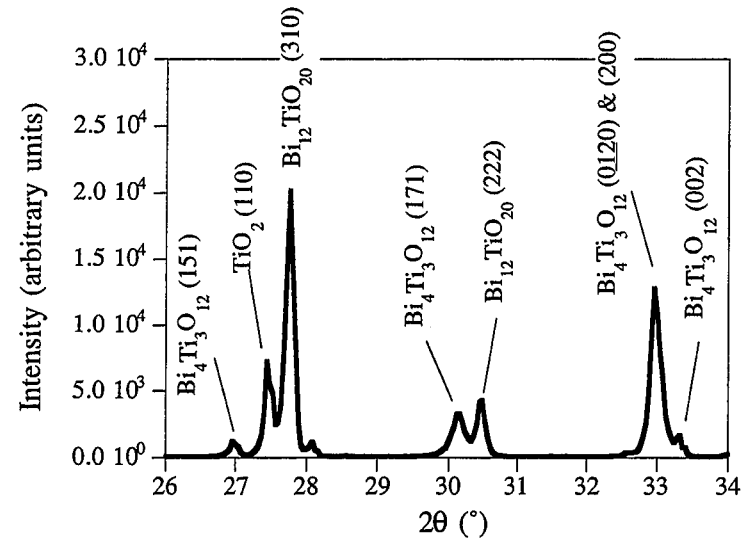

a)

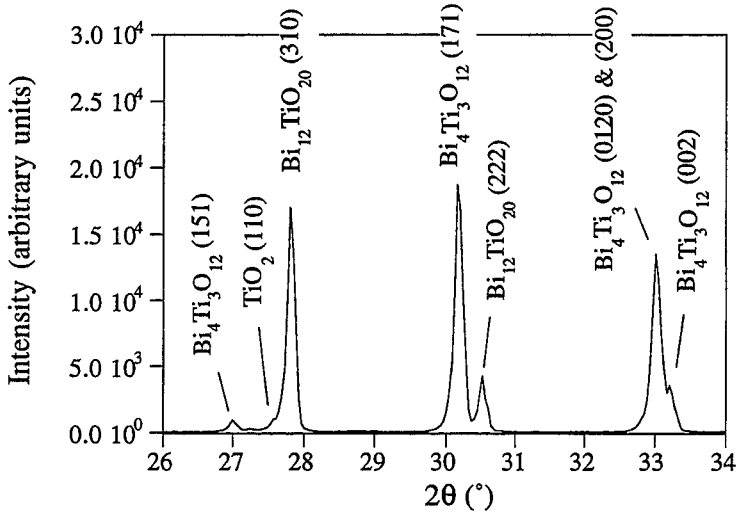

b)

Figure 3.4 Portion of the XRD traces showing phases in Bi_2O_3-TiO_2 mixture: a) calcined 1 hr 600 °C b) calcined 1 hr 600 °C and 1 min 800 °C.

Several points can be noted concerning the reaction of Bi_2O_3 with TiO_2. The initial reaction at 600 °C when Bi_2O_3 was still present may have involved direct formation of $Bi_4Ti_3O_{12}$ as in equation 3.1. and an indirect route through $Bi_{12}TiO_{20}$, as in equations 3.2 and 3.3. At the calcination temperature of 800 °C, the reaction must occur by the route

expressed in equation 3.3 since Bi_2O_3 was not present at the beginning of this calcination step. The reaction kinetics for the combination of $Bi_{12}TiO_{20}$ and TiO_2 at 800 °C is treated with a semi-quantitative analysis in section 3.4.2.

equation 3.1) **$2\,Bi_2O_3 + 3TiO_2 \text{---> } Bi_4Ti_3O_{12}$**

equation 3.2) **$6\,Bi_2O_3 + TiO_2 \text{---> } Bi_{12}TiO_{20}$**

equation 3.3) **$Bi_{12}TiO_{20} + 8\,TiO_2 \text{---> } 3\,Bi_4Ti_3O_{12}$**

Many references in the literature give calcination temperatures above the $Bi_{12}TiO_{20}$-Bi_2O_3 eutectic (790 °C) without mentioning a glassy phase formation (e.g.[8,15,85]). The ramp rate may have been slow enough to allow complete reaction of the Bi_2O_3 before reaching 790 °C. Another possibility is that a low temperature dwell was applied but not reported. It is likely that several researchers have observed the glassy phase due to the $Bi_{12}TiO_{20}$-Bi_2O_3 eutectic, but have not commented on the implications.

In summary, it was found that a mixture of Bi_2O_3 and TiO_2 to prepare $Bi_4Ti_3O_{12}$, melted at 800 °C, which is 40°C lower than the melting point for Bi_2O_3. An intermediate phase, $Bi_{12}TiO_{20}$, was formed which has a eutectic with Bi_2O_3 at 795 °C. The eutectic composition was avoided by applying a one hour dwell at 600 °C, after which the Bi_2O_3 was no longer present. The resulting phases included $Bi_{12}TiO_{20}$, $Bi_4Ti_3O_{12}$, and unreacted TiO_2. It was concluded that $Bi_4Ti_3O_{12}$ formed via a reaction route involving the intermediate phase, $Bi_{12}TiO_{20}$ and residual TiO_2. Bismuth titanate may have also formed directly from Bi_2O_3 and TiO_2, however, this could only have occurred while the Bi_2O_3 was still present, i.e. at < 600 °C. This reaction, if it occurs, would represent a minor contribution to the $Bi_4Ti_3O_{12}$ reaction product.

3.4.2 Reaction kinetics

In heterogeneous reactions, different kinetics are observed when the rate is controlled by the reaction or by transport (i.e. diffusion). The latter case is often responsible for the

kinetics of phase formation from mixed oxides.[97] A parabolic rate law[97] has been derived for the growth rate of the reaction layer thickness, **x**, as described by equation 3.4

equation 3.4 $$\mathbf{x = Kt^{\frac{1}{2}}}$$

where **t** is time, and **K** is a constant related to the diffusion of the rate limiting species.

Although, this law, in principle, also applies to reactions between powders when transport is limited by diffusion through a reaction layer, it is difficult to measure the reaction layer. One of the earliest treatments of this problem, by Jander[109], continues to be a useful approach. Jander related the volume fraction of the reaction product, α, to the radius of a spherical particle, **r**, which is reacting:

equation 3.5 $$(1-\sqrt[3]{1-\alpha})^2 = \left(\frac{K_x D}{r^2}\right)t$$

In equation 3.5, **t** is time, **D** is the diffusion coefficient of the slowest moving species and $\mathbf{K_x}$ is a constant determined by the geometry and the chemical-potential difference for the species diffusing across the reaction layer. A reaction rate constant equivalent to $\mathbf{K_xD/r^2}$ is characteristic of the reaction conditions. A constant molar volume and spherical particles are assumed, as well as a thin reaction layer.

An estimate of the volume percent of reacted $Bi_4Ti_3O_{12}$ calcined at 800 °C from 1 minute to 4 hours (with 1 hour dwell at 600 °C) was obtained from a ratio of the integrated 100% peak intensities. The intensities were not corrected for the differences in scattering or multiplicity factors.

The integrated peak intensity for $Bi_4Ti_3O_{12}$ was divided by the total from the three phases which were present: $Bi_4Ti_3O_{12}$, $Bi_{12}TiO_{20}$, and TiO_2. The integrated peak intensity for the $Bi_{12}TiO_{20}$ was taken to include the TiO_2 peak due to the overlap explained previously. Table 3.5 contains a list of the relevant integrated peak intensities and the approximation of the volume fraction of $Bi_4Ti_3O_{12}$.

Table 3.5 Integrated peak intensities used to calculate the approximate volume fraction of $Bi_4Ti_3O_{12}$.

time (min)	$Bi_4Ti_3O_{12}$(171)	$Bi_{12}TiO_{20}$(310) + TiO_2 (110)	total	$\approx \alpha$ vol fraction $Bi_4Ti_3O_{12}$
1	374.44	352.26	726.70	0.515
30	482.80	294.32	777.12	0.625
60	515.44	263.81	779.25	0.661
120	199.98	71.28	271.26	0.737
240	365.03	38.75	403.78	0.904

The results of applying Janders equation (equ. 3.5) to the approximate volume fraction, α (Table 3.5), is shown graphically in Figure 3.5. The reaction appears to follow the parabolic rate law for low volume fractions of $Bi_4Ti_3O_{12}$. The relationship did not hold for high volume fractions of $Bi_4Ti_3O_{12}$ (> 90 vol%), where the assumption of small reaction thickness was not valid. The reasonably good agreement with the parabolic rate law suggests that the rate limiting step for $Bi_4Ti_3O_{12}$ formation was diffusion of ions through the $Bi_4Ti_3O_{12}$ reaction layer.

According to the model, one of the species, Bi^{3+}, Ti^{4+}, or O^{2-} was responsible for limiting the rate of diffusion through the $Bi_4Ti_3O_{12}$ layer.* It is unlikely that O^{2-} is the rate limiting species since self diffusion coefficients for O^{2-} in various perovskites are much higher than the cation diffusion coefficients.[110-113] In addition, evidence is given in Chapters 4 and 5 which suggests that O^{2-} diffuses in $Bi_4Ti_3O_{12}$ at relatively low temperatures. It is reasonable to assume that Ti^{4+} or Bi^{3+} is the rate controlling species.

* This is a simplification of the problem which often involves ambipolar diffusion.

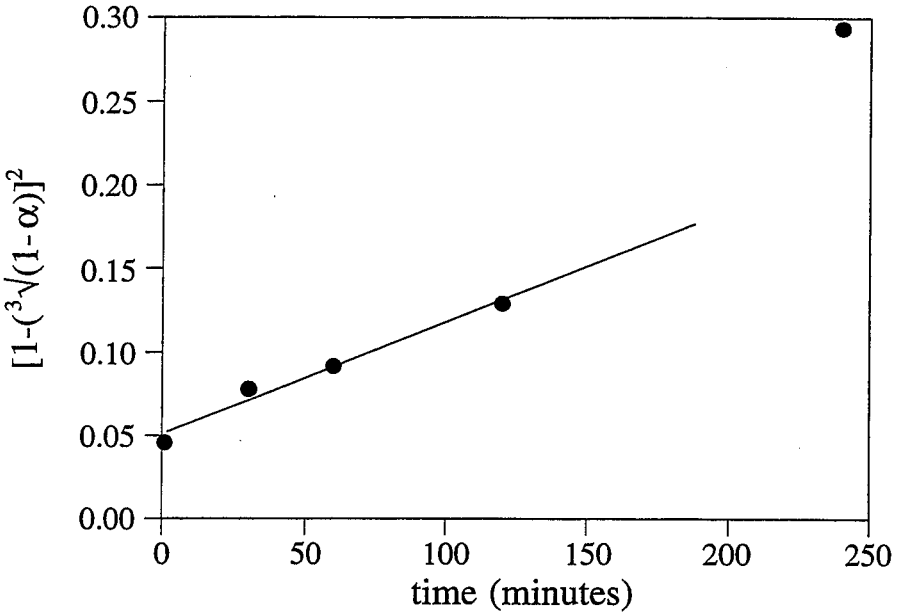

Figure 3.5 Dependence of approximate volume fraction (α) of $Bi_4Ti_3O_{12}$ on calcination time at 800 °C (after a one hour dwell at 600 °C). The model breaks down at high volume fractions of $Bi_4Ti_3O_{12}$, since the assumption of a thin reaction layer is no longer valid.

3.4.3 Raw materials and reaction rate

A number of variables can influence reaction rates including mean grain size, grain size distribution, specific surface area, impurities, and vapor pressure of the reactants.[103,114] Combinations of TiO_2 and Bi_2O_3 from different sources are expected to show different reaction rates. The starting materials and their impact on the calcination rate was investigated.

Sections of the XRD patterns for AC, TC, and TF BIT (calcined 1 hour 600 °C and 4 hours 800°C) can be compared in Figure 3.6. The 100% peak for $Bi_{12}TiO_{20}$ was observed in AC BIT (≈ 10 vol%), less strongly in TC BIT (≈ 3 vol%), and could not be detected in TF BIT.

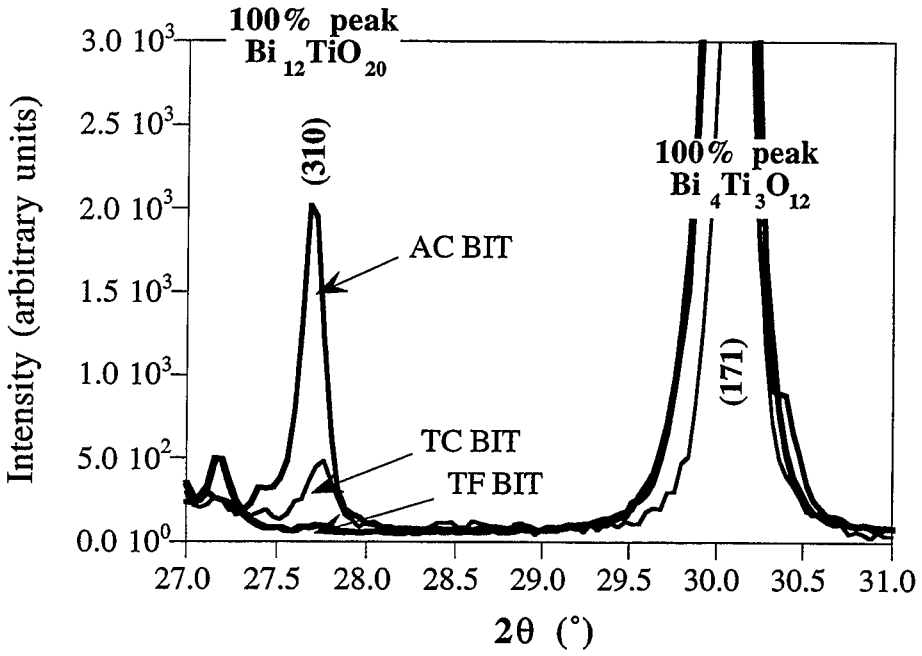

Figure 3.6 XRD trace comparing the $Bi_{12}TiO_{20}$ 100% peak for different combinations of Bi_2O_3 and TiO_2 powders (calcined 1 hour at 600 °C and 4 hours at 800 °C).

The disappearance of $Bi_{12}TiO_{20}$ follows a logical evolution when one considers the size of the starting powders. The rate of the reaction should be proportional to $\mathbf{1/r^2}$, from equation 3.5, i.e. smaller particles react faster. The Alpha TiO_2 and Cerac Bi_2O_3 mixture contained the largest particles and therefore required more time to react than the others. In the TC mixture, the TiO_2 was more reactive due to its small size and high surface area.[115] As a result the reaction rate increased. By combining the Tioxide TiO_2 with the fine Ferro Bi_2O_3 powder, the reaction was complete after calcining for 4 hours. This shows that as predicted by the parabolic rate theory, the particle sizes of the TiO_2 and Bi_2O_3 were significant in the reaction kinetics.

Other factors, such as the impurities and phase of the reactants, may also affect the reaction kinetics. Alfa TiO_2 contained more impurities, including Si, which would be

expected to increase the reactivity.[116] An additional factor is related to the phases of TiO_2 in the raw material. It was shown that Tioxide contained only anatase while Alfa contained a mixture of rutile and anatase. Studies on the early stages of sintering have shown that rutile is more reactive than anatase.[117] These considerations would lead to an increase in the reactivity of the AC mixture. Since $Bi_4Ti_3O_{12}$ formed more slowly in the AC composition, it can be concluded that the overwhelming influence was that of the particle sizes.

The AC and TC powders were re-calcined for 2 hours at 800 °C which eliminated the $Bi_{12}TiO_{20}$ phase. The powders were re-milled using the same process as described in section 3.3.2. The particle size distributions were not significantly changed from those reported in section 3.3.4, Table 3.4. Fully reacted $Bi_4Ti_3O_{12}$ powders were used in the following studies on densification and microstructural development.

It was found that when high levels of the Nb dopant ($\geq$ 0.5 at%) were added to fine grain Tioxide and Ferro starting materials, higher calcination temperatures were required to complete the reaction. The calcination schedule for these compositions was adjusted by increasing the second calcination temperature from 800 to 850 °C. These considerations suggest that Nb decreased the diffusivity of the rate limiting ion (Ti^{4+} or Bi^{3+}). It is possible that the diffusion of Ti^{4+} is suppressed since Nb substitutes for Ti in bismuth titanate. In perovskite titanates, it is generally accepted that Ti has a smaller diffusion coefficient than the B-site cations.[111,118]

In summary, given the same calcination procedure, the reaction between larger particle size raw materials was slower than for fine grain starting materials as evidenced by the residual $Bi_{12}TiO_{20}$ phase. These observations agree qualitatively with previous results which indicated that the reaction was controlled by diffusion through a reaction layer. It was found that Nb inhibited the reaction of the fine (TF) starting powders.

3.5 Densification and Microstructural Investigations

Microstructural features such as grain size, grain boundary phases, pores, inclusions, and fissures, can influence electrical properties of ceramics.[102] It is necessary to characterize the ceramic microstructure and include it, in some form, as part of the

experimental parameters for electrical measurements. In addition, a determination of the processing parameters which have the most significant effects on the microstructure is important for achieving the control and reproducibility desired in electroceramics.

Little is known about densification and grain growth in randomly oriented bismuth titanate. It is the goal here to classify the sintering behavior and characterize undoped and doped bismuth titanate ceramics. Grain growth in bismuth titanate, in relation to densification and the starting materials is explored. The effect of dopants on grain growth is discussed in general, and the effect of Nb doping is examined in more detail. General discussions on sintering, densification, and grain growth are found in many references.[17,97,119-122]

3.5.1 Densification and grain growth in bismuth titanate

In this section, the densification and grain growth in $Bi_4Ti_3O_{12}$ powders from different raw materials is explored. The density was determined either from the Archimedes method or from the weight and dimensions of the samples.

Figure 3.7 shows a graph of sample density as a function of sintering temperature for AC, TC, and TF $Bi_4Ti_3O_{12}$ compositions. The sintering time at each temperature was 12 minutes. The AC $Bi_4Ti_3O_{12}$ achieved 95.6% and 98.0% theoretical density at 1000 and 1050 °C, respectively. Representative microstructures of AC BIT from these sintering conditions are given in Figure 3.8. The higher purity TF and TC $Bi_4Ti_3O_{12}$ powders achieved much lower densities (~70% theoretical) after sintering at 1050 °C for 12 minutes.

The enhanced densification in AC $Bi_4Ti_3O_{12}$ can be explained by the presence of a liquid phase, which probably originates from the impurities in the Alfa TiO_2, such as Fe, Ni, Si and Mn (Table 3.2). Impurities produce a liquid phase by forming a eutectic composition with a melting temperature below that of the sintering temperature.[123] With a wetting liquid phase there is a rapid initial densification due to the capillary force exerted by the liquid on the particles.

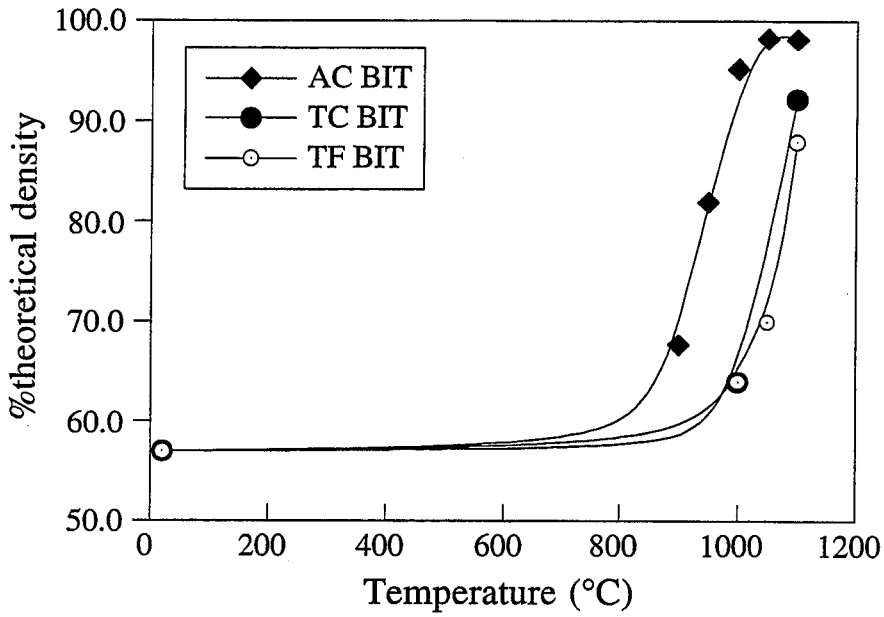

Figure 3.7 Densification of $Bi_4Ti_3O_{12}$ as a function of sintering temperature showing the effect of the raw materials. Sintering time was 12 minutes.

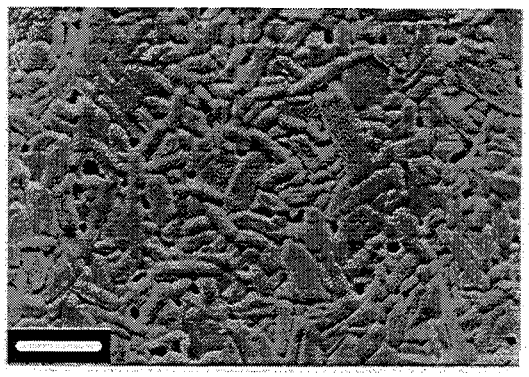

10 μm
a) sintered 1000 °C 12 min
(95.6% theoretical density)

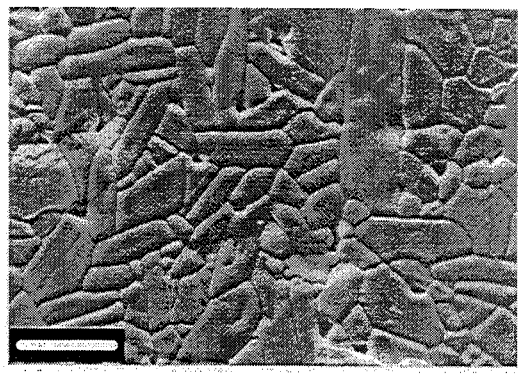

10 μm
b) sintered 1050 °C 12 min
(98.0% theoretical density)

Figure 3.8 Scanning electron micrographs of AC $Bi_4Ti_3O_{12}$ showing anisotropic grains and rounding at grain edges (ramp rate 5 °C/min).

Scanning electron micrographs of AC, TC, and TF $Bi_4Ti_3O_{12}$ sintered for one hour and 10 hours at 1100 °C can be compared in Figure 3.9. Some evidence of liquid phase assisted grain growth in AC $Bi_4Ti_3O_{12}$ can be observed in the microstructures in Figure 3.9 a and d. The rounded appearance of the grains, especially at the triple points, is a classic sign of liquid phase sintering.[123] In general, more angular junctions were observed in TC and TF $Bi_4Ti_3O_{12}$ (Figures 3.9 b and 3.9 c) than in AC BIT, however, some grain rounding was also evident. The accelerated densification and grain growth in AC BIT may be related to a greater degree of liquid phase. This is consistent with an example in the literature which shows that large grain bismuth titanate was obtained after sintering at 950 °C with an impurity related amorphous phase.[77]

Another observation from Figure 3.9 is that after 1 hour of sintering, the TC $Bi_4Ti_3O_{12}$ microstructure had the finest grains, AC the largest, and TF $Bi_4Ti_3O_{12}$ was in between the two. After sintering for 10 hours, large anisotropic grains were evident in all three compositions.

It is notable that the TC composition showed slower densification and smaller grains than TF $Bi_4Ti_3O_{12}$. The difference must originate in the Bi_2O_3 powder, since both compositions contain TiO_2 from the same source (Tioxide). The Cerac powder contains Fe (100 ppm) and Ti (100 ppm) impurities. These impurities added as oxides in higher concentrations, behave as grain growth inhibitors in $Bi_4Ti_3O_{12}$ (see section 3.5.2 for Fe doped BIT). It is likely that the differences observed are due to these impurities.

The characterization of microstructures with anisotropic grains has been discussed at length in the literature.[124-127] The problem is not trivial and requires adequate statistics. For the purposes of this study, it was sufficient to characterize the bismuth titanate ceramics with representative micrographs from Figures 3.8 and 3.9. This provides a qualitative description of the microstructures which can be referred to in the following chapters.

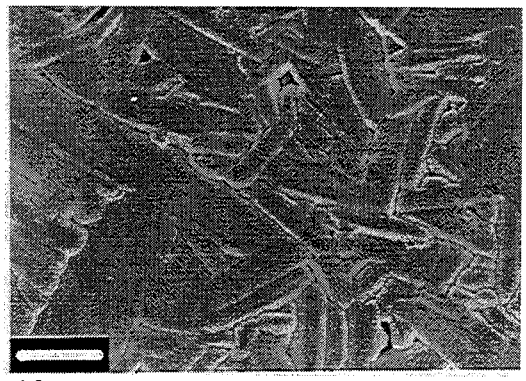

10 μm
a) AC BIT sintered 1100 °C 1 hour

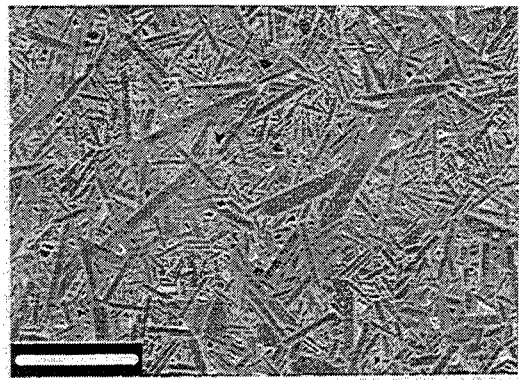

100 μm
d) AC BIT sintered 1100 °C 10 hours

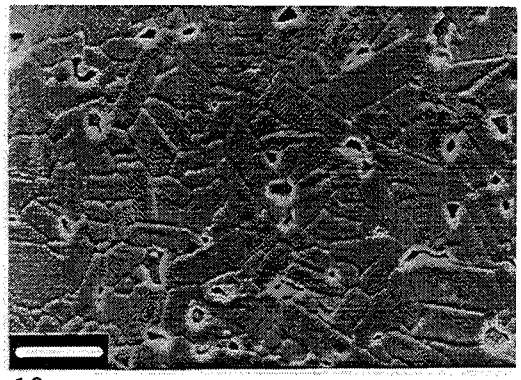

10 μm
b) TC BIT sintered 1100 °C 1 hour

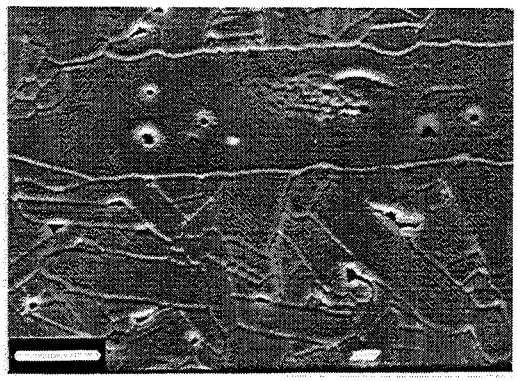

10 μm
e) TC BIT sintered 1100 °C 10 hours

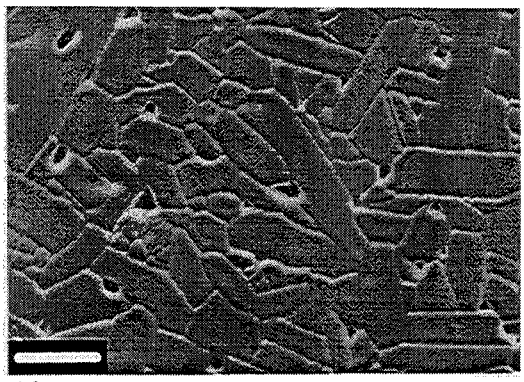

10 μm
c) TF BIT sintered 1100 °C 1 hour

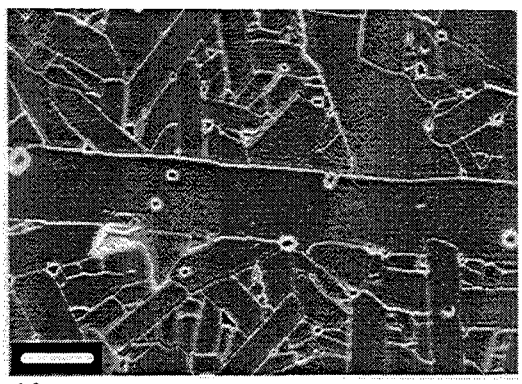

10 μm
f) TF BIT sintered 1100 °C 10 hours

Figure 3.9 Scanning electron micrographs showing microstructures of AC, TC, and TF $Bi_4Ti_3O_{12}$ sintered at 1100 °C for 1 hour and 10 hours (ramp rate 5 °C/min).

In summary, the raw materials had a significant impact on the densification and grain growth in $Bi_4Ti_3O_{12}$. It was proposed that one of the compositions, AC $Bi_4Ti_3O_{12}$, underwent liquid phase sintering due to impurities in the raw materials. A liquid phase may aid in densification, such that the sintering temperature was lowered by 75-100 °C compared to the higher purity bismuth titanate. The slow grain growth and densification of TC $Bi_4Ti_3O_{12}$ compared to TF $Bi_4Ti_3O_{12}$ was attributed to impurities in the Cerac Bi_2O_3. For long sintering times (10 hours at 1100 °C), large anisotropic grains were observed in all three compositions.

3.5.2 Densification and grain growth in doped bismuth titanate

Representative microstructures and densities of TF bismuth titanate (sintered 1100 °C 1 hr) with dopants are given in Figure 3.10. The 0.53 at% dopant level is shown for La, Sr, Ca, and Nb, and the 0.79 at% level for Fe. The undoped TF bismuth titanate microstructure is also shown for comparison.

The dopants can be separated into three categories: donors ($Nb_{Ti}^{\bullet} + e'$), acceptors ($Fe_{Ti}' + h^{\bullet}$, $Sr_{Bi}' + h^{\bullet}$ or $Ca_{Bi}' + h^{\bullet}$) and isovalent dopants (La_{Bi}). The acceptor dopants can be sub-divided into two types: those replacing Bi (Sr and Ca) and those replacing Ti (Fe). It can be seen that all of the dopants inhibited grain growth and densification, irrespective of their position in the lattice or of their ionic charge.

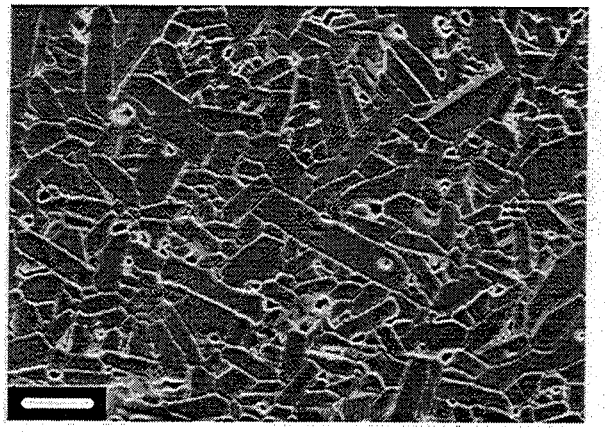

10 μm

a) undoped TF BIT (96.3% th. density)

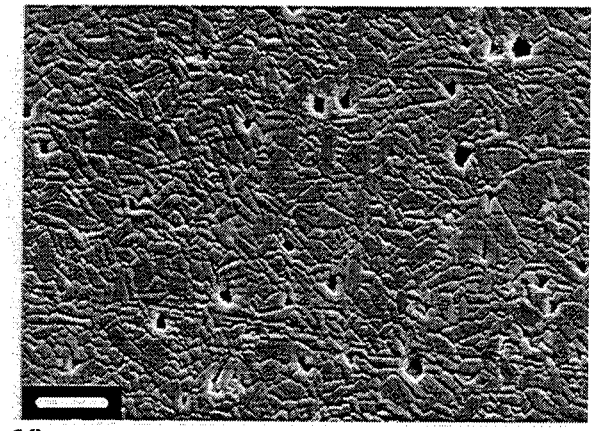

10 μm

d) TF BIT+ 0.53 at% Sr (83.4% th. density)

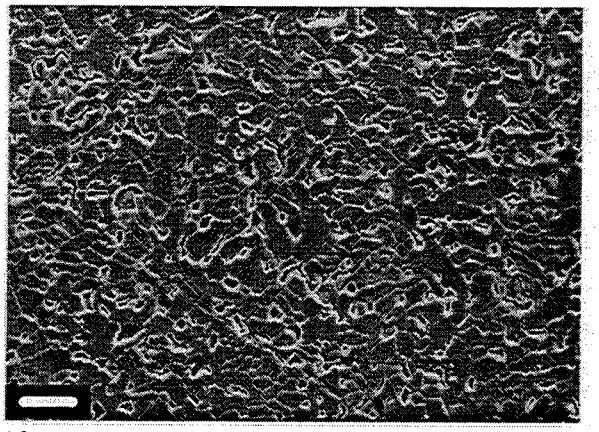

10 μm

b) TF BIT+ 0.53 at% La (94.1% th. density)

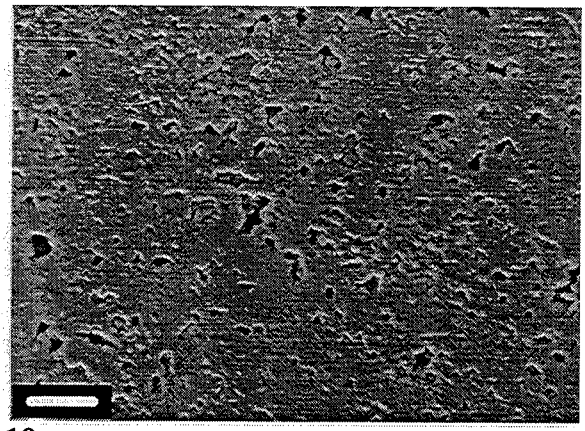

10 μm

e) TF BIT+ 0.53 at% Nb (93.4% th. density)

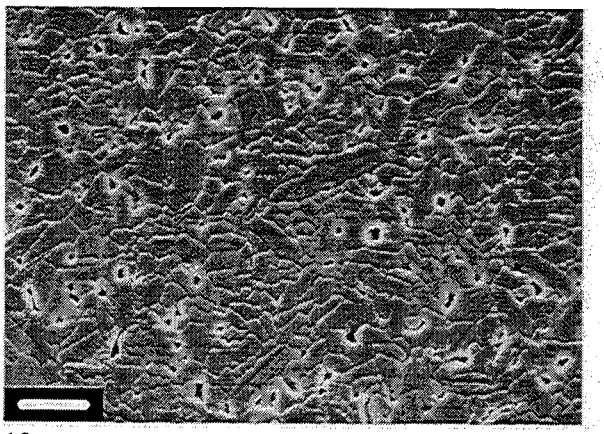

10 μm

c) TF BIT+ 0.53 at% Ca (94.9% th. density)

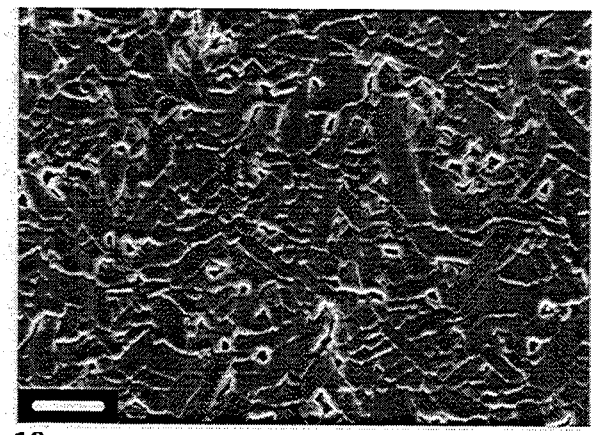

10 μm

f) TF BIT+ 0.79 at% Fe (94.8% th. density)

Figure 3.10 Scanning electron micrographs comparing the density and microstructure of bismuth titanate with various dopants after sintering at 1100 °C for 1 hour (ramp rate 5 °C/min).

3.5.3 Solubility limit of Nb in bismuth titanate

The solubility limit of Nb in bismuth titanate is of interest since Nb doping decreased the conductivity and improved the piezoelectric properties as discussed in the following chapters.

The grain boundaries and grain junctions in Nb doped bismuth titanate (0.05 at% and 0.74 at%) were analyzed by TEM. The sample with 0.05 at% Nb showed narrow grain boundaries. Nb was not detected by EDS in the grain boundaries or triple points. Although Nb was detected in the grains, the concentration was only slightly above the detection limit. Narrow grain boundaries (< 10 nm) were also observed in the 0.74 at% Nb doped sample as indicated in the micrograph in Figure 3.11. A Nb rich Ti deficient phase (with respect to the bismuth titanate grains) was detected in the triple point in this composition according to the EDS analysis, also shown in Figure 3.11. The standardless semi-quantitative elemental analysis which compares the grain and grain junction composition is given in Table 3.6. Oxygen was omitted from the analysis due to the low atomic number. A cation ratio of 4/3 for Bi/Ti or 1.33 Bi/Ti can be calculated from the formula for $Bi_4Ti_3O_{12}$. The measured ratio from the grain composition was 1.1 Bi/Ti which is in fairly good agreement with the calculated value. A ratio of 3.3 Bi/Ti was measured from the grain junction which reflects the Ti deficiency of this phase. The Nb peak accounts for 10 at% of the triple point composition (excluding oxygen) compared to < 2 at% for the grain.

Most triple points did not contain phases with notably different compositions than the grains. This suggests that the solubility limit of Nb in bismuth titanate is very close to, but slightly less than 0.74 at%. Lopatin, et al.[15] reported a change in the piezoelectric properties at 0.6 at% Nb dopant and concluded that the solubility limit of Nb in bismuth titanate was 0.6 at%. In Chapters 4 and 5, slight differences in the properties were observed between 0.53 and 0.74 at% Nb. This agrees with previously reported observations and supports the conclusion that the solubility limit of Nb in bismuth titanate is between 0.53 and 0.74 at%.

From the evidence given here, the solubility limit of Nb in bismuth titanate is slightly less than 0.74 at%.

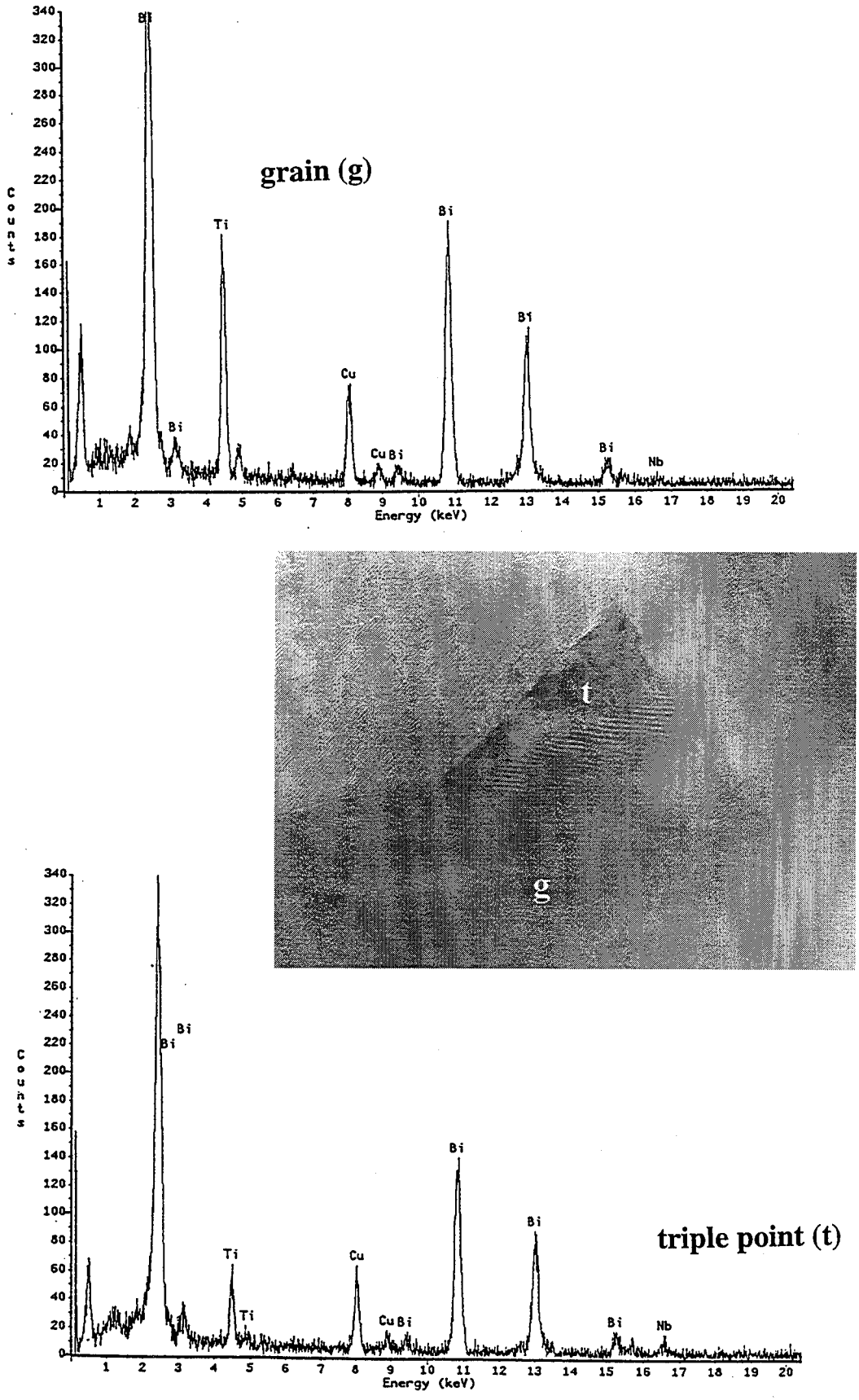

Figure 3.11 TEM showing grains and a triple point from the 0.74 at% Nb doped bismuth titanate. EDS analysis gave a different composition with a smaller Ti peak and higher Nb peak in the triple point than in the grain as indicated.

Table 3.6 Semi-quantitative (standardless) elemental analysis by EDS comparing the grain composition with a triple point, showing less Ti and more Nb in the triple point. Oxygen was not included in the analysis.

element	Ti	Bi	Nb
electronic shell	K	L	K
Grain composition (at%)	47	52	1.8
Triple point composition (at%)	21	69	10

3.5.4 Grain growth in Nb doped bismuth titanate

The effect of Nb doping on the microstructure (sintered 1100 °C, 1 hr) is demonstrated in the micrographs in Figure 3.12. Grain growth and densification were inhibited with the addition of ≥ 0.5 at% Nb. Bismuth titanate with 0.53 and 0.74 at% Nb showed fine grain microstructures with little evidence of anisotropy (Figure 3.12 d and e).

There are many mechanism by which dopants can inhibit grain growth. Since grain boundary migration requires mass transport, it follows that grain growth is suppressed when the rate controlling process for mass transport is adversely affected by a dopant. These processes can include surface or lattice diffusion, vapor transport, coalescence or solution of a second phase, diffusion through a continuous second phase, and impurity drag.[128]

A second phase was observed by TEM/EDS at some triple points in 0.74 at% Nb doped bismuth titanate, however, precipitates or a continuous second phase were not found at the grain boundaries. This excludes the mechanisms of particle drag and diffusion through a second phase. In addition, grain growth inhibition was observed for Nb doping below the solubility limit. This disagrees with grain growth controlled by coalescence of a second phase. Vapor transport is not usually critical in oxides and is unlikely to be related to grain growth in bismuth titanate.

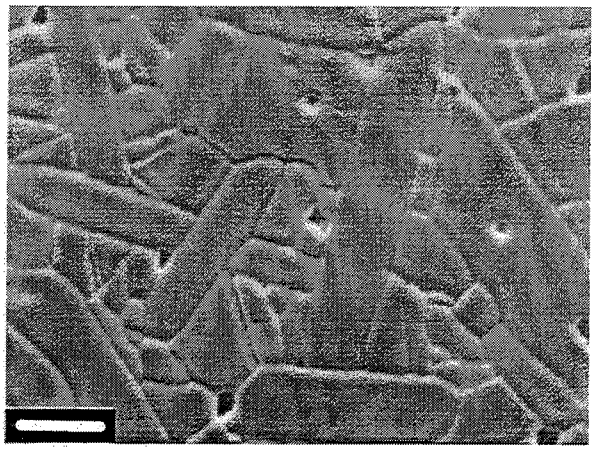

5 μm
a) undoped TF BIT (96.3 % th. density)

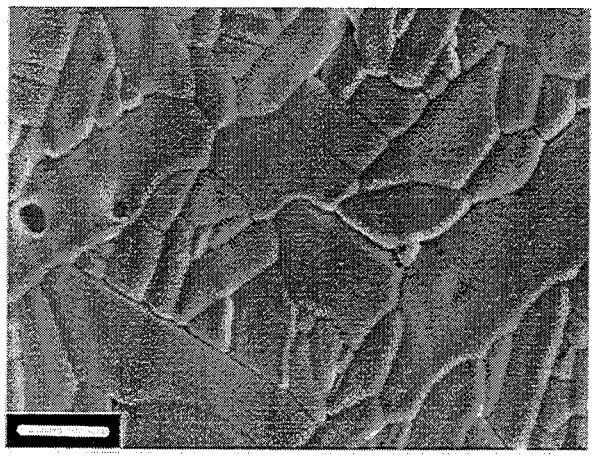

5 μm
b) TF BIT + 0.05 at% Nb (96.0% th. density)

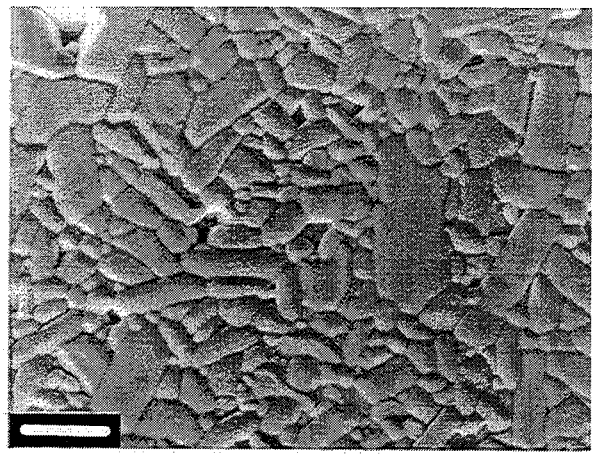

5 μm
c) TF BIT + 0.21 at% Nb (96.0% th. density)

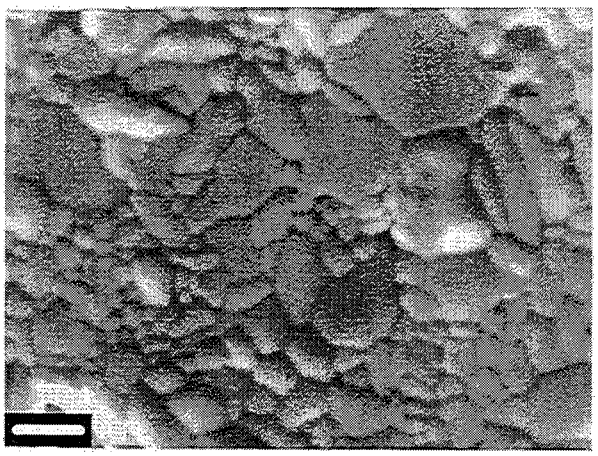

1 μm
d) TF BIT + 0.53 at% Nb (92.5% th. density)

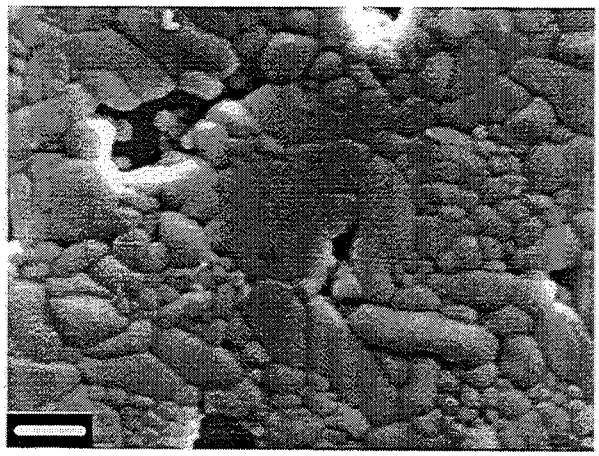

1 μm
e) TF BIT + 0.74 at% Nb (82.8% th. density)

Figure 3.12 Scanning electron micrographs of Nb doped bismuth titanate (sintered 1 hour, 1100 °C, ramp rate 5 °C/min).

A possible mechanism for grain growth inhibition is that lattice diffusion was suppressed by Nb. Several observations agree with a mechanism by which Nb slows diffusion in bismuth titanate. It was shown in section 3.4.3 that a higher calcination temperature was required to form bismuth titanate when doped with Nb. In addition, the particle size of the calcined powder was affected by Nb doping. Finer particles were obtained in 0.74 at% Nb doped than in undoped TF $Bi_4Ti_3O_{12}$ powder.

It is plausible that since Nb substitutes for Ti, the diffusion of Ti is inhibited. This would suggest that Ti^{4+} is the rate limiting ion for diffusion. In fact, diffusion in ionic solids is a complicated subject. The defect $Nb_{Ti}^{\bullet}$ may control the diffusion process in bismuth titanate in any number of ways. The most direct possibility is suggested above. Other mechanisms may include i) a decrease in the concentration of oxygen vacancies which can affect the diffusivity of the cations by limiting ambipolar diffusion, or ii) a decrease in the free hole population ($Nb_{Ti}^{\bullet} + e'$) may render hole migration rate limiting.[112] Determining the rate limiting specie for diffusion in undoped and Nb doped bismuth titanate is a subject of interest for future work.

To summarize the results of this section, Nb inhibits grain growth in bismuth titanate. For highly Nb doped compositions ($\geq$ 0.5 at%), anisotropic grain growth was suppressed.

3.5.5 Hot forged bismuth titanate

Grain oriented bismuth titanate was prepared by hot forging so that the conductivity could be compared with randomly oriented materials. The subject of hot forging and grain alignment has already been discussed at length in the literature (e.g. [8,19,92]).

Cylindrical powder compacts of TF bismuth titanate, 15 mm in diameter and 15 mm in length were uniaxially pressed and sintered at 1100 °C for 1 hour before hot forging. The density was approximately 95% theoretical. Hot forging was performed in an Instron press with an alumina chamber and SiC rams. The sample was placed between sapphire plates and forged at 1100 °C with a strain rate of approximately 10^{-4} sec^{-1}. The diameter after hot

forging was ~21 mm and the length was 7 mm. The **ab** plane is measured from the cut perpendicular to the hot forging direction. The cut parallel to the forging direction allows the properties to be measured in the **c**-direction.

Representative micrographs of hot forged samples from the directions parallel and perpendicular to the hot forging axis are shown in Figures 3.13 a and b, respectively. The degree of alignment was measured from the XRD traces using the Lotgering method.[101] The (00l) peaks from the cut parallel to the hot forging axis (**c**-direction) were compared to a non-oriented sample to calculate the Lotgering factor.

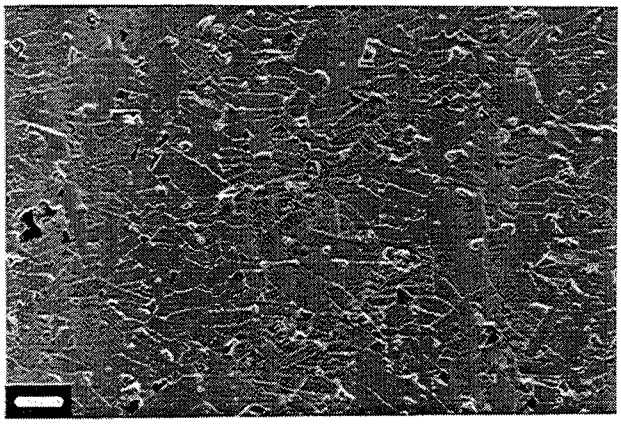

10 μm

a) view parallel to the hot forging axis (**ab** plane)

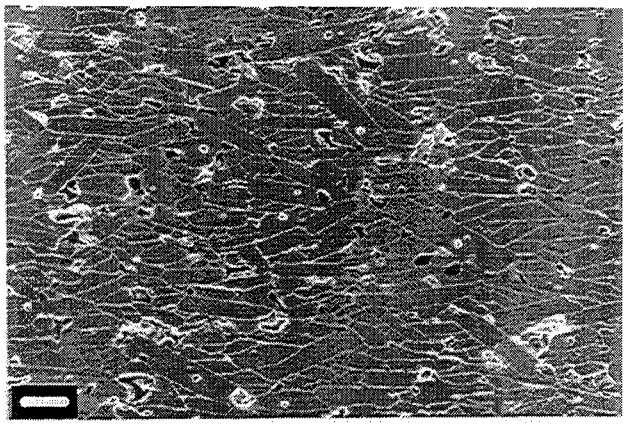

10 μm

b) view perpendicular to the hot forging axis (**c**-direction)

Figure 3.13 Scanning electron micrographs showing the microstructure of hot forged bismuth titanate parallel to and perpendicular to the hot forging axis.

The c-direction (Figure 3.13 b) showed an alignment of 70 (±1)%. Alignments as high as 95% have been reported in bismuth titanate by the hot forging method[8] and 100% by tape casting platy particles.[19] Higher strain rates during hot forging may give better orientation. The degree of orientation obtained here was sufficient to confirm the anisotropy of the conductivity in the following chapter.

3.6 Chapter Summary

Phase pure $Bi_4Ti_3O_{12}$ was prepared via the mixed oxide method using Bi_2O_3 and TiO_2 powders. A dwell at temperatures below 790 °C was necessary to avoid a eutectic melt. A calcination temperature of 800 °C was sufficient to form $Bi_4Ti_3O_{12}$ in less than 6 hours, however, a higher temperature was required when ≥ 0.5 at% Nb was added. This is one indication that Nb affects the diffusivity of the ionic species in bismuth titanate.

It was shown that the formation of $Bi_4Ti_3O_{12}$ from coarse powders > 1 μm involved a two step reaction; 1) the reaction of Bi_2O_3 with TiO_2 to form $Bi_{12}TiO_{20}$ occurred before or during a 1 hour dwell at 600 °C, and 2) $Bi_{12}TiO_{20}$ reacted with residual TiO_2 to form $Bi_4Ti_3O_{12}$. The second reaction followed a parabolic rate law indicating that the rate was limited by bulk diffusion through the product $Bi_4Ti_3O_{12}$ phase. The reaction rate increased by combining raw materials with finer particle sizes. It was demonstrated that if the direct reaction of Bi_2O_3 with TiO_2 (coarse powders) occurs, it represents a minor contribution to the formation of bismuth titanate.

The choice of raw materials affected the densification and grain growth in undoped bismuth titanate. The differences in sintering behavior were attributed to impurities in the raw materials. Niobium was effective as a grain growth inhibitor in $Bi_4Ti_3O_{12}$ for levels of dopant ≥ 0.5 at%. It was suggested that grain growth inhibition with Nb was related to a decrease in the diffusivity of the rate limiting specie. This conclusion agrees with the observed effects of Nb doping on the reaction kinetics and particle size in bismuth titanate.

Chapter 4. Electrical Conductivity in Bismuth Titanate

4.1 Introduction

The original premise in this work was that a deeper understanding and control of the conductivity in bismuth titanate would be essential for the application of this material as a high temperature piezoelectric ceramic. The approach taken in this chapter was to measure the electrical conductivity and observe trends due to the raw materials, atmosphere, quenching temperature, dopant type, and dopant level. It can be noted that the microstructures were matched* by adjusting the sintering conditions for the various compositions in sections 4.3-4.6. The difference in conductivity between fine and coarse grain materials was studied separately in section 4.7.

The important questions which must be addressed concerning the conduction mechanisms are as follows:

1. Is the conductivity controlled by the grains or grain boundaries in bismuth titanate ceramics? It is demonstrated in this chapter that the conductive path is through the grains.

2. Is the conductivity predominantly ionic or electronic? The literature suggests electronic conductivity.[91] Evidence for electronic rather than ionic conductivity is given for grain oriented and randomly oriented ceramics.

3. Is the conductivity p-type or n-type in bismuth titanate? Single crystal data suggests p-type conductivity, however, the crystal direction was not specified.[91] Annealing studies in reducing and oxidizing atmospheres agree that the conductivity is p-type for undoped bismuth titanate ceramics.

---

* In general, a slightly finer grain ceramic for the highly Nb doped compositions (d~1-2 μm) is compared to the undoped and lightly doped bismuth titanate (equivalent d~5 μm). It is shown in Chapter 5 that these differences did not affect the piezoelectric properties. Also, see discussion in section 4.7.

4. Since the conductivity is highest in the **a**-direction, does the perovskite or the bismuth oxide layer form a resistive layer? It is suggested that the conductivity is controlled by the perovskite layer, however, the conduction path may be related to the charge distribution in the crystal.

5. What impact do the raw materials and dopants have on the conductivity in bismuth titanate? A better understanding of the defect structure in bismuth titanate was achieved by analysis of these variables. Adding a sufficient concentration of a donor dopant, which depends on the purity of the raw materials, was essential for decreasing the conductivity in bismuth titanate ceramics.

6. How does the grain size of undoped and Nb doped bismuth titanate affect the conductivity? It is shown that an increase in grain size increases the p-type conductivity in undoped bismuth titanate. In contrast 0.05 at% Nb doped BIT changes from a p-type to an n-type conductor with increased sintering time. The possible mechanisms for this unusual behavior are discussed.

The relationships between Nb doping, conductivity, polarization, and the piezoelectric response are addressed in Chapter 5.

4.2 Experiment Procedures

4.2.1 Sample preparation for electrical measurements

Sintered and polished discs (~8 mm diameter, ~0.8 mm thick) were prepared for conductivity, dielectric, and piezoelectric measurements by sputtering on Au or Pt electrodes with a Balzers SCD 050 Sputter Coater. Platinum coated samples were annealed at 900°C for half an hour to improve mechanical and electrical properties of the electrodes. The resistance of the electrodes was less than 1.5 Ω on each faces and usually less than 1 Ω.

4.2.2 AC measurement method

Capacitance and loss were measured with a Hewlett Packard 4284A Precision LCR meter in the temperature range from 100 °C to 900 °C from 20 Hz to 1 MHz (1 V). The dielectric loss was measured at more than twenty frequencies in the range 20 Hz to 1 MHz. The data were recorded automatically by a program on a Hewlett Packard 4153C computer.

In the temperature range 300-900 °C, an AC method was used to calculate the "static" conductivity from the imaginary component of the dielectric permittivity (dielectric loss) ε", as a function of angular frequency , ω. The total measured ε" is given by equation 4.1[129]:

equation 4.1 $$\varepsilon''(\omega) = \frac{\sigma_{DC}}{\omega} + \frac{\omega\tau(\varepsilon_0 - \varepsilon_\infty)}{1+\omega^2\tau^2} + \textbf{higher order terms}$$

where σ_{DC} is the "static" or DC electrical conductivity. The other terms describe various relaxational contributions to the total measured dielectric loss. At low frequencies and high temperatures, the first term in equation 4.1 usually dominates resulting in a linear relationship between ε" and 1/ω. An example is shown in Figure 4.1 for undoped bismuth titanate at 250 and 300 °C.

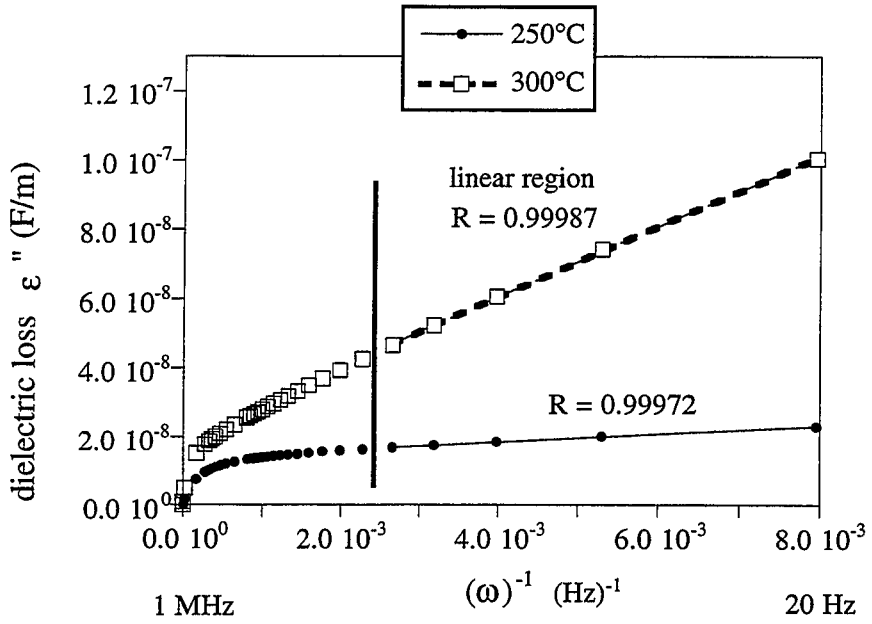

Figure 4.1 Dielectric loss as a function of reciprocal angular frequency. The criteria for accepting the slope as the "DC" conductivity was a correlation R > 0.9998 considering the five lowest frequencies.

The dielectric relaxation begins to have a significant impact on the loss at ~300 °C as evidenced by the curving towards lower loss at higher frequencies. The criterion for accepting a value of the DC or static conductivity, was that a correlation factor of the linear least square fit, R > 0.9998, could be obtained from $\varepsilon''(\omega)$ versus $1/\omega$ for at least the 5 lowest frequencies (20 to 60 Hz). In general, this was not achieved at temperatures below 300 °C. The conductivity was taken from the slope of the linear relationship, typically at temperature intervals of 50 °C.

4.2.3 Charge-discharge method

Electrical conductivity was measured using the 2-electrode charge-discharge method[130] in the temperature range of 50-225°C in a Delta 9023 furnace. A step voltage was applied with a Keithley 230 Programmable Voltage Source and the current was measured

with a Keithley 486 Picoammeter or a Keithley 617 Electrometer. The upper temperature was limited by the Delta chamber and the lower temperature was limited by the sensitivity of the picoammeter or electrometer. The data was collected automatically by a program on a Hewlett Packard 4153C computer.

The charging current and discharge currents contain a time dependent term equal in magnitude but opposite in sign. By adding the charge and discharge currents, the value remaining is due to the conductivity of the material.[97] The currents during charging and discharging were measured, each for 1 hour. This was sufficient to obtain a nearly constant current with time. An example of a typical charge-discharge measurement is shown in Figure 4.2.

It was demonstrated that the DC conductivity measurements must be carried out at fields less than or equal to 10 kV/m in order to remain in the Ohmic region. An example is given in Figure 4.3 for TF bismuth titanate measured at 200 °C.

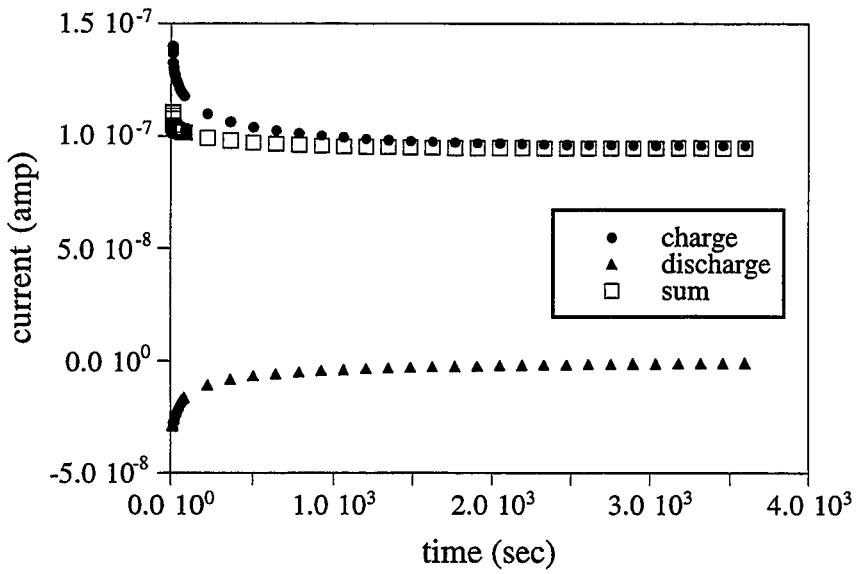

Figure 4.2 Example of charging and discharging currents as a function of time (TF bismuth titanate measured at 200 °C).

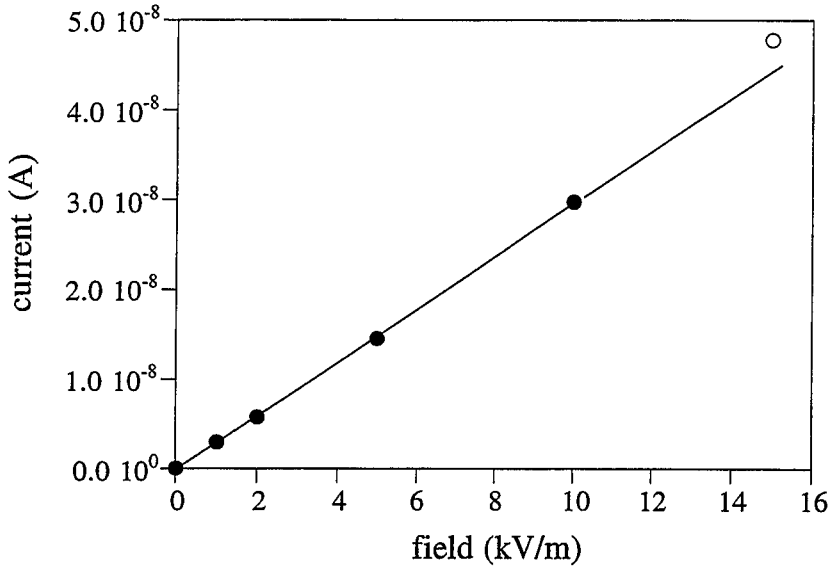

Figure 4.3 Example of Ohmic behavior for fields up to 10 kV/m
(TF bismuth titanate measured at 200 °C).

4.3 Discussion of Band Structure, Defects , and Conductivity

Basic knowledge of the defect chemistry of $Bi_4Ti_3O_{12}$ would be useful for understanding the conduction mechanisms, however, very little work has been published on this subject. The important features of the defect structure and band structure in perovskites are discussed in this section and some justification will be given for making a comparison with bismuth titanate.

The $Bi_4Ti_3O_{12}$ crystal structure has several features which are unique to the bismuth layer structure perovskites, for example overbonding of the O in the bismuth oxide layer.[65] On the other hand, the band gap in BIT*, 3.4 eV[25], is similar to that of the perovskites, such as $SrTiO_3$, $BaTiO_3$, $PbTiO_3$, and PZT which have band gaps in the range 3.1-3.4 eV.[131] All of these materials in an "undoped" state, show extrinsic conductivity due to impurities and non-stoichiometry which provide donor or acceptor levels within the band gap.[132]

Electronic conductivity and electronic band structures are closely linked to the stability of various oxidation states of the constituent atomic species. The band structure is

* Calculated from optical transmission spectra of single crystals along the c-axis.

derived from the electronic states of the ions, which retain their relative stabilities.[133] Valence bands can be viewed as the collective states from the uppermost filled electronic states of the ions, while conduction bands involve the lowest empty electronic states. Band structure is discussed in detail in many texts, for example[133-135]. Band theory is used here as a descriptive model for discussing defect chemistry.

The band gap in perovskites is similar to that in TiO_2 (3.1 eV) and is attributed to the TiO_6 bonding. Taking TiO_2 as an example, the oxygen atoms are strongly electronegative. Oxygen gains 2 electrons to fill the 2p orbital which results in the stable electron configuration of the rare gas neon. The 2p oxygen orbitals form a filled valence band. The conduction band can be viewed as the overlap of the Ti 3d shells. The alkaline earth cations such as Ba^{2+} and Sr^{2+} have empty orbitals considerably higher in energy than the transition metal d levels. They contribute very little to the electronic structure of the alkaline earth perovskites because of their closed-shell, inert gas structures. From this description, it follows that the value of the band gap is directly related to the coordination of Ti to the oxygens.[133,136] A schematic illustration of the band structure for pure stoichiometric TiO_2 or alkaline earth perovskite is given in Figure 4.4.

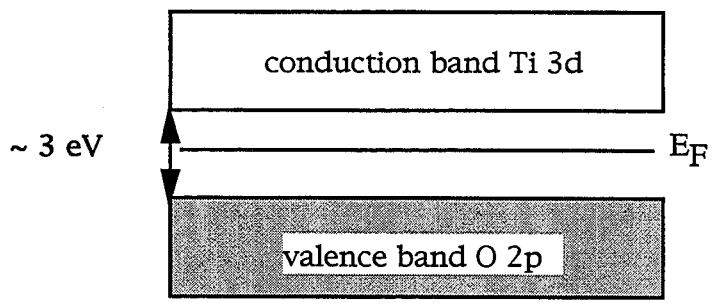

Figure 4.4 Schematic illustration of the band structure in alkaline earth perovskites and TiO_2.

In general, reducible cations are receptive to shallow electron traps and deep hole traps while the reverse is true for oxidizable cations. For example, Ti^{4+} can be reduced but not oxidized. Pure TiO_2 is n-type due to the shallow electron traps from oxygen vacancies, even with high pO_2 at high temperatures. Pure alkaline earth perovskites are also expected to be n-type, however, minor acceptor impurities almost always produce p-type conductivity.[132]

A difference in the band structure can be expected with perovskites containing Pb^{2+} or Bi^{3+} ions, which unlike the alkaline earths, have a "lone pair" of electrons in the 6s shell. The band structure of cubic $PbTiO_3$ has recently been calculated by Robertson, et al.[137] using a tight binding method. The upper valence band state has a 45% Pb 6s and 55% O 2p character.

A simplified model of the band structure[137] for PZT or $PbTiO_3$ is given in Figure 4.5. Vacancies of oxygen ($V_O^{\bullet\bullet}$ + 2e') provide shallow donor levels, 0.1 to 0.2 eV below the conduction band, as is the case in TiO_2 and other perovskites.[111,138] Deep hole traps exist approximately 0.7 eV above the conduction band and are related to cation vacancies (i.e. V_{Pb}'' + 2h$^\bullet$) or acceptor impurities, A' (i.e. Fe_{Ti}' + h$^\bullet$).[139] Lead vacancies are an important defect in PZT, since they contribute to the p-type conductivity.[38] It has recently been proposed that the trapping of an electron as Ti^{3+} in $PbTiO_3$ and PZT occurs at centers at least 1 eV below the conduction band, which is a deep electron trap, while Pb^{3+} centers* are believed to form shallow hole traps.[137,141] Donor dopants, D$^\bullet$, such as Nb^{5+} ($Nb_{Ti}^\bullet$ + e') form shallow donor levels which easily relinquish their electrons to the conduction band.[135,139]

It is often the case in layer structures, that the electronic levels are dominated by the overlap of atomic orbitals within a layer and that a good approximation can be obtained by ignoring the interaction between layers.[133] In bismuth titanate, it is postulated that the electronic structure is dominated by the perovskite rather than the Bi_2O_2 layer due to the chemical bonding between Ti and O which produces the characteristic band gap of 3.0-3.4 eV.

---

* According to the quantum mechanical definition of the band gap, electron traps such as Ti^{4+} and hole traps due to the Pb^{2+} ion are not appropriate terminology,[140] however, these terms are useful in describing the defect chemistry and are commonly combined with band structure representations.[139]

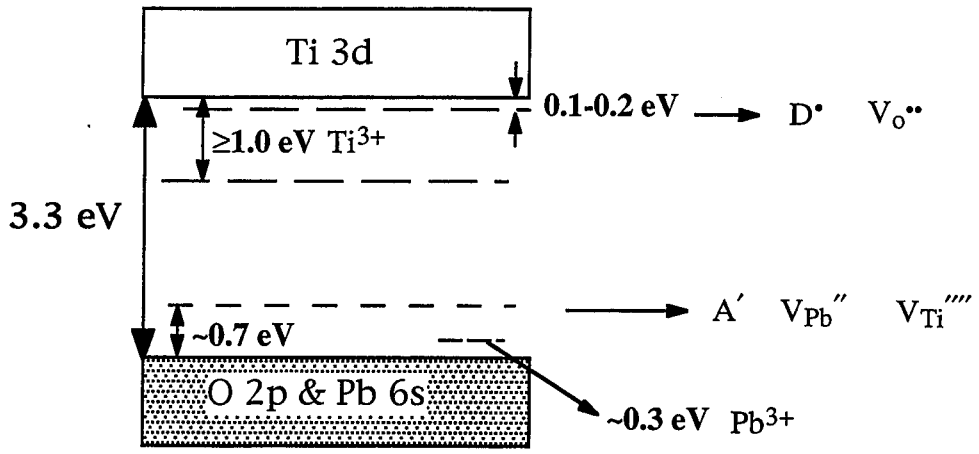

Figure 4.5 Schematic illustration of band structure in lead based perovskite titanate such as PZT.

Several possible features of the defect structure in bismuth titanate can be kept in mind. These include shallow donors from oxygen vacancies (responsible for n-type conductivity in TiO_2), acceptor impurities in the raw materials (promotes p-type conductivity in $BaTiO_3$), and A-site vacancies (contributes to p-type conductivity in PZT). One difference between bismuth titanate and the Pb perovskites, is that the Bi^{3+} ion can be both reduced (Bi^{2+}) and oxidized (Bi^{5+}), while Pb^{2+} can only be oxidized (Pb^{3+}), therefore, the possibility of electron traps as well as hole traps can be considered in bismuth titanate.

It is beyond the scope of this thesis to determine a band model for the defect structure in bismuth titanate. The focus here is to understand the relationship between the conductivity and several variables, including impurities, dopants, and microstructure. In order to achieve this goal, however, all interpretations of the conductivity data must be consistent with a proposed defect structure. It will be shown that the conductivity in bismuth titanate follows a trend which can be explained in terms of a defect chemistry which has similarities with that of the alkaline earth perovskites and the lead based perovskites.

In summary, a description of the band structure and defect structure of perovskites was given to develop a tentative model for bismuth titanate. It was proposed that the Bi_2O_2 layer has a minor impact on the electronic structure in BIT, however, extrinsic defects related to the Bi_2O_2 layer may add additional levels within the forbidden zone. The concept of hole

traps (Bi^{5+}), similar to those observed in PZT (Pb^{3+}) was introduced. It was also suggested that BIT may contain electron traps, due to the lower oxidation state of Bi^{2+}.

4.4 Conductivity in Undoped Bismuth Titanate

The electrical conductivity of undoped bismuth titanate was investigated with respect to the orientation, raw materials, and annealing atmosphere. In addition, a realistic representation of the "conductive layer" in bismuth titanate is formulated.

4.4.1 The conductive layer in bismuth titanate

In the previous discussions, it was suggested that the perovskite layer controls the conductivity in bismuth titanate. This implies that the bismuth oxide layer is more resistive than the perovskite layer. The plausibility of this model is discussed.

There are four possibilities which can be considered for the conductive path. These are as follows: 1) the bismuth oxide forms a resistive layer, 2) the perovskite is a resistive layer, 3) the resistivities are about the same, and 4) the conductive path depends on the conducting species.

The bismuth oxide layer $(Bi_2O_2)^{2+}$ must be compared to Bi_2O_3 with caution, since the relationship between the ions in each structure is very different. Bismuth oxide typically forms in the monoclinic structure of bismite (space group P21/c), however, oxygen deficient rhombohedral, tetragonal and cubic structures are also found. Oxygen deficient cubic Bi_2O_3 is a fast ion conductor at high temperatures.[142] At first glance, it is tempting to relate the high conductivity in the **a**-direction to this material, however, it is shown in the following sections that the conductivity is non-ionic.

The more common monoclinic form of Bi_2O_3 is a p-type conductor due to hole compensation of Bi vacancies[143] (e.g. $3[V_{Bi}'''] = [h^{\bullet}]$). The conductivity of monoclinic Bi_2O_3 is compared with $Bi_4Ti_3O_{12}$ and PZT in Figure 4.6. Bismuth titanate is actually more resistive than either the perovskite or the Bi_2O_3. It is interesting to note that the activation energy for conduction in bismuth titanate (1 eV) is similar to the activation energy in PZT.

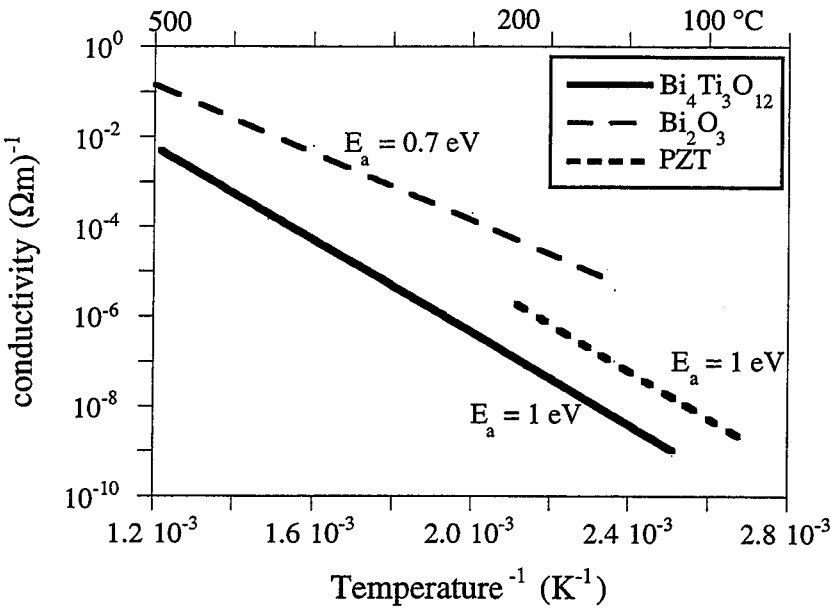

Figure 4.6 Comparison of conductivity in ceramics of undoped Bi_2O_3[143], $Bi_4Ti_3O_{12}$[144], and PZT.[145]

The question of a conductive layer was addressed by Huanosta, et al.[146] using an AC impedance method. They modeled the $Bi_4Ti_3O_{12}$ structure with an equivalent circuit to represent the separate resistances of the perovskite and bismuth oxide layers. Large single crystals were studied which cleaved along the bismuth oxide layers.* The results indicated a higher resistivity in the bismuth oxide layer or "plate boundary". An activation energy of 1.0 eV was obtained for the perovskite layer while a much higher activation energy of 1.7 eV was calculated for the bismuth oxide layer. An activation energy for conduction of 1.0 eV agrees with the results obtained for bismuth titanate in Figure 4.6. This analysis implies that the bismuth oxide forms a more resistive layer than the perovskite.

A more complex formulation of the "resistive layer" problem is shown in Figure 4.7. If one separates the perovskite and bismuth oxide layers on planes perpendicular to **c**, the resulting pieces each have a net charge. In this case the $Bi_4Ti_3O_{12}$ crystal consists of $(Bi_2O_2)^{2+}$ and $(Bi_2Ti_3O_{10})^{2-}$. Since the layers are not only held together by electrostatic

* The cleavage planes were called "boundaries" and the perovskite layers were called "crystalline plates".

forces, the charge density would not be expected to change abruptly from one layer to the next. The change in charge is shown schematically in Figure 4.7. From this representation, it can be seen that an electrical barrier is formed as either electrons or holes move in the **c**-direction. In contrast, the **a**- or **b**-directions show no such barrier.

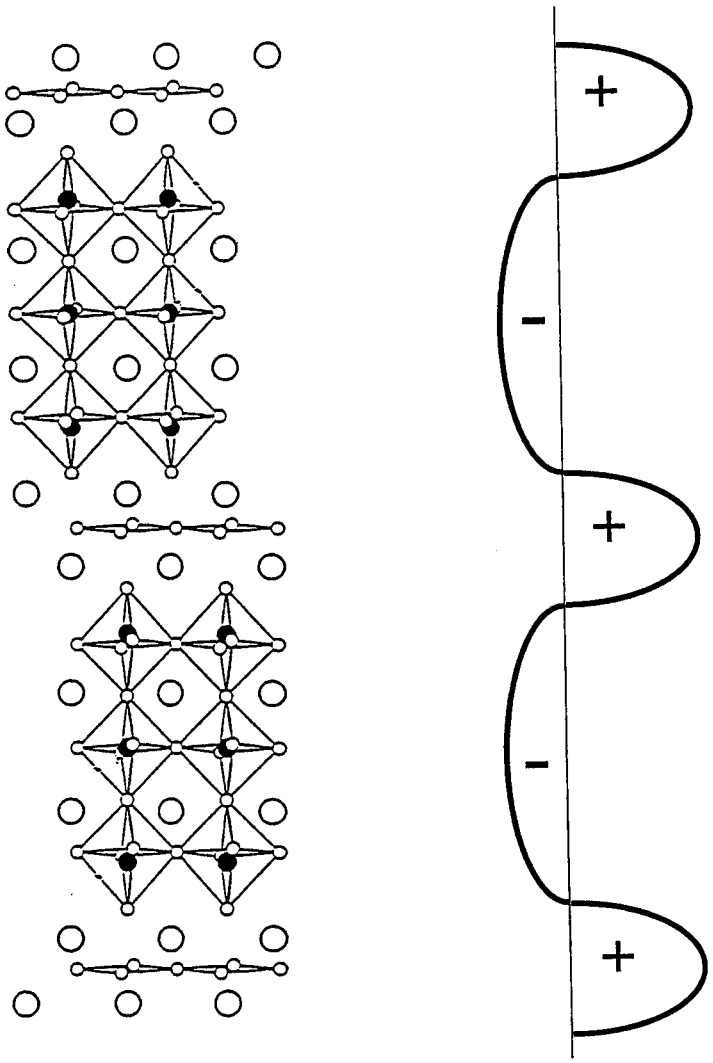

Figure 4.7 Schematic illustration of the change in electronic charge between the layers in the bismuth titanate unit cell.

This poses an interesting possibility whereby the resistivities of the $(Bi_2O_2)^{2+}$ and $(Bi_2Ti_3O_{10})^{2-}$ layers may be similar, with oppositely charged conducting species in each layer. This could potentially result in a large current in the **a**-direction which is blocked in the **c**-direction by the electrical barrier. It is difficult to envision for this model, a *decrease* in the conductivity with the addition of a donor dopant, as described in section 4.6.

To summarize, the true source of the higher conductivity in the **a**-direction appears to be more complicated than a conducting perovskite layer and an insulating bismuth oxide layer. The charge distribution may cause an electrical barrier for holes and electrons in the **c**-direction.

4.4.2 Comparison of single crystals and oriented ceramics

In this section, single crystals are compared to grain oriented ceramics. Conductivity data for hot forged samples described in Chapter 3 will be presented along with results from the literature.

Data from Fouskova and Cross[20] is reproduced in Figure 4.8 and shows that the conductivity in the **a**-direction is approximately 30 times higher than in the **c**-direction* in a single crystal of $Bi_4Ti_3O_{12}$. At temperatures below ~600 °C, the data was skewed towards high values of conductivity due to the measurement method§. The data from Gurevich[91] on single crystal BIT is also shown which was measured with a DC method and is therefore more reliable over the entire temperature range. The crystal direction was not stated in the reference, but is most likely to be the **c**-direction+, and agrees well with the data from Fouskova and Cross[20] for the **c**-direction when extrapolated to the same temperature range. The conductivity of a randomly oriented sample of TF bismuth titanate falls between the **a**- and **c**- single crystal directions.

---

* The **b**-direction is not included since it was very similar to the **a**-direction.

§ The AC method was used with frequencies greater than 5 kHz. At low temperatures (< 500 °C) there are significant contributions to the dielectric loss which are not related to the conductivity.

+ Crystals grow in platelets which are easier to measure in the **c**-direction. In addition, this data was collected before it was known that the **a**-direction is of interest due to the much greater polarization.

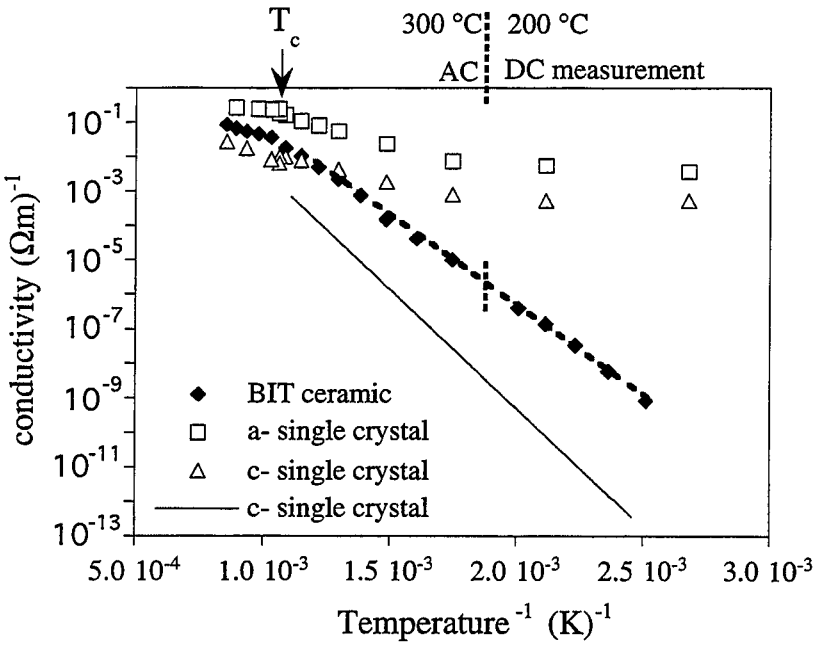

Figure 4.8 Comparison of single crystal conductivity[20,91] and randomly oriented $Bi_4Ti_3O_{12}$.

In Figure 4.8, it can be noted that if the conductivity (TF BIT) from the DC method is extrapolated to higher temperatures, an excellent agreement with the AC method is observed. This is evidence that the conduction mechanism is predominantly electronic. The total conductivity (σ_T) is comprised of the electronic (σ_e) and ionic (σ_i) contributions.

equation 4.2 $$\sigma_T = \sigma_e + \sigma_i$$

An ionic contribution would appear in the charging current and increase the level of conductivity by the DC measurement. With the AC method, the ionic species would not be expected to follow the field at higher frequencies,[130] and therefore the measured conductivity would be diminished. Since the measurement methods agree and give a single activation energy, the ionic contribution can be considered negligible. This is not to say that ionic species and other charged defects don't move in the electric field during the DC

measurement, only that their contribution to the total conductivity is much smaller than the electronic component[112] ($\sigma_e >> \sigma_i$ therefore $\sigma_T \approx \sigma_e$).*

The conductivity of the hot forged samples was measured perpendicular to and parallel to the axis of hot forging. The orientation is such that the measurement across the parallel cut is the direction of the conductive **ab** plane. A comparison of the conductivity between a randomly oriented sample, the hot forged **ab**-direction, and hot forged **c**-direction is shown in Figure 4.9. The conductivity was higher in the **ab** plane than in the **c**-direction for the entire temperature range. The conductivity of the randomly oriented bismuth titanate falls roughly in between. This agrees with the trend shown in single crystals in Figure 4.6.

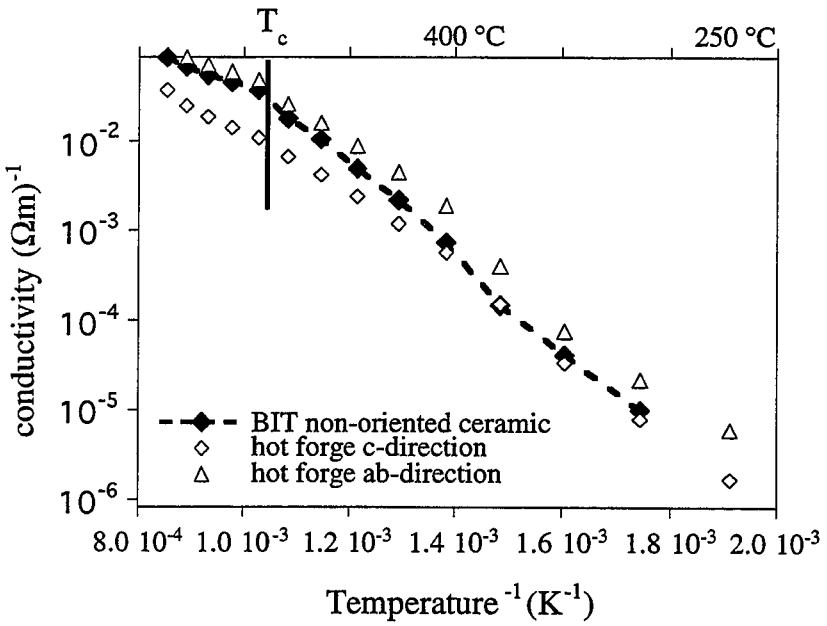

Figure 4.9 Comparison of the conductivity in randomly oriented and hot forged bismuth titanate ceramics.

The results in Figures 4.8 and 4.9 indicate that the conduction path in the ceramic is through the grains rather than the grain boundaries. If this were not the case one would expect a higher conductivity in the ceramic than in the **a**-direction in single crystal bismuth titanate.

* Further evidence for this conclusion is given in the following sections.

Instead, an averaging affect of the conductivity in the different crystal directions was indicated.* This assessment agrees with other workers, who have treated the grain boundaries as insulating compared to the bismuth titanate grains (e.g.[8,19,146]). Insulating grain boundaries are also typical of perovskite ceramics.[113]

Swartz, et al.[92] prepared grain oriented samples by tape casting bismuth titanate platelets. They obtained a difference of approximately 10 times between the **c**-direction and **ab**-directions in well oriented (98%) samples. The hot forged ceramics prepared here, were less well oriented (70%) and showed a difference of approximately 4 times between the two directions. A decrease in the anisotropy can be expected due to the imperfect alignment, however, the trend is clearly that of higher conductivity in the **ab** plane.

In summary, evidence was presented that the conductive path in bismuth titanate ceramics is through the grains rather than the grain boundaries. The agreement between AC and DC measurements indicates that the ionic contribution to the conductivity is negligible. The trend of higher conductivity in the **a**- or **b**-directions than the **c**-direction was similar for grain oriented ceramics and single crystals.

4.4.3 Reducing and oxidizing atmosphere

In this section a study of the effect of annealing in oxidizing and reducing atmospheres reveals the type of charge carrier.

Samples were annealed in flowing argon (pO_2 nominally 10^{-5} atm)§, the conductivities measured, annealed in flowing oxygen (pO_2 nominally 1 atm) and measured again. Gold electrodes were applied before the measurements and removed before the thermal treatments. The experiments were reproduced using Pt electrodes which were annealed at 900 °C in the same atmosphere as the treatments. The results were not affected by the different electrodes. It is assumed that the defect structure is due to the annealing temperature rather than the measurement temperature.

---

* An attempt was made to further substantiate this argument by comparing grain oriented and single crystal data. Unfortunately, the single crystal data varies considerably so that conclusive evidence was not obtained.

§ This pO_2 was estimated from the known concentration of oxygen (~10 ppm) in the argon.

Figure 4.10 shows that the conductivity of AC bismuth titanate decreased after the treatment in argon and increased due to the treatment in oxygen.* In order to observe the trend more clearly, the conductivity measured at 175 and 200 °C is graphed versus the log of the approximate partial pressure of oxygen (from the annealing treatment) in Figure 4.11. The conductivity increased with increasing pO_2 which is indicative of p-type behavior. The annealing treatments were also applied to the higher purity TF bismuth titanate. A similar trend of increasing conductivity with increasing pO_2 was observed as shown in Figure 4.12.

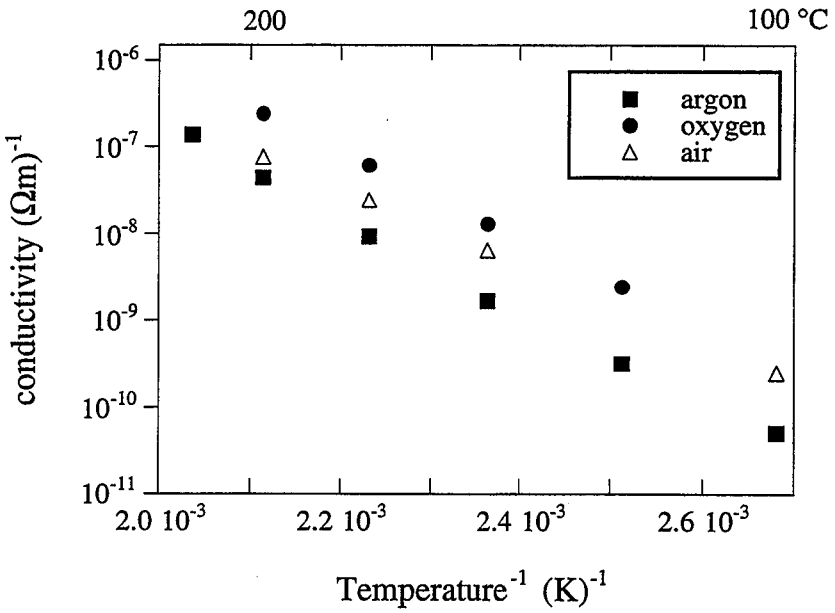

Figure 4.10 The effect of oxidizing and reducing treatments on the conductivity in AC bismuth titanate (sintered 1100 °C 10 hours).

* A difference in slope can be noted in the curves in Fig. 4.10 which results in slightly different activation energies: 1.0 eV compared to 1.1 eV. It is possible that the sample in air was reducing during the measurement, however, one would also expect the oxidized sample to reduce and have a lower slope. One factor which is not well explored in perovskite ceramics is the effect of moisture on the conductivity. Oxygen vacancies may allow the formation of mobile OH^- species (effective +1 charge) which are extracted as temperature increases.[147] This can explain a slight decrease in the slope as additional electrons become available to compensate holes.

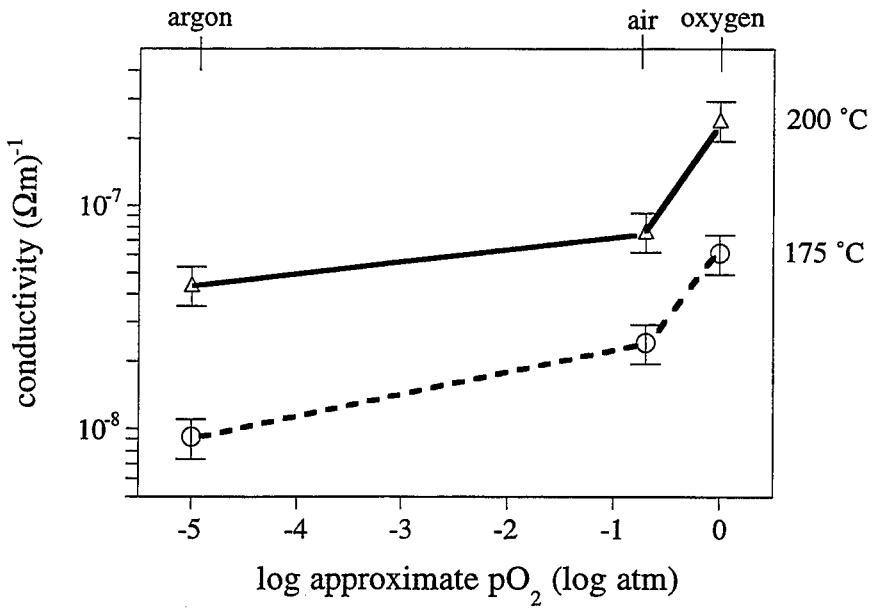

Figure 4.11 Conductivity as a function of approximate annealing atmosphere in AC bismuth titanate showing p-type trend.

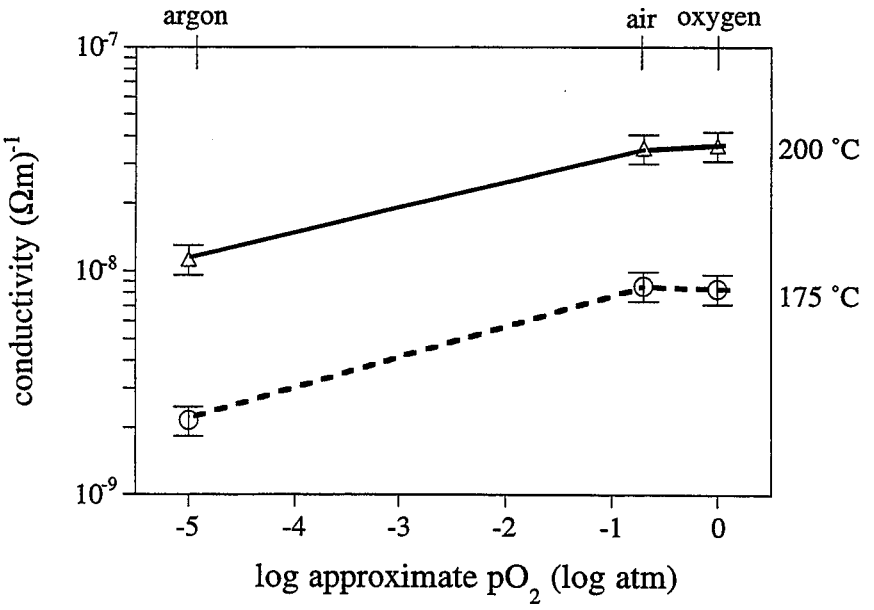

Figure 4.12 Conductivity as a function of approximate annealing atmosphere in TF bismuth titanate showing p-type trend.

For an ionic oxygen conductor* an increase in the vacant oxygen sites (i.e. oxygen vacancies formed in a reducing atmosphere) should increase the conductivity, the reverse of what was observed. The mechanism of polaronic hopping through Ti ions (Ti^{4+} --> Ti^{3+} --> Ti^{4+}) or Bi ions (Bi^{3+} --> Bi^{2+} --> Bi^{3+}) is n-type. i.e. the *reduction* of Ti or Bi would *increase* the conductivity.

The possibility of cation migration should be considered since this can also produce an increase in conductivity with increasing pO_2. It was reasoned that the conductivity in bismuth titanate was not ionic due to the agreement between the AC and DC measurements. This analysis agrees with data from Gurevich[91] which showed that the conductivity in bismuth titanate single crystals§ (700 °C) was p-type (measured by the Seebeck effect) and electronic (non-ionic) in the temperature range 300-500 °C (by verification of Faraday's law).

The origins of the holes responsible for the p-type conductivity can be explored by a comparison with perovskites which display p-type conductivity in "undoped" materials. In alkaline earth perovskites such as $BaTiO_3$, p-type conductivity is attributed to hole compensation of acceptor impurities[132,139] (i.e. Fe_{Ti}' + $h^{\bullet}$). In the case of Pb based perovskites, lead vacancies (V_{Pb}'' + $2h^{\bullet}$) become an important contributor of holes.[38] Identifying the controlling defects requires a precise analysis of the equilibrium conductivity with varying partial pressure of oxygen which was beyond the scope of this thesis, however, the possibilities can be analyzed for the most probable defect structure.

There are three sources of holes which can be considered. These include intrinsic electronic disorder, Schottky defects, and ionized acceptor impurities. The first of these possibilities can be excluded since the activation energy in undoped bismuth titanate is approximately 1 eV which is much less than the half the band gap of 3.3 eV. It can be seen that a measured activation energy equal to half the band gap ($\mathbf{E_a=E_g/2}$) indicates intrinsic conduction from the following equation[97] for intrinsic conductivity (σ_i):

---

* Assuming the ions migrate through lattice sites and not intersticially.

§ Crystal direction not given, probably **c**-direction.

equation 4.3 $$\sigma_i = \left[2|e| \left(\frac{2\pi kT}{h^2} \right)^{\frac{3}{2}} \left(m_e^* m_h^* \right)^{\frac{3}{4}} \exp\left(-\frac{E_g}{2kT} \right) \right] (\mu_e + \mu_h)$$

In equation 4.3, **h** is Planck's constant, **k** is Boltzmann's constant, **T** is temperature, $\mathbf{m}^*$ is effective mass, μ is the mobility, and **e** and **h** refer to electrons and holes, respectively.

It was shown in Chapter 3 (Table 3.2) that AC bismuth titanate contains a substantial amount of acceptor type impurities in the Alfa TiO_2 raw material. The incorporation of acceptor impurities in $Bi_4Ti_3O_{12}$ can be written as follows, taking Fe ($Fe_{Ti}'+h^\bullet$) as an example:

equation 4.4 acceptor doped reaction

$$2Bi_2O_3 + (3-x)TiO_2 + \tfrac{x}{2}Fe_2O_3 \Rightarrow 4Bi_{Bi} + (3-x)Ti_{Ti} + \left(12 - \tfrac{x}{2}\right)O_o + \tfrac{x}{2}V_o^{\bullet\bullet} + xFe_{Ti}'$$

Equation 4.4 is not an equilibrium reaction since the impurity is incorporated during the preparation, rather than by equilibration with an external source of fixed activity. The resulting composition, $Bi_4Ti_{3-x}Fe_xO_{12-(x/2)}$ is chemically stoichiometric with respect to the starting oxides, but oxygen deficient relative to the ideal $Bi_4Ti_3O_{12}$ reference structure.*

The reaction which occurs in an oxidizing atmosphere can be written as:

equation 4.5 $$\tfrac{x}{4}O_2 + \tfrac{x}{2}V_o^{\bullet\bullet} + xFe_{Ti}' \Leftrightarrow \tfrac{x}{2}O_o + xFe_{Ti}$$

P-type conduction occurs by ionization of the trapped holes[136]:

equation 4.6 $$xFe_{Ti} \Leftrightarrow xFe_{Ti}' + xh^\bullet$$

The neutrality equation which considers ionized Fe_{Ti}' defects is as follows:

equation 4.7 $$[Fe_{Ti}'] = 2[V_o^{\bullet\bullet}] + [h^\bullet]$$

---

* This type of a defective structure is considered to be stoichiometric by Smyth.[136]

The p-type conductivity may be the result of partial or complete compensation of acceptors by holes. (equation 4.7 becomes $[Fe_{Ti}']=[h^{\bullet}]$) Holes are typically more mobile than point defects. Alternatively, the acceptors may be compensated by oxygen vacancies. For complete compensation (equation 4.7 becomes $[Fe_{Ti}']=2[V_o^{\bullet\bullet}]$), the observed p-type conductivity would result from compensation of cation vacancies which exist due to Schottky disorder*.

equation 4.8 $$\mathbf{nil} \Leftrightarrow 4V_{Bi}''' + 3V_{Ti}'''' + 12V_o^{\bullet\bullet}$$

such that the neutrality equation becomes

equation 4.9 $$4\left[V_{Ti}''''\right] + 3\left[V_{Bi}'''\right] = 2\left[V_o^{\bullet\bullet}\right]$$

A comparison can be made between the defect chemistry in acceptor "doped" AC bismuth titanate and the higher purity TF composition. Although acceptor impurities exist in the TF raw material, such as CaO and Na ($^{\S}Ca_{Bi}'$, Na_{Bi}'), donor impurities were also present, including Sb and Nb ($Sb_{Ti}^{\bullet}$ and $Nb_{Ti}^{\bullet}$). The acceptors are incorporated as in the example in equation 4.4 while the donors (taking Nb as an example) can be compensated by cation vacancies, V_{Bi}''' and V_{Ti}'''' (equation 4.10), or by adding oxygen to existing vacant oxygen sites (equation 4.11):

equation 4.10

$$2Bi_2O_3 + (3-x)TiO_2 + \tfrac{x}{2}Nb_2O_5 \Rightarrow$$
$$4Bi_{Bi} + (3-x)Ti_{Ti} + xNb_{Ti}^{\bullet} + \left(12+\tfrac{x}{2}\right)O_o + \tfrac{x}{6}V_{Bi}''' + \tfrac{x}{8}V_{Ti}''''$$

equation 4.11

$$2Bi_2O_3 + (3-x)TiO_2 + \tfrac{x}{2}Nb_2O_5 \Rightarrow 4Bi_{Bi} + (3-x)Ti_{Ti} + xNb_{Ti}^{\bullet} + 12O_o + \tfrac{x}{4}O_2 + xe'$$

It is well known in perovskite titanates, that the equilibrium concentration of oxygen vacancies increases with acceptors and decreases with donors.[38] In the case of AC BIT, the

---

* The idealized BIT structure is considered for simplicity.

§ Ca may also substitute on the A site in perovskites and behave as a doubly charged acceptor. Results in section 4.5 indicate that Ca behaves similarly as Sr and therefore is a singly charged acceptor.

high concentration of acceptors may promote oxygen vacancies. Since the TF bismuth titanate was also p-type, the function of the donor impurities may be to suppress oxygen vacancy formation.

In summary, bismuth titanate ceramics displayed p-type conductivity. Holes responsible for the p-type conductivity may originate from cation vacancies and/or acceptor impurities. It was suggested that acceptor impurities in the raw materials increase the concentration of oxygen vacancies.

4.4.4 Quenching study

A quenching study was performed to gain additional information on the defect structure in undoped TF bismuth titanate. A sample sintered at 1100 °C for 1 hour was quenched from 250, 300, 400, 500, 600, and 900 °C to room temperature after a 1 hour dwell at each temperature. The results on the DC conductivity measured at 200 °C are given in Figure 4.13.

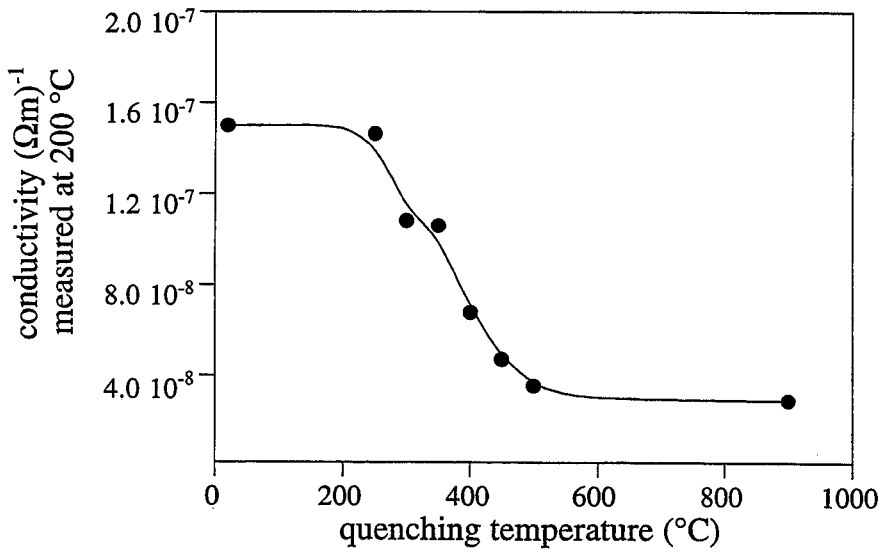

Figure 4.13 Conductivity measured at 200 °C as a function of quenching temperature (TF bismuth titanate).

It was shown that the conductivity in TF bismuth titanate is p-type in air at 200 °C. The decrease in conductivity with increased annealing temperature indicates that there is a defect structure with less charge carriers frozen in at higher temperatures. Since the charge carriers are holes, a decrease in the hole population can be achieved by an increase in the concentration of oxygen vacancies as described in the following relationship:

$$T\uparrow \quad [V_o^{\bullet\bullet}]\uparrow \quad [e']\uparrow \quad [h^{\bullet}]\downarrow \quad \sigma\downarrow$$

The conductivity was not affected by quenching from temperatures below 200 °C (Figure 4.13). The diffusion of oxygen out of the sample was too slow to have a significant effect. As a result samples quenched from low temperatures had the same level of conductivity as the slow cooled sample.

In the following chapter, the dielectric properties show a relaxation process in the temperature range from 250 °C to 500 °C which is attributed to oxygen ions jumping between nearly equivalent sites. The results from these quenching experiments indicate that oxygen ions diffuse in bismuth titanate in this temperature range. This is consistent with perovskites, where, oxygen is considered to be a mobile species at relatively low temperatures.[112,113]

It has been established that the conduction mechanism in bismuth titanate is by holes and not oxygen migration. Several studies on conductivity[111] and diffusion[112] in perovskites address the combination of p-type conductivity with mobile oxygen vacancies. Müller and Härdtl[112] state that although the concentration of electrons and holes is governed by the concentration of ionized oxygen vacancies, the mobility of the oxygen vacancies is much smaller than that of the electronic carriers. The electrical conductivity as a first approximation is therefore governed by the electronic defects.

It is appropriate to note here that a sample annealed for 50 hours at 900 °C showed a further decrease in the conductivity. This suggests that diffusion for shorter times at lower temperatures was not sufficient for equilibration of oxygen with the atmosphere. In other words, the measured conductivity (Figure 4.13) does not represent the equilibrium oxygen vacancy concentration from the quenching temperature.

In summary, when quenched from temperatures greater than 200 °C, a decrease in the conductivity of bismuth titanate was observed. This effect was attributed to the creation of oxygen vacancies. Oxygen vacancies act as donors which decrease the p-type conductivity. This result indicates that oxygen vacancies are mobile defects in bismuth titanate at relatively low temperatures, but not sufficiently mobile to achieve an equilibrium with the atmosphere.

4.4.5 Raw materials

In Chapter 2 it was noted that the reported conductivity in single crystals varied between samples due to impurities. In this section, the differences between AC, TC, and TF bismuth titanate with similar grain sizes will be examined more closely. In Chapter 3, it can be recalled that these materials are all nominally the same composition, however, they were prepared from different sources of TiO_2 and Bi_2O_3. which contained different levels and types of impurities (Table 3.2).

The behavior of the conductivity with temperature for the three undoped bismuth titanate compositions is shown in Figure 4.14. It can be seen that TF and TC BIT were similar, while AC bismuth titanate showed a slightly lower conductivity which converged with the others at higher temperatures.*

All of the materials were p-type, but AC bismuth titanate contained the highest concentration of acceptor impurities (~2000 ppm). One might expect AC bismuth titanate to have the highest conductivity if all of the acceptors were compensated by holes. Since the opposite was the case, a portion of the acceptor impurities in AC BIT may be compensated by promoting oxygen vacancies and/or defects with trapped holes (e.g. Fe_{Ti}).

It is difficult to explain the lower conductivity in AC than TF BIT, even if one assumes that the equilibrium concentration of oxygen vacancies is higher due to the acceptor impurities. If one examines perovskite materials in the p-type region in equilibrium with the atmosphere, increased acceptor concentrations should provide higher conductivities.

---

* The same trend was also observed for large grain size samples.

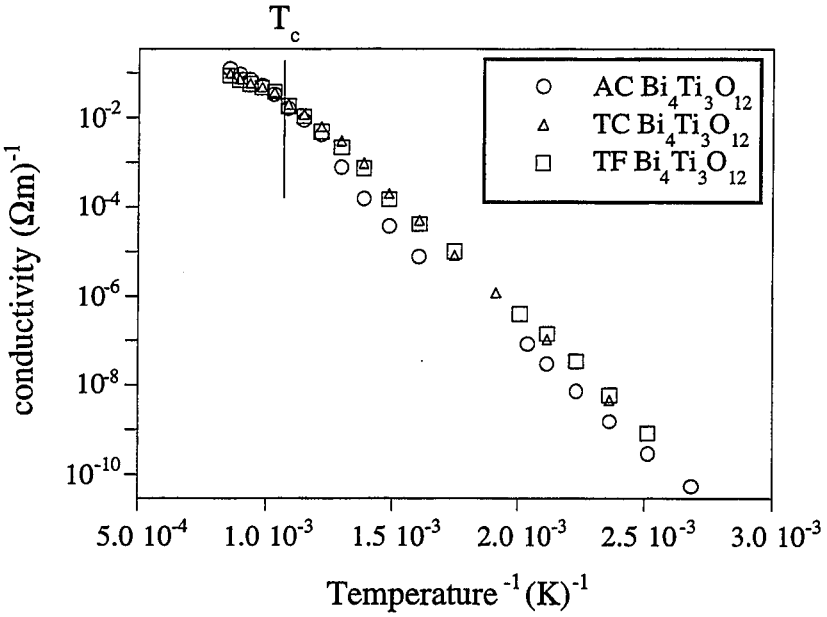

Figure 4.14 Comparison of conductivity as a function of reciprocal temperature in AC, TC, and TF bismuth titanate. See representative micrographs: AC BIT Fig. 3.8b, TC BIT Fig. 3.9b, TF BIT Fig. 3.9c. (note: Error bars for the measurements are smaller than the symbol sizes.)

In fact, it is highly improbable for the low temperature measurements, that equilibration of the oxygen in the bismuth titanate samples with the atmosphere was attained.[113] In the previous section, it was noted that even at 900 °C, an equilibrium in air was not achieved after 1 hour.

The equilibrium reaction for oxygen is written as in equation 4.12:

equation 4.12 $$V_O^{\bullet\bullet} + \tfrac{1}{2}O_2(g) \Leftrightarrow O_O + 2h^{\bullet}$$

In the low temperature regime, the reaction is expected to be slow compared to the measurement time, such that the oxygen vacancy content is "frozen in" from some higher temperature.[113]

It is conceivable that the low conductivity in AC BIT compared to the others in Figure 4.14 is due to a higher concentration of "quenched in" donor oxygen vacancies*. The conductivities converge at higher temperatures where the diffusivity of oxygen increases and equilibration may occur to a greater extent during the measurement. This suggestion is supported by the work of Müller and Härdtl[112] who show that the diffusion of oxygen in perovskites is enhanced with acceptor doping. From the study in section 4.4.4, it appears that higher temperatures promotes oxygen vacancy formation. Accelerated oxygen diffusion at higher temperatures would provide more oxygen vacancies (more donor electrons) and a lower conductivity as observed in AC BIT§ .

In summary, the conductivity in AC bismuth titanate was lower than in TF or TC bismuth titanate, even though AC BIT contained the highest concentration of acceptor impurities. It was suggested that AC BIT contains a higher concentration of oxygen vacancies due to the kinetics of equilibration with the atmosphere. The oxygen vacancies act as donors to partially compensate the acceptors.

4.5. Analysis of Acceptor and Isovalent Dopants in Bismuth Titanate

The impact of acceptor and isovalent doping on the conductivity is described in this section. Acceptor dopants were added to TF bismuth titanate including Fe_{Ti}', Sr_{Bi}', and Ca_{Bi}' and an isovalent ion, La_{Bi}. The acceptor Mn_{Ti}' was added to AC bismuth titanate.

It can be seen in Figures 4.15 and 4.16 that the conductivity increased with acceptor doping. There was no effect from an isovalent substitution of La for Bi. The increase in conductivity was observed whether Bi (Fig. 4.15) or Ti (Fig. 4.16) was replaced by the acceptors. The addition of acceptors in high enough concentrations increases the hole concentration (e.g. $Fe_{Ti}'+h^{\bullet}$). These results agree qualitatively with the behavior of acceptor and isovalent dopants in perovskites.[38,111,141]

---

* The term "quenched" is used here to signify a non-equilibrium concentration rather than completely immobile oxygen vacancies.

§ This assumes that the "quenching in" of the defect structure occurs at similar temperatures upon cooling. This probably depends on the grain size and should be true for bismuth titanate with similar microstructures, as compared here. The subject is discussed in section 4.7.

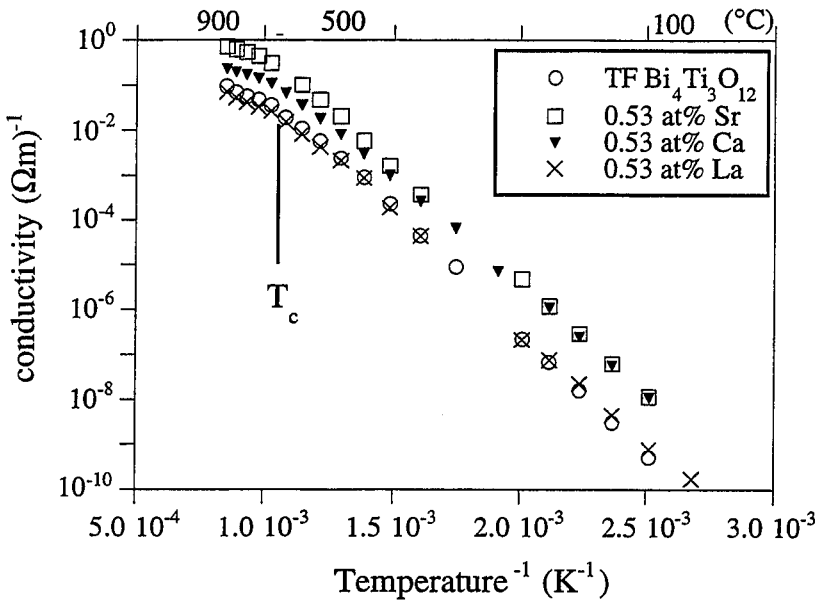

Figure 4.15 Acceptor dopants Ca and Sr which replace Bi in bismuth titanate increase the conductivity. La, an isovalent ion which substitutes for Bi, does not have a significant effect on the conductivity.

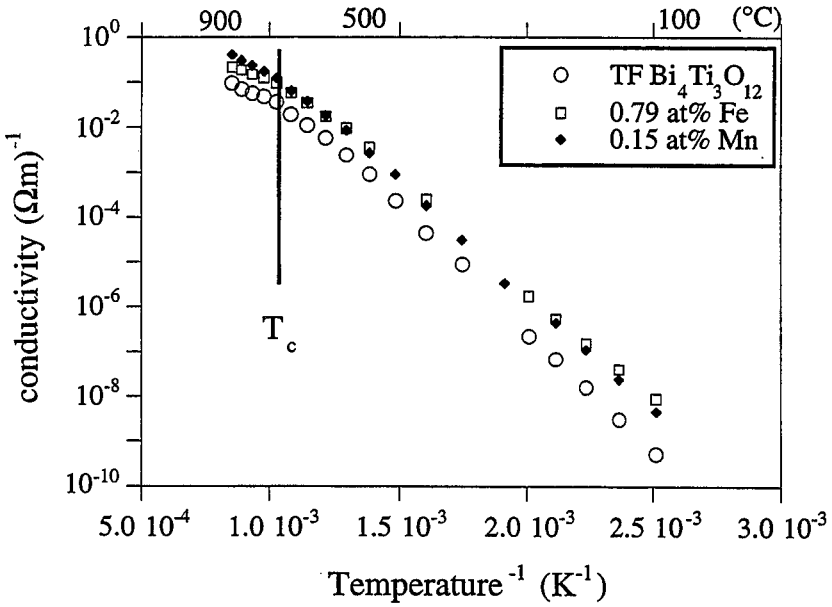

Figure 4.16 Acceptor dopants Fe and Mn which replace Ti in bismuth titanate increase the conductivity.

It can be noted from Figures 4.14 to 4.16 that acceptor doped bismuth titanate followed a similar Arrhenius type relationship to the undoped bismuth titanate. The activation energy does not appear to be effected by impurities or acceptor dopants.* Considering undoped and acceptor doped samples from Figures 4.15 and 4.16, the average value for activation energy was 0.99 ± 0.06 eV below T_c and 0.43 ± 0.07 eV above T_c. A change in the conductivity at the phase transition temperature has also been observed in single crystals.[20]

In summary, acceptor dopants increased the conductivity in TF bismuth titanate which is consistent with p-type conductivity in the ceramics. Acceptor doped bismuth titanate followed the same Arrhenius relationship as undoped bismuth titanate with an activation energy of ~1 eV for temperatures below T_c and ~0.5 eV above T_c.

4.6. Analysis of a Donor Dopant in Bismuth Titanate

4.6.1 Niobium concentration

A cursory investigation of the effect of Nb on the conductivity in bismuth titanate ceramics can be found in the literature.[15] A more in depth study of the effect of Nb concentration on the conductivity is given in this section. It will be shown in Chapter 5 that the composition with the lowest conductivity does not correspond to the optimum piezoelectric properties.

Niobium was added in concentrations of 0.05, 0.21, 0.53, and 0.74 at% to TF bismuth titanate as described in Chapter 3. Since Nb is a grain growth inhibitor, the sintering temperature and time were adjusted to match the microstructures.

With the Nb donor dopant, the conductivity showed a different response from the "pure" and acceptor doped bismuth titanate. The log of the conductivity is graphed versus the reciprocal temperature in Figure 4.17. It can be seen that Nb doping decreased the conductivity and changed the relationship between the conductivity and reciprocal temperature.

---

* The activation energy below T_c appears to be slightly lower for 0.79 at% Fe doped BIT, (0.9 eV compared to 1.1 eV).

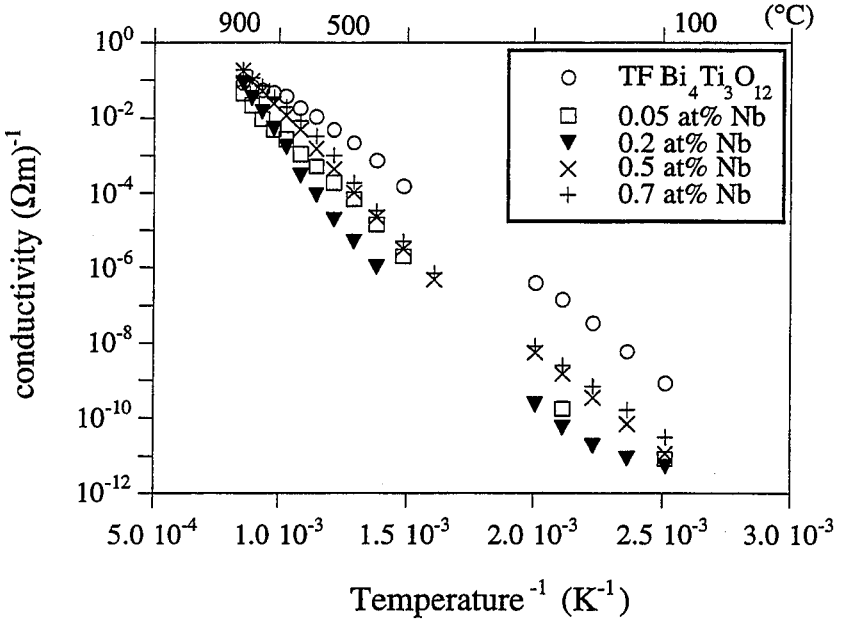

Figure 4.17 The effect of Nb concentration on the conductivity in bismuth titanate

A conductivity minimum was observed for the dopant level 0.21 at% Nb, corresponding to the composition $Bi_4Ti_{2.95}Nb_{0.04}O_{12}$. The conductivity measured at 200 °C is shown versus the dopant concentration in Figure 4.18. With 0.21 at% Nb, the hole compensation was complete and with higher levels of donor dopant the increase in the conductivity can be explained in terms of a transition to n-type conduction.

In Figures 4.17 and 4.18 one observes that the conductivity changed slightly between 0.53 at% and 0.74 at% Nb doping. This agrees with the conclusions from Chapter 3 that the solubility limit for Nb is slightly greater than 0.53 at%.

In order to confirm that a transition from p-type to n-type conductivity occurred with Nb doping, the samples were annealed in flowing oxygen (pO_2 ~1 atm, 1000 °C, 24 hours). The treatment resulted in an increase in the conductivity for the Nb concentration < 0.2 at% (p-type) and a decrease in conductivity for > 0.2 at% Nb (n-type). An example is shown in Figure 4.19. With the low dopant levels, the p-type conductivity increased due to a decrease in the compensating oxygen vacancies $[V_O^{\bullet\bullet}]\downarrow$ $[e']\downarrow$ $[h^{\bullet}]\uparrow$ $\sigma\uparrow$. For higher dopant levels, the reverse effect was observed since the electrons from oxygen vacancies were suppressed and could not contribute to the n-type conductivity $[V_O^{\bullet\bullet}]\downarrow$ $[e']\downarrow$ $\sigma\downarrow$.

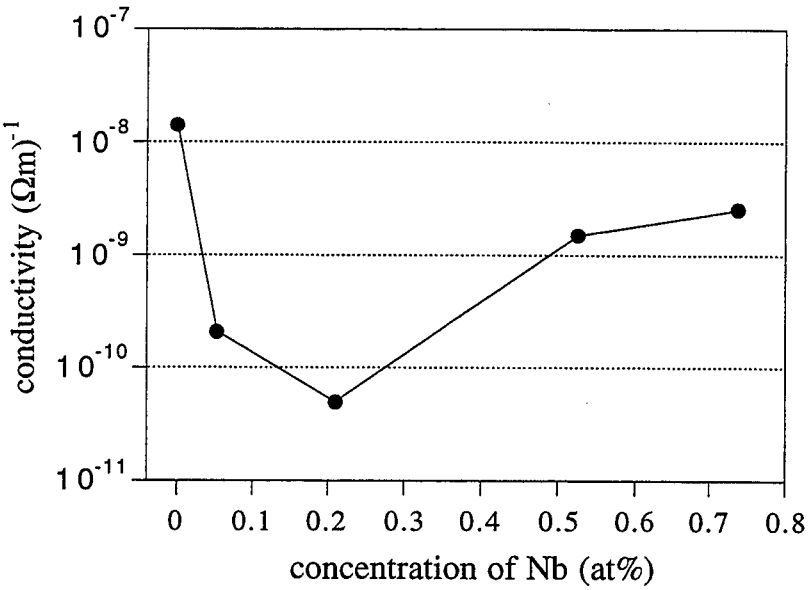

Figure 4.18 The effect of Nb doping on the conductivity (measured at 200 °C) in TF bismuth titanate showing a minimum at approximately 0.2 at%. Bismuth titanate becomes n-type above this concentration.

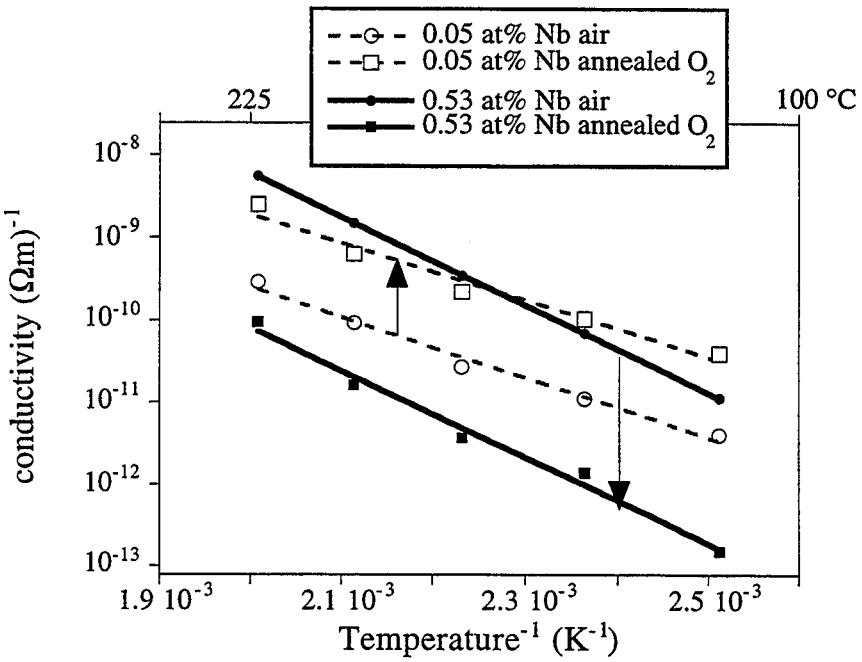

Figure 4.19 A comparison of the effect of oxygen annealing on 0.05 at% Nb doped and 0.53 at% Nb doped bismuth titanate. The conductivity increased for the low level of dopant (p-type) and decreased for the high dopant level (n-type).

The shape of the curve in Figure 4.17 for the 0.21 at% Nb doped bismuth titanate warrants further investigation. A more detailed study of this composition in the temperature range 50-650 °C is shown in Figure 4.20. An activation energy of 1.69 eV was measured in the range 400-650 °C which agrees well with the energy of half the band gap, 1.65 eV, in bismuth titanate[25], indicating intrinsic conduction in this temperature regime. Since the composition corresponds to nearly complete compensation of the free holes by donors, it is reasonable to expect that the intrinsic regime would be observed at lower temperatures than in undoped bismuth titanate.

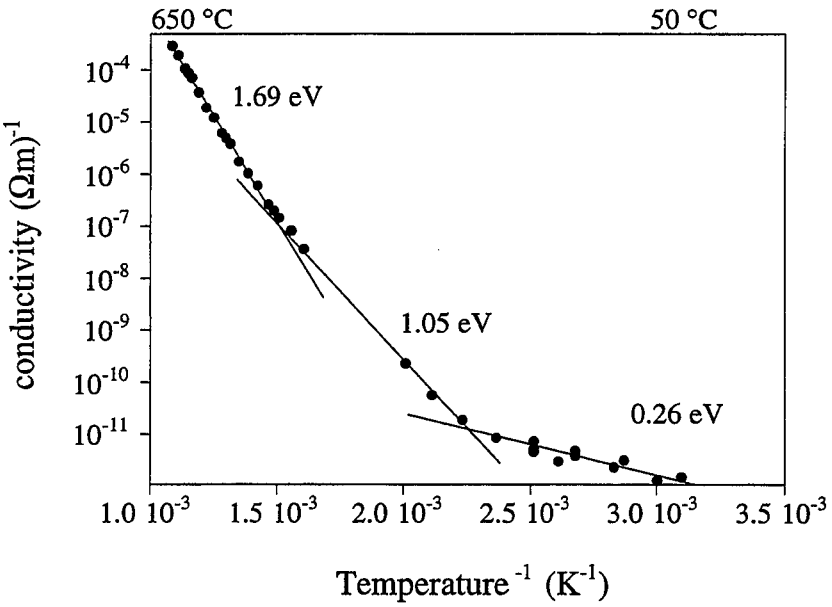

Figure 4.20 Arrhenius relationship for conductivity in 0.21 at% Nb doped bismuth titanate illustrating the changes in the activation energy.

An activation energy of 0.26 eV was measured at low temperatures, 50-200 °C as shown in Figure 4.20. The slope of the Arrhenius plot may contain a temperature dependence of the mobility as well as the enthalpy of the reaction to form free charges. In the case of completely compensated Nb doped bismuth titanate, it is possible that an activation for

mobility is observed at low temperatures where very few carriers can be ionized. The value obtained, 0.26 eV, is on the order of the activation energy reported in PZT[137,139,141,148] (0.26-0.30 eV), for the trapping of holes by Pb^{2+} ions in the temperature range 500-700 °C. A similar mechanism, namely the trapping of holes by Bi^{3+} ions, is possible in bismuth titanate.

The intermediate activation energy of 1.05 eV from 200-400 °C in the Nb compensated BIT was similar to what was observed in p-type undoped and acceptor doped BIT in the range 100-650 °C. The value of ~1 eV may be composed of an activation energy for hole mobility, (~0.3 eV) and the enthalpy of ionization (~0.7 eV). This implies that the energy levels for holes in the band model are approximately 0.7 eV above the valence band which agrees well with Pb containing perovskites as discussed in section 4.3.

In summary, the addition of Nb to TF bismuth titanate decreased the conductivity. A transition from p-type to n-type behavior was observed with increasing concentration of Nb. The composition with 0.21 at% Nb represented a nearly compensated condition where the acceptor states were compensated by electrons from the Nb donor. The conductivity of this composition showed an interesting behavior which can be represented by three separate thermally activated processes using Arrhenius relationships. It was suggested that the activation energy in the low temperature regime (50-200 °C) represents a thermally activated hole mobility.

4.6.2 The impact of raw materials on donor doping

In this section, it is shown that the impurities in the raw materials have a significant impact on donor doped bismuth titanate.

TC and TF bismuth titanate, undoped and with 0.05 at% Nb dopant can be compared in Figure 4.21. The conductivity decreased drastically in TF bismuth titanate, while for the same amount of additive, a less significant effect was observed in TC BIT.

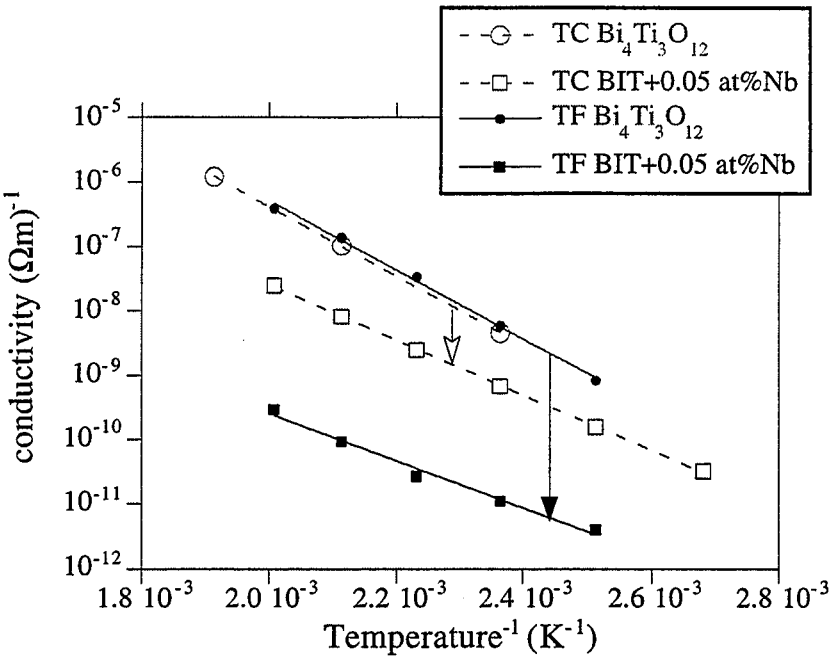

Figure 4.21 The conductivity as a function of reciprocal temperature for undoped and 0.05 at% Nb doped TF and TC bismuth titanate. It can be noted that the same level of dopant showed a greater effect in TF than in TC bismuth titanate.

Since the undoped conductivities were nearly the same, the initial concentration of ionized holes in both undoped compositions must have been nearly equal*, and yet the same quantity of Nb decreased the conductivity more in TF than TC BIT. This behavior can be understood by examining the initial concentration of impurities in the raw materials. The TiO_2 source (Tioxide) was the same for both while the Bi_2O_3 in TC BIT contained a higher concentration of acceptors, including 100 ppm Fe (Fe_{Ti}'), and 50 ppm Ni (Ni_{Ti}'').

To decrease the p-type conductivity the free holes from the native acceptor impurities and cation vacancies must be compensated. There are two mechanisms which may account for the differences with Nb doping. 1) Nb may *compensate* defects in TC BIT which do not contribute holes. For example the compensation for $[Fe_{Ti}'] = 2[Vo^{\bullet\bullet}]$ becomes $[Fe_{Ti}'] = [Nb_{Ti}^{\bullet}]$. 2) Nb may *suppress* defects in TF BIT which contribute holes such as $3[V_{Bi}''']=h^{\bullet}$ or $[Fe_{Ti}']=h^{\bullet}$.

* It is assumed that the hole mobility is the same in both compositions.

Another comparison can be made concerning the concentration of a donor dopant. A minimum in the conductivity was reported for 0.5 at% Nb doped bismuth titanate ($Bi_4Ti_{2.91}Nb_{0.09}O_{12}$)[15], while it was shown in the previous section that a minimum exists for 0.21 at% Nb doping in TF BIT ($Bi_4Ti_{2.95}Nb_{0.04}O_{12}$). These data are compared in Figure 4.22. It is evident that the compositions identify the same level of conductivity where the holes were fully compensated. Compensation required 0.5 at% Nb in the powder used by Lopatin, presumably due to a higher level of acceptor impurities. From these results it is clear that in order to prescribe a formula for Nb doping, the naturally occurring impurities must be considered.

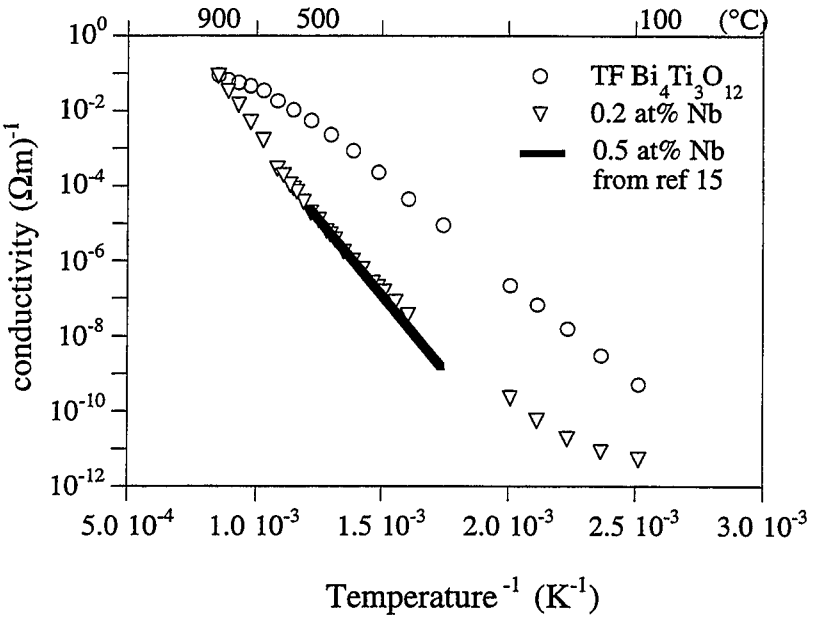

Figure 4.22 Comparison of the conductivity in a 0.5 at% Nb doped bismuth titanate composition from the literature[15] with 0.2 at% Nb doped TF bismuth titanate. It can be noted that different dopant levels produced the same level of conductivity.

In summary, the level of Nb dopant required to decrease the conductivity in bismuth titanate depends on the concentration and type of impurities in the raw materials.

4.7 Grain Size Effect in Undoped and Nb doped Bismuth Titanate

Grain size can affect the properties of electroceramics, although the reasons are not always clear. In the previous sections, the microstructures were matched in order to analyze the impact of raw materials and dopants on the conductivity. In this section, the grain size effects in undoped and a lightly donor doped (0.05 at% Nb) bismuth titanate composition are discussed.

Representative microstructures for "small", and "large" grain samples of AC bismuth titanate can be found in Chapter 3, Figures 3.8a and 3.9d, respectively. The conductivity of different grain size samples is shown over the temperature range of 100 °C to 900 °C in Figure 4.23. The conductivity of the large grain samples was approximately 10 times higher than the fine grain samples in the temperature range 100-500 °C. Similar behavior was observed in TF and TC bismuth titanate.

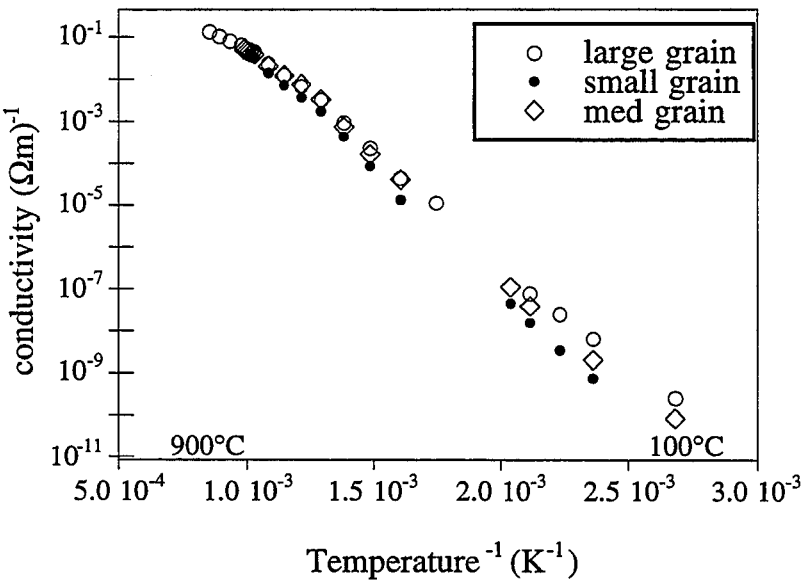

Figure 4.23 Conductivity in AC bismuth titanate as a function of reciprocal temperature showing the effect of grain size.

One contribution can be explained in terms of the anisotropic grain growth. Grains grow preferentially in the **a-** and **b**-directions which are more conductive than the **c**-direction. It can be noted from Figure 4.23 that the conductivities converge at higher temperatures. This convergence was also observed in TC and TF bismuth titanate. According to the results from grain oriented samples (section 4.4.2), a convergence is not expected between the conductivity in the **ab-** and **c**-directions. The grain size effect therefore can not be attributed to the relative increase in the **ab**-directions from the anisotropic grain growth. By the same reasoning, the effect cannot be due to a change in the quantity of insulating grain boundaries. This mechanism also predicts that the conductivities would not converge at high temperatures.

Two possibilities can be suggested for the observed behavior. 1) Grain growth may promote cation vacancies which are compensated by holes, e.g. $\mathbf{V_{Bi}'''} \uparrow \mathbf{h^{\bullet}} \uparrow \sigma \uparrow$. Again, one would not expect a convergence in the conductivity with increased temperature. 2) The grain size may control the concentration of oxygen vacancies. This mechanism suggests that the grain size effect is related to a difference in the "quenched in" defect structure.

Support for the second possibility can be found in the literature on diffusion of oxygen in perovskites.[112,113,149] Waser[113] states that the equilibration of oxygen in perovskites is partly controlled by the mobility of oxygen through the grain boundary. The oxygen vacancy concentration in fine grain samples is quenched in at a higher temperature than in large grain samples. This is due to the barrier character of grain boundaries for the transport of oxygen vacancies.

If the comparison with perovskites is valid, *fine grain* bismuth titanate samples should have a "frozen in" defect concentration from a *higher temperature* than the coarse grain samples. In section 4.4.4, it was shown that the higher temperature quenching gives *lower conductivity* (i.e. higher $[V_O^{\bullet\bullet}]$). This is consistent with the proposed mechanism that the microstructure affects the conductivity through the defect structure. A convergence of the conductivities at high temperature would also be anticipated, since the oxygen vacancies become more mobile and the structure may begin to equilibrate with the atmosphere.

Figure 4.24 shows the affect of sintering time on the conductivity for undoped and 0.05 at% Nb doped TF bismuth titanate. The Nb doped samples showed an unusual behavior in that the conductivity decreased and then increased to nearly the level of undoped (fine grain) bismuth titanate. These results indicate that the 0.05 at% Nb composition became fully compensated after 1 hour and changed from p-type to n-type with increased sintering time. The minimum conductivity achieved at 1 hour ($9x10^{-11}$ $(\Omega m)^{-1}$) was similar to the value in the fully compensated 0.21 at% Nb doped composition ($7x10^{-11}$ $(\Omega m)^{-1}$).

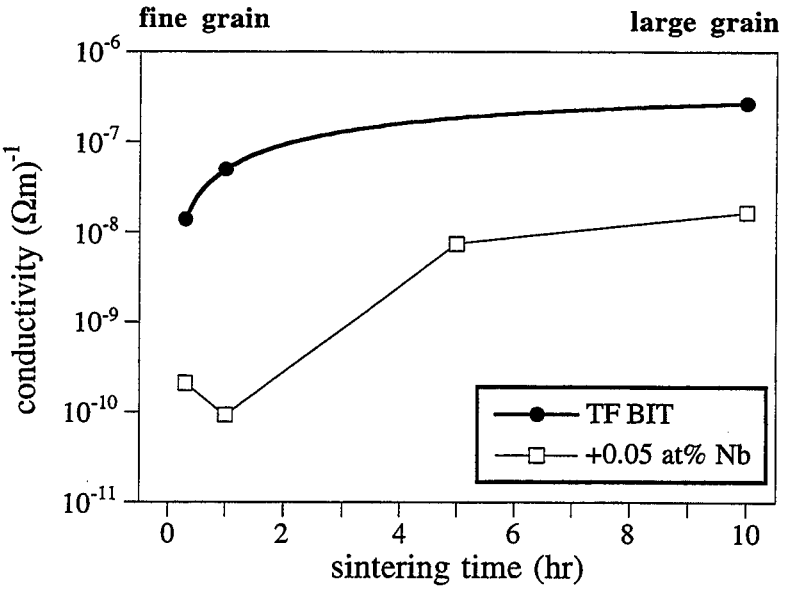

Figure 4.24 Conductivity measured at 200 °C in undoped and 0.05 at% Nb doped bismuth titanate as a function of sintering time.

In order to support this conclusion, the small grain Nb doped samples (sintered 12 min) and large grain (sintered 10 hr) samples were annealed in flowing oxygen as described previously. In Figure 4.25, it can be seen that the conductivity of the small grain sample increased due to the oxygen treatment, while the reverse was observed for the large grain sample. This agrees with a change from p-type to n-type with the increased sintering time.

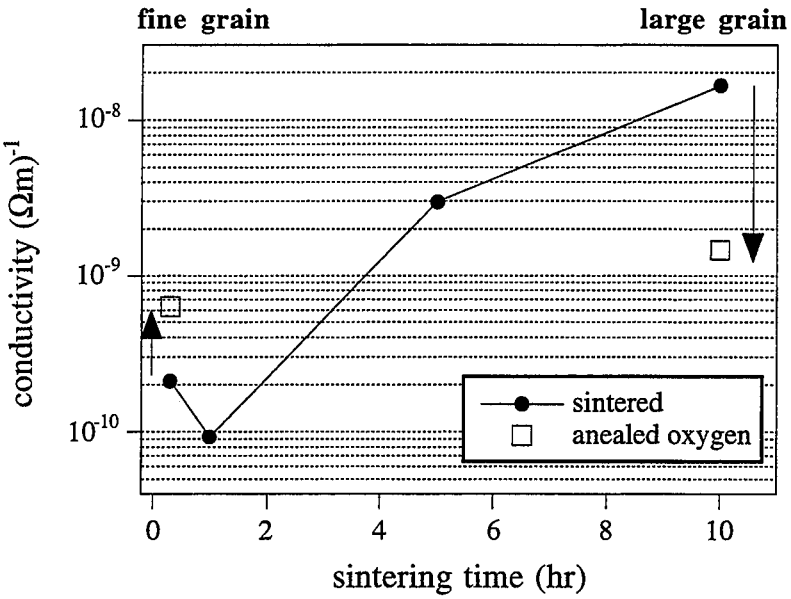

Figure 4.25 The effect of annealing small and large grain 0.05 at% Nb doped bismuth titanate in oxygen. It can be noted that the oxidation reaction increased the conductivity in fine grain and decreased the conductivity in large grain Nb doped bismuth titanate.

For the fine grain samples (short sintering times), the conductivity was slightly p-type which can be attributed to an excess of cation vacancies or ionized acceptor impurities as in undoped bismuth titanate, but with lower concentrations. Since the concentration of donors was the same in the large grain sample, the high n-type conductivity signifies an increase in the oxygen vacancy concentration. After annealing in oxygen the conductivities of the small and large grain samples were similar. The initial difference in the conductivity was due to a difference in the oxygen vacancy concentration rather than the grain size. These results differ from undoped bismuth titanate in which the oxygen vacancy concentration appeared to decrease with increasing grain size.

From these considerations, it appears that oxygen progressively diffuses out of the Nb doped samples during sintering. The longer sintering times allow the system to move towards an equilibrium oxygen vacancy concentration which is *higher* than the starting concentration. This does not conflict with the defect equation (equ. 4.11) which predicts an overall *decrease* in the equilibrium concentration of oxygen with Nb doping. The actual concentration of oxygen vacancies may be much smaller in the Nb doped BIT than in the undoped BIT. A

comparison of the conductivity of p-type and n-type BIT does not reflect the relative concentration of charge carriers, since the charge carriers (holes vs. electrons) can have widely different mobilities.

It can be suggested that the rate of oxygen vacancy formation is restricted by the diffusion of oxygen through the grains in Nb doped bismuth titanate rather than through the grain boundaries. This implies that the oxygen self-diffusion coefficient is decreased by Nb doping. A study of oxygen diffusion in $SrTiO_3$ bicrystals reveals that the lattice diffusion coefficient in Nb doped crystals is about three orders of magnitude smaller than in undoped crystals.[149] The **grain boundary diffusion** coefficient of oxygen, D_{gb}, may be similar for the doped and undoped bismuth titanate, but of a magnitude between that of the respective **lattice diffusion** coefficients in undoped ($D_{O}undoped$) and Nb doped ($D_{O}Nb$) compositions (i.e. $D_{O}undoped > D_{gb} > D_{O}Nb$).

Further evidence that Nb inhibits the mobility of oxygen in bismuth titanate, is found in the dielectric behavior in the following chapter. A set of peaks in the dielectric loss tangent were indicative of ionic motion in bismuth titanate and were attributed to oxygen diffusion. The suppression of these peaks with Nb doping also suggests the suppression of oxygen diffusion i.e. a decrease in oxygen mobility. A parallel is found in the literature for $BaTiO_3$. Donor doped $BaTiO_3$ equilibrates more slowly after a change in pO_2, than undoped or acceptor doped $BaTiO_3$. This behavior is attributed to low oxygen mobility.[150]

In summary, a grain size effect was investigated. In undoped bismuth titanate, finer grained microstructures showed lower conductivity than those with large grains. A mechanism was proposed in which the grain boundaries play a role as a barrier to oxygen vacancy diffusion, such that fine grain ceramics contain a higher concentration of oxygen vacancies.

Nb doped bismuth titanate underwent a transition from p-type to n-type conduction with increasing sintering time. It was suggested that equilibration with the atmosphere is slow in the Nb doped compositions, such that the defect structure changed with sintering time. The mobility of oxygen appears to be impeded by Nb doping. It was suggested that the sintering time rather than the grain size led to differences in the conductivity.

4.8 Binding Energy in Undoped and Nb doped Bismuth Titanate

Another approach to understanding the effect of dopants is to compare the binding energies of the constituent ions. One might expect that the replacement of Ti with Nb would impact the valence state and binding energies. The binding energy depends on the atom and its position in a specific crystal structure, however, the energy can be affected by defects which influence the charged state of the ions. The characteristic binding energies for the Bi, Ti, and O ions were observed using X-ray photo-electron spectroscopy (XPS). The effect of Nb doping on these energies is discussed in this section.

The XPS study was performed using a Perkin-Elmer Physical Electronics 5500 Spectrometer with an Al Kα X-ray source operating at 350 W and 15 kV. Data acquisition was performed in two steps. First, a survey spectrum was acquired in the range of 0 to 1100 eV. The peaks identified from the survey were then analyzed in a narrow window of 15-25 eV. The C 1s peak was used to correct the position of the spectrum. The data were acquired from a thickness of 5 nm.

An XPS survey spectrum of undoped bismuth titanate is presented in Figure 4.26. The O 1s peak typically occurs at 531 eV and overlaps with adsorbed OH groups at 533 eV.[151] The binding energies for the core level photo-emission of Ti 2p and Bi 4f electrons were used to obtain information on the valence states of the elements. These peaks can be located in Figure 4.26 and are expanded in Figures 4.27 and 4.28 with a comparison to Nb doped bismuth titanate.

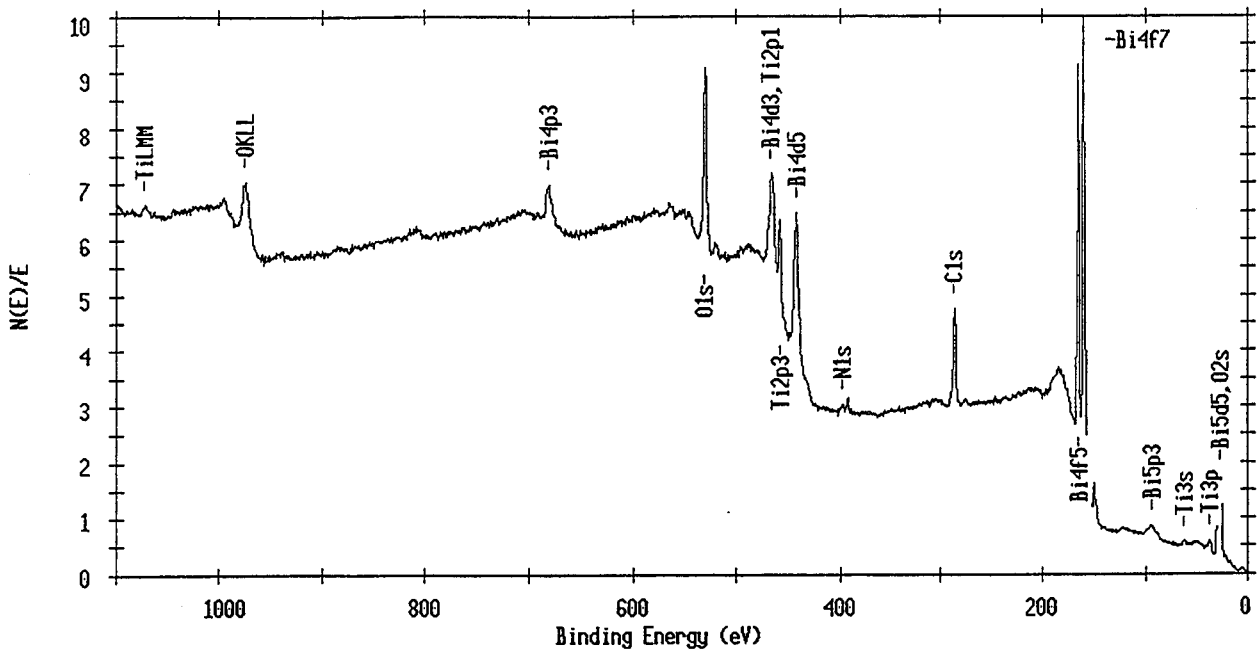

Figure 4.26 Survey spectrum by XPS showing the energy due to bonding of Bi, Ti, and O in undoped TF bismuth titanate (sintered at 1100 °C 1 hr).

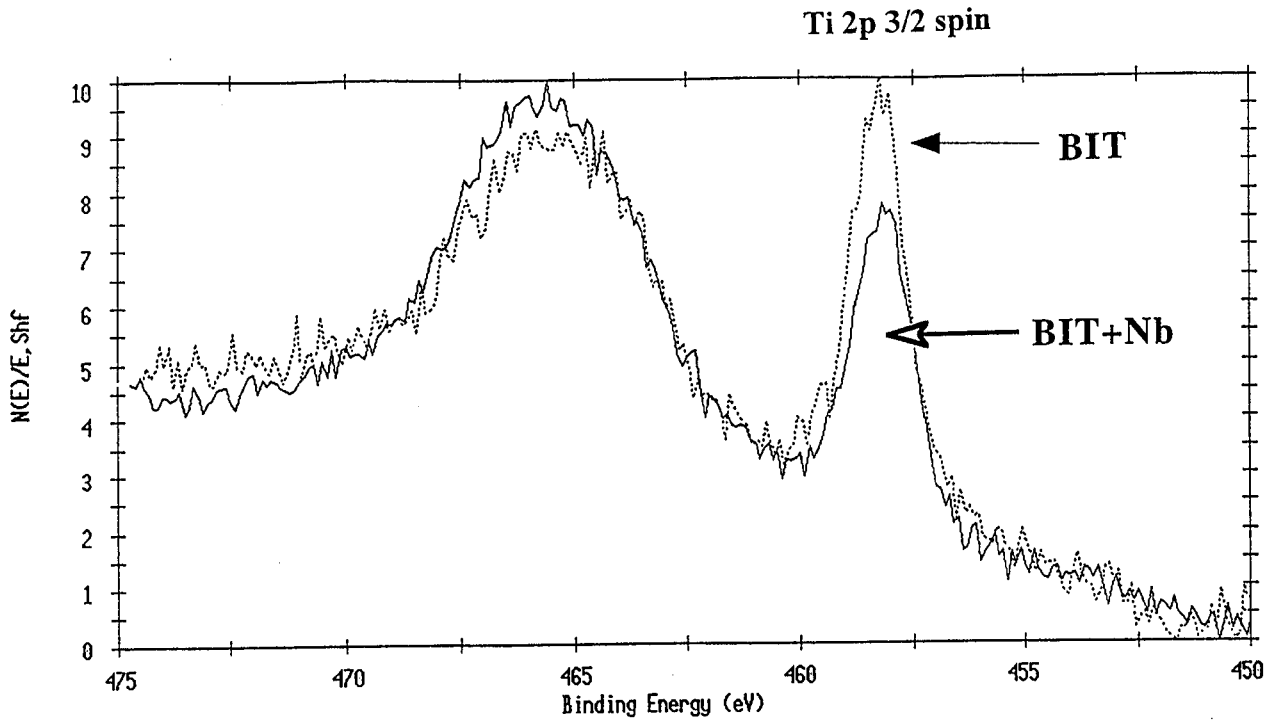

Figure 4.27 Spectrum showing the effect of 0.74 at% Nb doping on the binding energy of Ti in bismuth titanate.

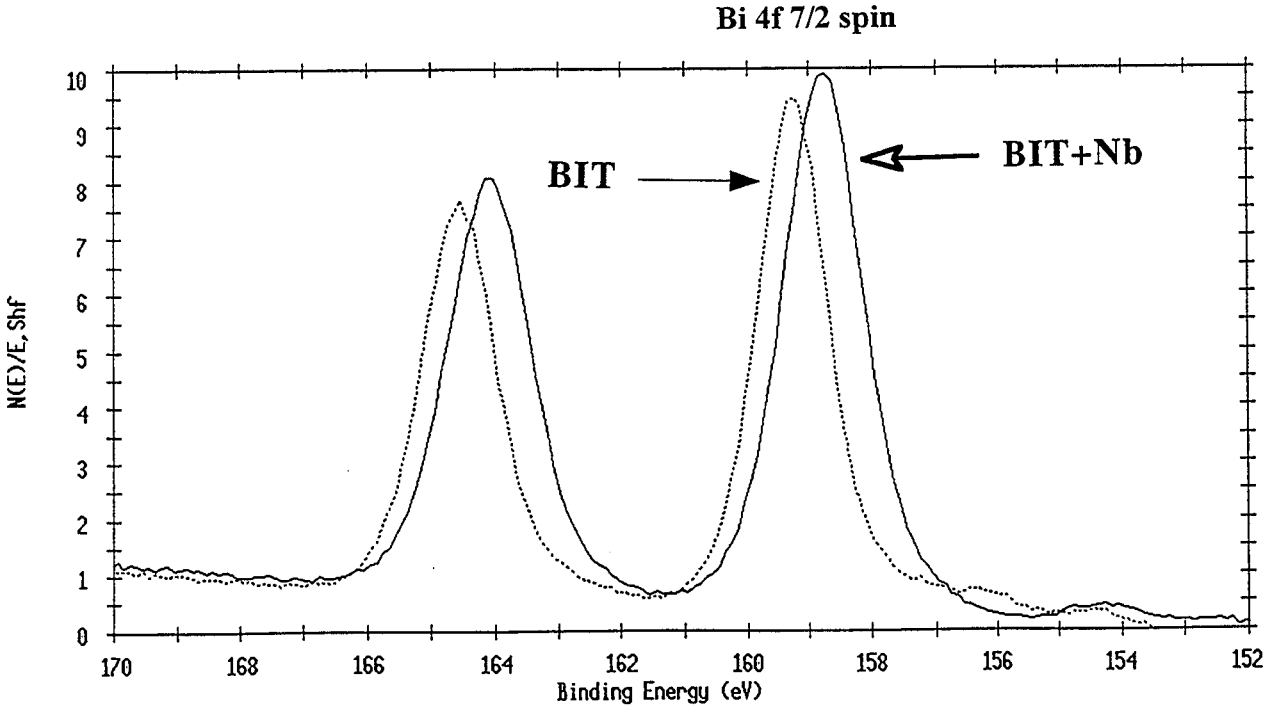

Figure 4.28 Spectrum showing the effect of 0.74 at% Nb doping on the binding energy of Bi in bismuth titanate. A shift toward lower energy for the Bi^{3+} peak is observed.

The Ti 2p 3/2 peak shown in Figure 4.27 occurred at an energy of 458.8 eV which agrees with reports in the literature for Ti in the 4+ valence state.[151] The position of the peak was not affected by Nb doping so that the binding energy of Ti remains characteristic of the 4+ ion. The decrease in magnitude or area of the Ti 2p peak reflects the decrease in the concentration, due to the replacement of Ti with Nb.

The 7/2 and 5/2 components of the Bi 4f spin-orbit doublet were located at 159.2 and 164.6 eV in Figure 4.28, which gives the expected energy (5.4 eV) for the splitting.[151] The binding energies were slightly higher than those reported in Bi_2O_3 with 4f 7/2 at 158.7 eV[151] which suggests a higher valence state than 3+ for the Bi ion. The average Bi valence calculated from the structure using a bond valence method[152] was +3.1, which agrees with this analysis. The Bi valence state of $3+\delta$, (where $0< \delta <1$) can be interpreted as characteristic of the binding in $Bi_4Ti_3O_{12}$. This is supported by the similarity with another Bi compound, $Bi_2Mo_3O_{12}$ which has a 4f 7/2 peak at 159.7 eV, signifying overbonding of the Bi ion.[153]

These results contradict a previous study[89] which reports a value of 158.4 eV for the Bi 4f 7/2 peak. This represents a reduced state for the Bi when compared with Bi_2O_3. It was suggested by the authors that oxygen vacancies were responsible for reducing the Bi ions.

The spectrum from undoped bismuth titanate is a useful base-line to compare with Nb doped bismuth titanate so that one can observe the changes rather than define the exact valence state. The Nb dopant caused a shift of 0.5 eV to lower energy for the Bi 4f peaks as shown in Figure 4.28. This shift is significant considering the reproducibility of the measurement and the well resolved high intensity Gaussian peaks. A shift to lower binding energy represents a decrease in the Bi valence state.

From the results in Figures 4.27 and 4.28 it is clear that Nb, a donor dopant which replaces Ti ($Nb_{Ti}^{\bullet} + e'$), promoted reduction of the Bi ion rather than Ti, even though Ti^{4+} is also a reducible ion. An explanation for this behavior can be found if one considers the effect of the bismuth titanate crystal structure on the valence states of Bi and Ti.

The valence states of the ions from Withers, et al.[152] for the parent orthorhombic structure and the monoclinic phase of bismuth titanate are shown in Table 4.1. The position of the atoms are indicated in Figure 4.29. It is interesting to note that the parent structure

requires Bi in an underbonded reduced state, while the Ti is overbonded. The parent structure (Fmmm) for $Bi_4Ti_3O_{12}$ must lower its symmetry to satisfy the bonding requirements. The monoclinic distortion (Bmab mode) in which the TiO_6 octahedra rotate about an axis parallel to the polar **a**-direction, allows the Ti ions to achieve lower valence states closer to 4+. Reducing the Ti even further may not be possible due to the restrictions already imposed on the bonding. In the monoclinic phase, most of the Bi ions are overbonded, therefore, Bi in preference to Ti, would be reduced by the donors.

Table 4.1. Calculated valences for ions in $Bi_4Ti_3O_{12}$ in the parent orthorhombic structure and monoclinic structure. The positions are defined in Figure 4.29. Note the overbonding of Ti in the parent structure.

ion	Fmmm orthorhombic	B1a1 monoclinic
Bi 1	2.36+	3.21+
Bi 1'	2.36+	3.10+
Bi 2	2.84+	3.23+
Bi 2'	2.84+	2.91+
Ti 1	4.45+	4.14+
Ti 2	4.27+	3.88+
Ti 2'	4.27+	4.09+
O 1	1.94-	1.95-
O 1'	1.94-	2.04-
O 2	2.28-	2.36-
O 2'	2.28-	2.30-
O 3	1.72-	2.04-
O 3'	1.72-	2.04-
O 4	1.73-	1.79-
O 4'	1.73-	1.87-
O 5	2.01-	2.03-
O 5'	2.01-	2.06-
O 6	2.01-	2.04-
O 6'	2.01-	2.05-

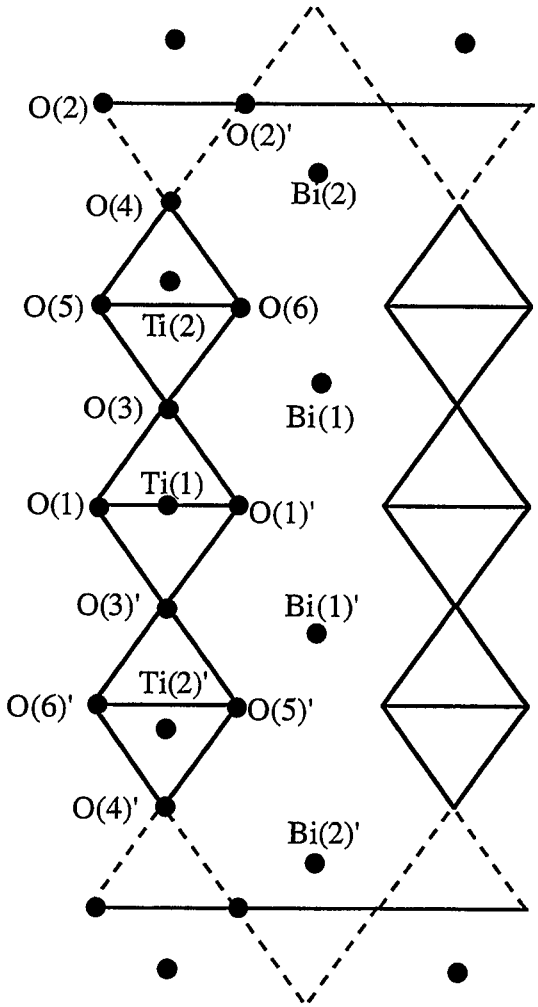

Figure 4.29 One half of the bismuth titanate unit cell projected down the b-axis showing the position of the atoms referred to in Table 4.1.

Alternatively, it can be envisioned that the excess electrons from the donor satisfy the bonding requirements for Ti and eliminate the driving force for the monoclinic distortion. The net change in the valence for Ti would be zero so that the Ti 2p peak in Figure 4.27 was not shifted from its original position. In this case, the Bi would appear to be in a reduced state, since the structure would be closely related to the parent structure in which the Bi ions are underbonded.

In summary, 0.74 at% Nb addition to bismuth titanate caused a shift to lower binding energy in the Bi core electrons, while the Ti binding energy was not effected. It was proposed

that the donor dopant preferentially reduced the Bi ion rather than the Ti due to the structural conditions which require Ti to be overbonded while Bi can be either overbonded or underbonded. Alternatively, the same results can be achieved if Nb suppresses the monoclinic distortion in bismuth titanate.

4.9 Summary of Defect Chemistry in Bismuth Titanate

A summary of the understanding which has been gained in the defect chemistry of bismuth titanate is given in this section. The results have been compiled from the effects of variables including the purity of the raw materials, annealing atmosphere, quenching temperature, microstructure, and dopants on the conductivity. The evidence shown in this chapter supports the original assumption that the band model for bismuth titanate has many important similarities to lead containing perovskites.

Undoped bismuth titanate is p-type, however, the source of holes may depend on the impurities in the raw materials. Different sources of holes, (e.g. Fe_{Ti}' and Ca_{Bi}') may exist which correspond to specific energy levels, however, the similar activation energies (~1 eV below T_c) indicate that these levels are very close in energy in the band gap. In addition, if cation vacancies (e.g. V_{Bi}''') provide a significant contribution of free holes, these defects would also be of similar ionization potential.

The possibility of a thermally activated hole mobility was presented in section 4.6.1 with an activation energy of 0.26 eV. The activation energy of 1.05 eV in undoped TF bismuth titanate may therefore indicate an ionization energy 0.79 eV below the valence band with an additional 0.26 eV corresponding to the energy required for a hole to hop from one site to another. These values compare favorably with calculations in Pb containing perovskites. In addition, it appears that Nb additions and oxygen vacancies behave as electron donors with low ionization potentials similar to the titanate perovskites.

A schematic illustration of the band model for bismuth titanate which incorporates the defects suggested in this chapter is shown in Figure 4.30. This is an oversimplification of the band structure, however, it is the first attempt to date at identifying and quantifying the defects in bismuth titanate which are significant in the conduction process.

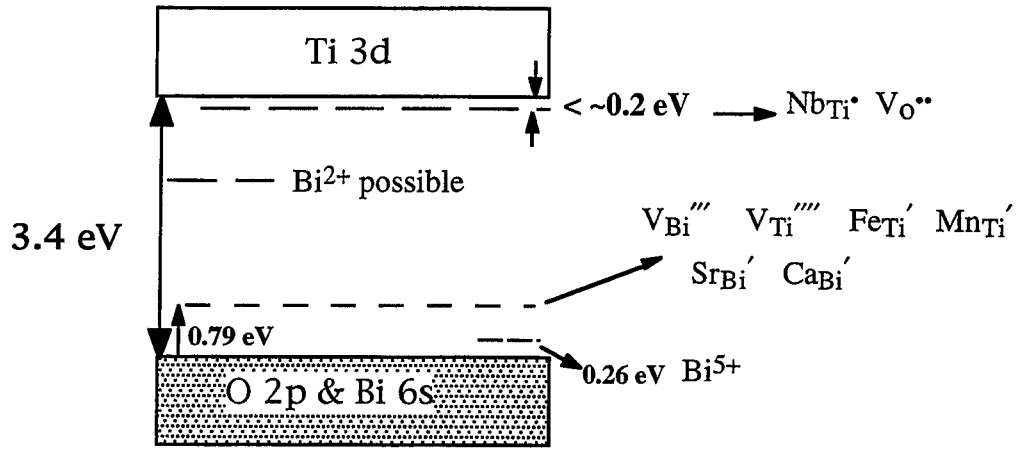

Figure 4.30 Schematic illustration of the suggested defect band model for bismuth titanate.

4.10 Chapter Summary

In this chapter, a first approximation of the defect structure in bismuth titanate with acceptors and donors was presented using the band model. It was established that undoped bismuth titanate ceramics containing different purity levels displayed electronic p-type conductivity. The level of conductivity was not greatly effected by the raw materials, however, the impurities became an important factor in determining the concentration of donor dopant required to minimize the conductivity.

A conductivity minimum was observed for 0.21 at% Nb doping in TF bismuth titanate which represents a nearly fully compensated composition. The activation energy of 0.26 eV from the Arrhenius behavior suggests a thermally activated hopping mechanism which can be observed in the low temperature region (50-200 °C). Intrinsic conduction was observed in the temperature range of 500-650 °C. The intermediate temperature range showed an activation energy of 1.0 eV which was similar to undoped or acceptor doped bismuth titanate. It was suggested that this value represents a combined activation for the hole mobility and

generation of new carriers. The Arrhenius behavior changed as bismuth titanate became n-type with higher concentrations of Nb.

Other important results from this chapter include a binding energy study which shows that the Bi ion is reduced by Nb doping, in preference to the Ti ion. This was explained in terms of the difference between the binding energies in the orthorhombic parent phase and monoclinic phase. Several results indicate that O^{2-} is a mobile species in bismuth titanate at relatively low temperatures (300-500 °C). It appears that the addition of Nb decreases the mobility of oxygen and shifts the equilibrium to lower concentrations of oxygen vacancies.

Chapter 5. Dielectric Properties and Piezoelectricity in Bismuth Titanate Ceramics

5.1 Introduction

In Chapter 3, processing variables and dopant additions were investigated in terms of the microstructural effects. The impact of microstructural variations and dopants on the conductivity was explored in Chapter 4. Undoped bismuth titanate was p-type for the materials studied. The conductivity decreased by as much as three orders of magnitude with Nb donor doping. The transition to an n-type material with a high level of Nb (0.53 at%) corresponded to the conditions for grain growth inhibition. Acceptor dopants increased the conductivity in bismuth titanate, therefore, these materials were eliminated from the following study.

It is the goal of this chapter to determine the relative significance of the microstructure, conductivity, and Nb dopant concentration on the piezoelectric properties. The Curie temperature can also be affected by dopants, therefore, the effect of Nb on the temperature of the ferroelectric phase transition was investigated. In addition, a study of the unusual dielectric properties of bismuth titanate gives insight into one of the polarization processes.

The experimental realization of these goals includes the following steps:

1. Impurities and dopants often affect the Curie temperature in ferroelectrics. The impact of the raw materials and Nb doping on the phase transition will be determined by measuring the permittivity as a function of temperature.

2. An anomalous peak in permittivity at ~500 °C in bismuth titanate has been reported.[19,20,24,25] A study of the dielectric data including the permittivity, dielectric loss, and loss tangent is conducted to reveal the nature of this anomaly.

3. The original premise in this thesis was that a more effective poling regime could be applied to bismuth titanate if the conductivity were suppressed. The effect of conductivity and Nb doping on the poling is explored.

4. The microstructure as well as the concentration of free charges can influence the domain structure of a ferroelectric ceramic. Nb doping changes both of these conditions in bismuth titanate and therefore can affect the polarization process and piezoelectric properties by different routes. Ideally, one would compare the piezoelectric properties of samples with:

a. the same grain size and dopant level, but different conductivity
b. the same grain size and conductivity, but different dopant level
c. the same dopant level and conductivity, but different grain size

In practice, not all of these conditions can be obtained, however, several important trends will be shown.*

5.2 Ferroelectric to Non-Ferroelectric Phase Transition

Since the feature of bismuth titanate which stimulated this investigation was the high temperature of the ferroelectric to non-ferroelectric phase transition (675 °C), it is of interest to observe the impact of Nb doping on this temperature.

The Curie temperature ($\mathbf{T_0}$) can be determined from the susceptibility (χ) as a function of temperature. Ideally, the Curie-Weiss law is observed. For temperatures above the ferroelectric to non-ferroelectric phase transition (first order), the behavior is described in equation 5.1:

equation 5.1 $$\chi^{-1} = \frac{\mathbf{T - T_0}}{\mathbf{C}}$$

where **C** is the Curie constant and T is the temperature. The susceptibility, χ, is related to the dielectric constant, **k'**, by equation 5.2.

equation 5.2 $$\chi = \mathbf{k' - 1}$$

* Bismuth titanate in this chapter refers to the TF composition unless otherwise specified.

An example of the dielectric susceptibility as a function of temperature for undoped bismuth titanate is shown in Figure 5.1a.* It can be noted that the behavior was not ideal when compared to the theoretical curve in Figure 5.1b. Although, it is not clear from the dielectric response, it has been determined previously that the phase transition in bismuth titanate is of the first order.[71] A contribution to the permittivity which is discussed in section 5.3 is partly responsible for the deviation below T_c. With Nb dopant, the behavior resembles that of the first order phase transition.

Above the transition temperature, the reciprocal slope of the linear relationship gives a Curie constant of 1.6 x 10^5 °C. This value agrees well with the Curie constant in ferroelectric perovskites. For example, the Curie constants in $PbTiO_3$ and $BaTiO_3$ are 1.1 x10^5 and 1.7 x10^5 °C, respectively.[154] A Curie constant of 2.2 x 10^5 °C was previously reported for bismuth titanate.[155]

The Curie temperature (T_0), as defined in equation 5.1, does not necessarily coincide with the temperature of the transition between a ferroelectric and a non-ferroelectric phase (T_c). The difference is usually less than a few degrees Celsius for first order phase transitions§[156], and in much of the literature, the term "Curie temperature" is used interchangeably with "phase transition temperature" (e.g.[157]). In general, the reported values for the "Curie temperature" in high temperature ferroelectrics are actually the phase transition temperatures. In order to be consistent with the literature, in this thesis the transition temperature is called "Curie temperature" and is determined by the temperature at which the permittivity achieves a maximum value when measured at 1 MHz.

---

* The measurement technique for the dielectric measurements was described in Chapter 4.

§ In second order phase transitions, the Curie temperature always equals the phase transition temperature.

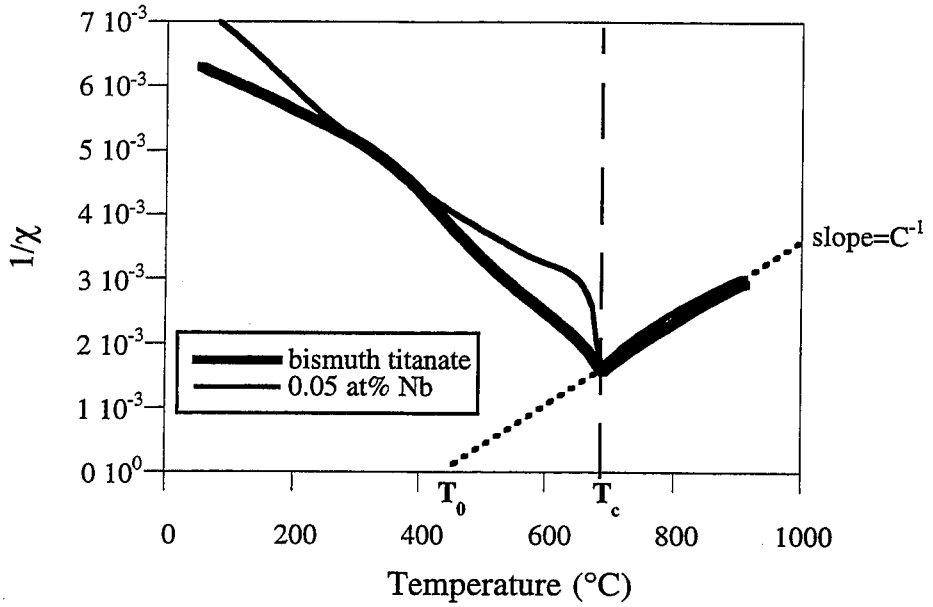

Figure 5.1a) The reciprocal of the susceptibility as a function of temperature in undoped and 0.05 at% Nb doped bismuth titanate. Note that T_0, the Curie temperature is significantly lower than T_c, the transition temperature. The Nb dopant affects the shape of the curve below T_c (suppresses the anomaly), such that the behavior resembles a first order phase transition (Fig. 5.1b).

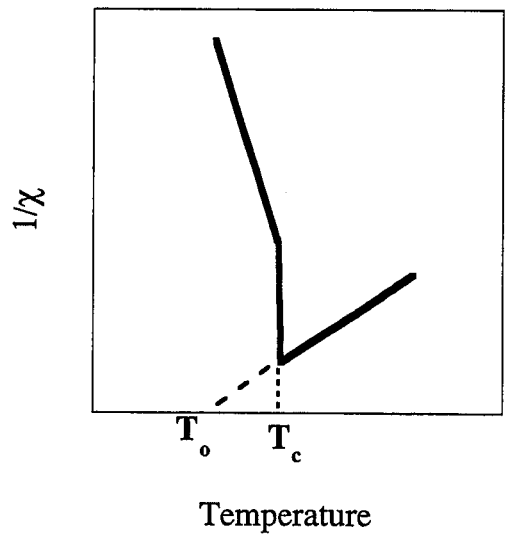

Figure 5.1b) Theoretical Curie-Weiss behavior for a first order phase transition.

The Curie temperature of bismuth titanate ceramics prepared from different raw materials (AC, TC, and TF) was 685 ± 5 °C. The choice of raw materials did not significantly affect T_c. The value obtained for T_c in bismuth titanate agrees well with that reported for high purity single crystals.[6] Other reports place T_c at 675 °C (e.g.[4]). It has been noted that impurities decrease T_c in single crystals.[11] This was not observed here, however, the type and concentration of impurities may be significant. The value of 675 °C for T_c in bismuth titanate is widely quoted from Cummins and Cross[4], however, Hopkins and Miller[11] believe that this value is about 10 °C too low. The method of measuring T_c may also contribute to the apparent discrepancy.

It is known that dopants can drastically shift the Curie temperature in ferroelectrics.[38] The Curie temperature in bismuth titanate as a function of Nb dopant is shown in Figure 5.2. With the highest dopant level (0.74 at% Nb), T_c was decreased by 20 °C. The decrease of ~3% occurred in the composition very near the solubility limit of Nb in bismuth titanate, therefore further decreases would not be expected.

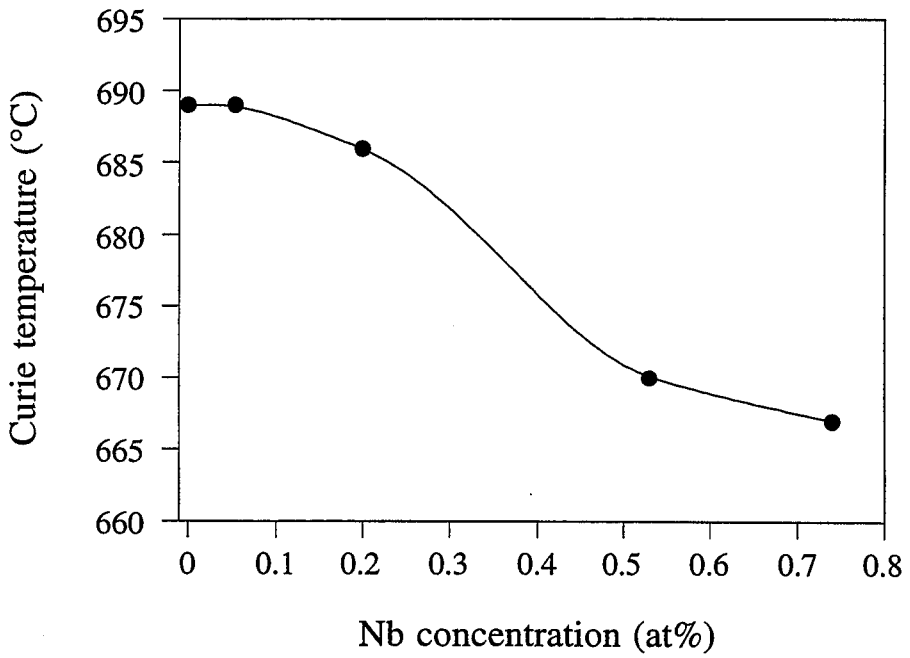

Figure 5.2 Curie temperature in bismuth titanate as a function of Nb dopant.

In summary, impurities in the raw materials did not affect the Curie temperature in bismuth titanate. A 20 °C decrease in the Curie temperature was observed by Nb doping which does not interfere with the original goal of developing bismuth titanate ceramics for high temperature piezoelectric applications.

5.3 Additional Dielectric Anomalies

In the following sections, an improved understanding of the dielectric properties of bismuth titanate allows an interpretation of several anomalies in the permittivity and the loss. In addition, the effect of Nb doping on these anomalies is investigated.

5.3.1 Relative permittivity

A peak in the relative permittivity at ~500 °C in bismuth titanate ceramics and single crystals has been observed by several authors.[19,20,24,25] This peak has been attributed to various phenomena including a phase transition[158], space charge relaxation[20,24], and ion jump relaxation.[19] In several cases, the magnitude of this peak was larger than the anomaly related to the phase transition (~675 °C). Such a large anomaly was not observed in this study, however, in Figure 5.3 it appears that the peak at T_c, measured at 1 MHz, contains a contribution from an additional peak centered at approximately 550 °C. It was discovered in the course of this investigation that Nb affects the dielectric properties including this anomalous peak. It is evident that the Nb dopant suppressed this anomaly, resulting in a sharp transition at T_c. The example in Figure 5.3 is for 0.05 at% Nb, however, the result was similar for all of the Nb dopant concentrations.

A more complete view can be achieved by comparing the dielectric permittivity at several frequencies as shown in Figure 5.4 for undoped bismuth titanate. It is clear that the anomaly at ~550 °C measured at 1 MHz is actually a combination of two peaks which are both frequency dependent. A third anomaly is also indicated at temperatures around T_c which distorts the peak at the phase transition. These phenomena give the appearance of a broad phase transition in undoped bismuth titanate and contribute to the unusual behavior around the phase transition temperature(Figure 5.1a).

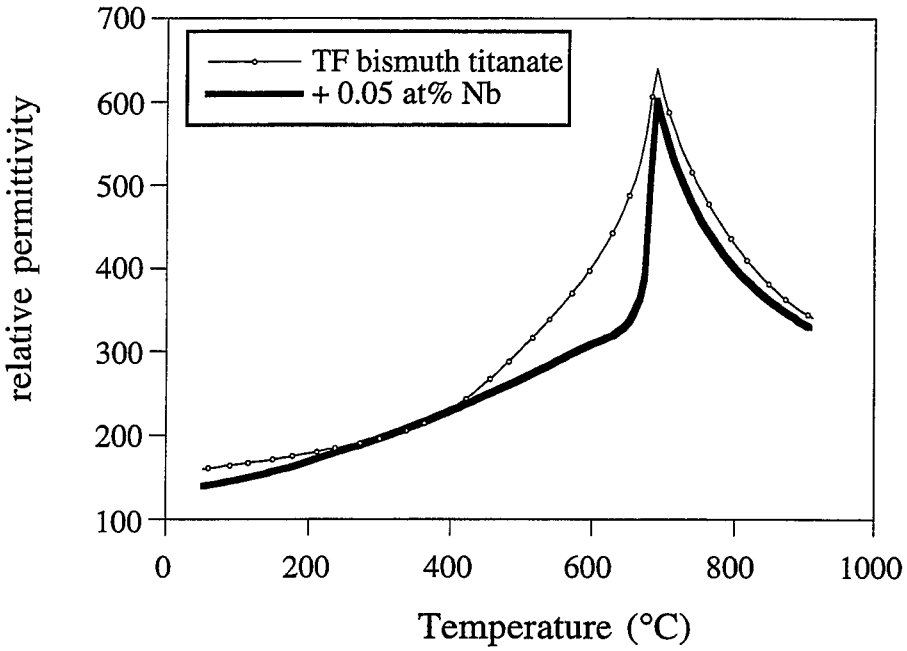

Figure 5.3 Relative permittivity (1 MHz) as a function of temperature showing the effect of 0.05 at% Nb on an anomalous peak at ~550 °C.

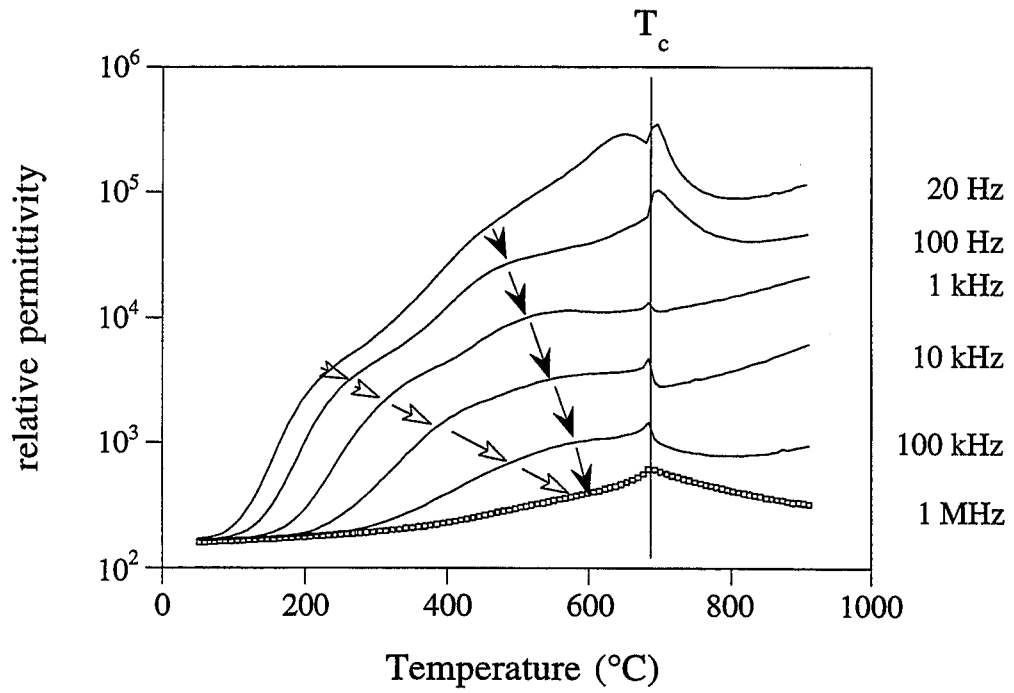

Figure 5.4 Relative permittivity of undoped bismuth titanate as a function of temperature for six frequencies (note the semi-log scale).

The relative permittivity of bismuth titanate doped with a low and high level of Nb (0.05 at%, 0.74 at%) is shown in Figures 5.5 and 5.6. as a function of temperature and frequency. The large anomalous peaks in the low temperature range (around 200 °C) have been suppressed, however, a frequency dependence persists in the higher temperature regions.

It can be shown that dispersion and absorption are two different aspects of the same phenomenon which is defined as a relaxational process.[26,129] The diminishing frequency dispersions presented in Figures 5.4 to 5.6 suggest that one or more relaxational processes become less significant with Nb doping. Relaxation is often better understood from the changes in the dielectric loss or loss tangent.[97,154] This subject will be addressed in more detail in the following section.

In summary, an understanding of the anomaly at ~550 °C in the relative permittivity of bismuth titanate requires a more complete analysis of the temperature and frequency dependence of the dielectric properties. Two separate frequency dependent peaks were observed which merged at ~550 °C at 1 MHz. These phenomena indicate relaxational processes which were suppressed with Nb doping.

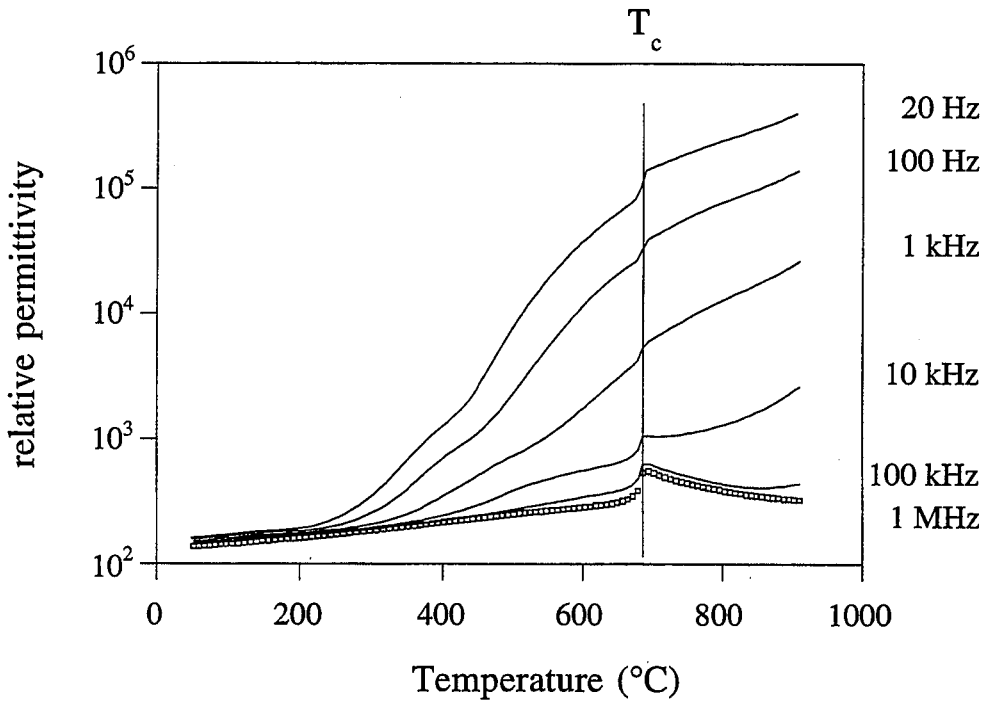

Figure 5.5 Relative permittivity as a function of temperature and frequency showing the frequency dependence with 0.05 at% Nb (note the dispersion has disappeared in the low temperature region ~ 200 °C).

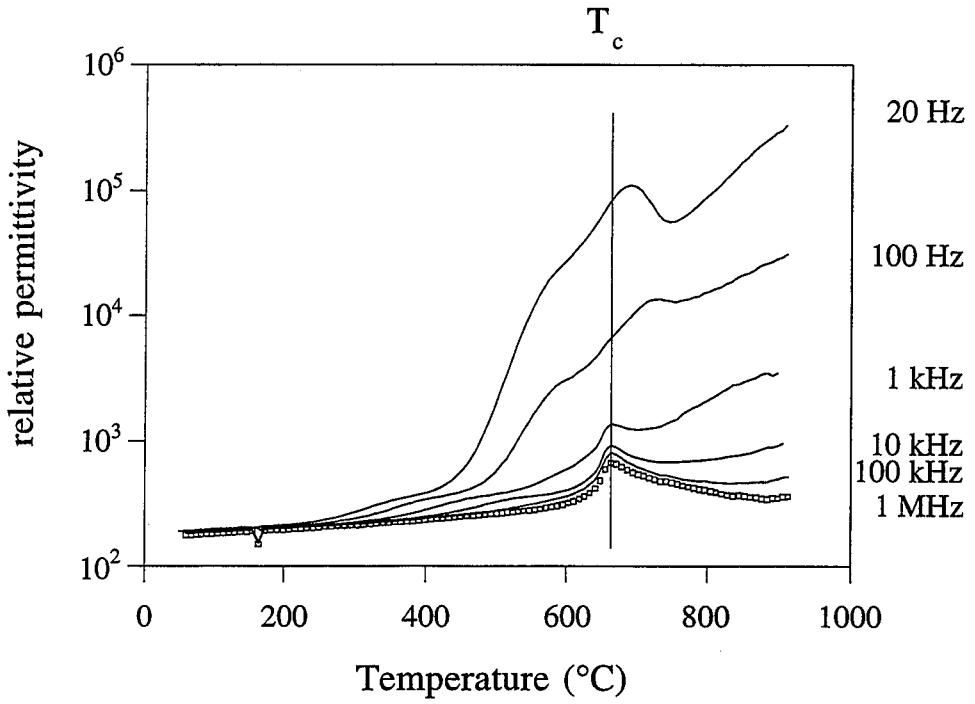

Figure 5.6 Relative permittivity as a function of temperature and frequency showing the frequency dependence with 0.74 at% Nb (note the dispersion has disappeared in the low temperature region ~ 200 °C).

5.3.2 Dielectric relaxation

In this section, the characteristics of the dielectric relaxational processes in bismuth titanate are discussed. In the following section, the mechanism by which Nb suppresses the dielectric relaxation will be explored.

The primary contributions to the permittivity, (electronic, atomic, dipolar (including ionic), and space charge polarization) involve the short range motion of charge.[154] The contributions in an alternating field are limited by the inertia for charge motion. This results in a characteristic relaxation time, and a frequency above which, the charge cannot follow the field. The relation between the real and imaginary parts of the permittivity requires that each mechanism leading to polarization will give rise to correspondingly high losses in the frequency spectrum in the frequency range where relaxation or resonance occur, as illustrated in Figure 5.7. The relationship is defined by the Kramers Kronig equations for the complex susceptibility and is discussed in detail in the literature.[129]

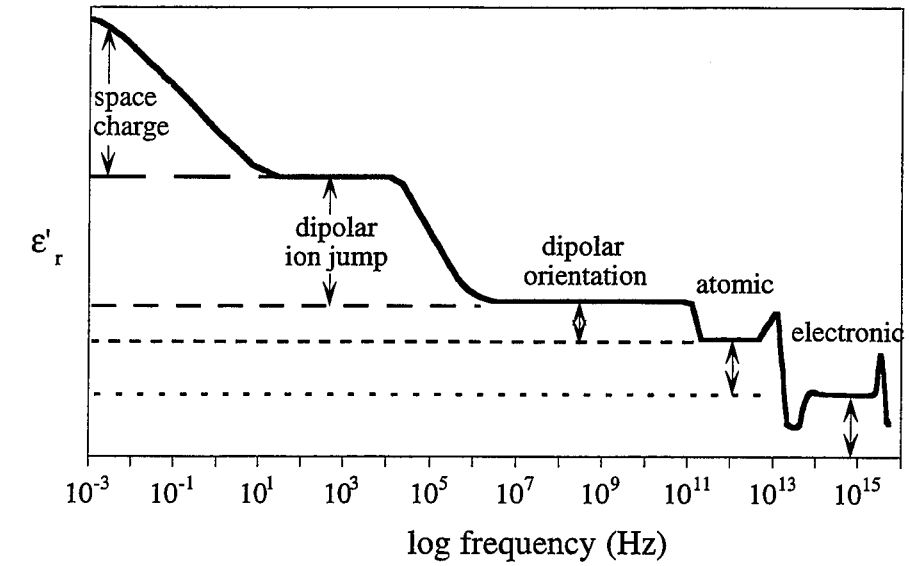

a)

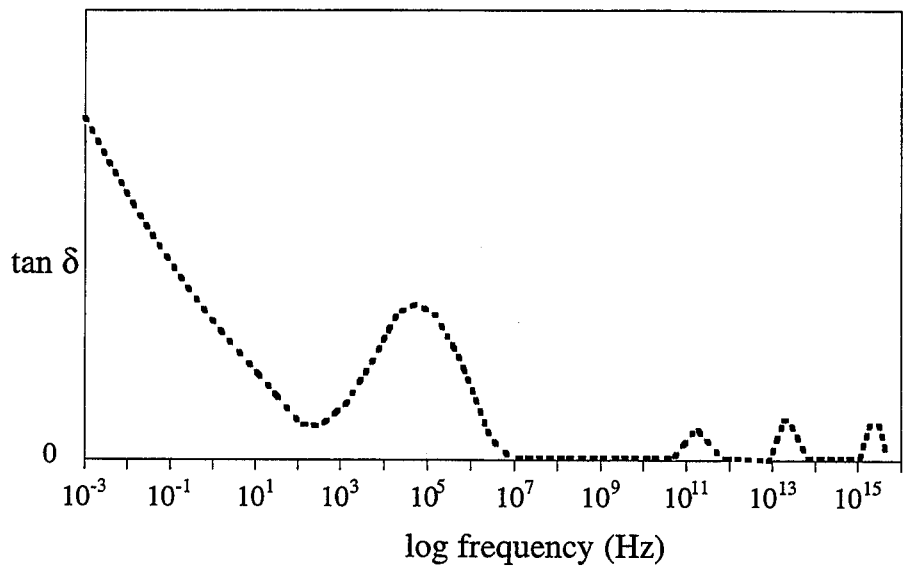

b)

Figure 5.7 Frequency dependence of the polarization mechanisms in dielectrics showing the relationship between a) the permittivity and b) the loss tangent

It can be shown that a relaxation which occurs in a certain frequency range will be shifted to higher frequencies as the temperature is increased. Loss peaks in the frequency domain must appear as peaks somewhere in the temperature domain. In this work, the complex permittivity was measured continuously in the temperature domain for several frequencies.

Two sets of peaks in the dielectric loss and loss tangent for undoped bismuth titanate are observed in Figure 5.8a and 5.8b, respectively. It is clear, when one compares the relative permittivity and the dielectric loss (Figures 5.4 and 5.8a), that the anomalies are related. The frequency dispersions indicate two relaxational processes and perhaps a third at higher temperatures.

One set of peaks can be clearly distinguished between 50 and 500 °C, especially in the loss tangent (Figure 5.8b), which is shown in more detail in Figure 5.9. The second set of peaks occurred at higher temperatures, where conduction losses interfere with resolution of the peaks.

According to the Debye model*, the reciprocal frequency of each peak gives the relaxation time, τ (sec).[154] When the log of the relaxation times are graphed versus the reciprocal of the temperature, a straight line is observed as shown in Figure 5.10. The relaxation fits an Arrhenius relationship where the slope is equal to the activation energy as in equation 5.3.[159]

equation 5.3 $$\tau = \tau_0 \exp\left(\frac{E_a}{KT}\right)$$

A single relaxation time and activation energy was sufficient to describe the behavior in Figure 5.9. The activation energy was 0.73 eV with a time constant t_0 of 1.1 $x10^{-11}$ sec (frequency of 0.9 x 10^{11} Hz) for TF bismuth titanate. These values were not significantly affected by the choice of raw materials or the grain size. The reciprocal of the time constant compares well with the frequency of the lattice for ionic solids from 1 $x10^{11}$ to 1 $x10^{14}$ Hz.[97,154] These are parameters indicative of ionic jump relaxation.[97,159]

---

* The Debye model usually refers to the frequency domain, but it is also valid for the temperature domain.[97]

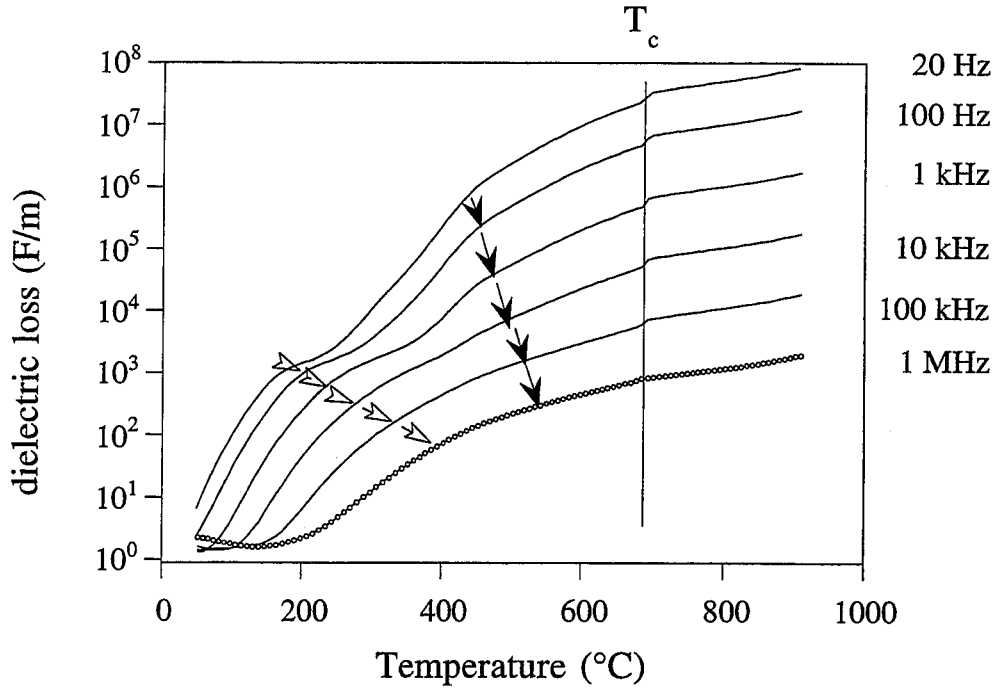

Figure 5.8a) Dielectric loss in bismuth titanate as a function of temperature and frequency showing two frequency dependent peaks. This behavior can be compared with the permittivity in Figure 5.4.

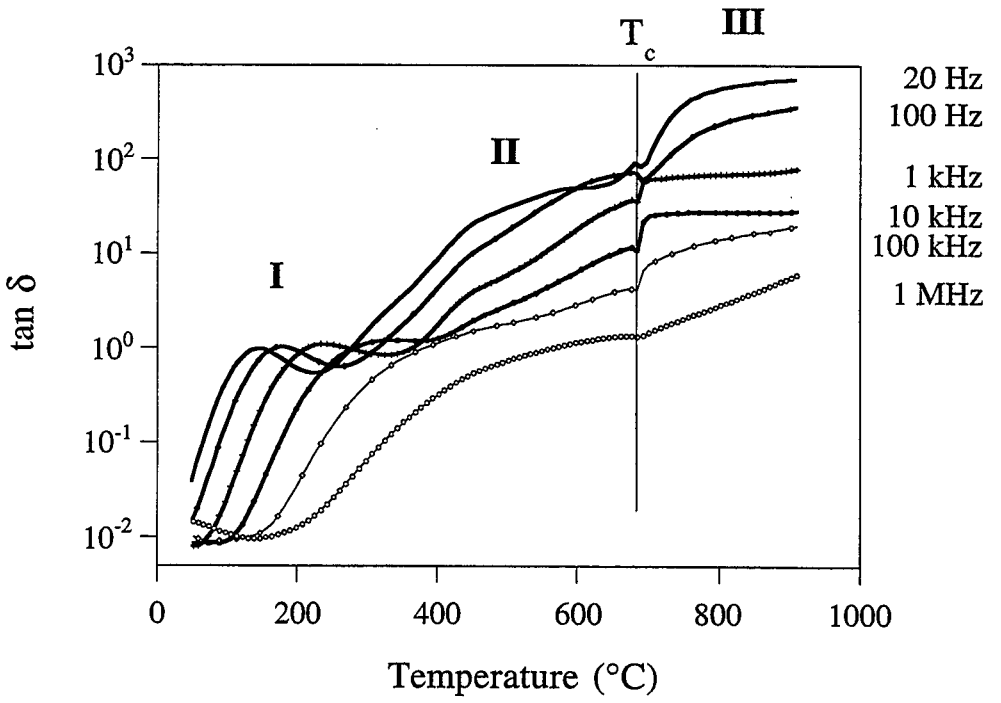

Figure 5.8b) Dielectric loss tangent in bismuth titanate as a function of temperature and frequency clearly showing the low temperature set of frequency dependent peaks. Note regions I, II, and III are referred to in the text.

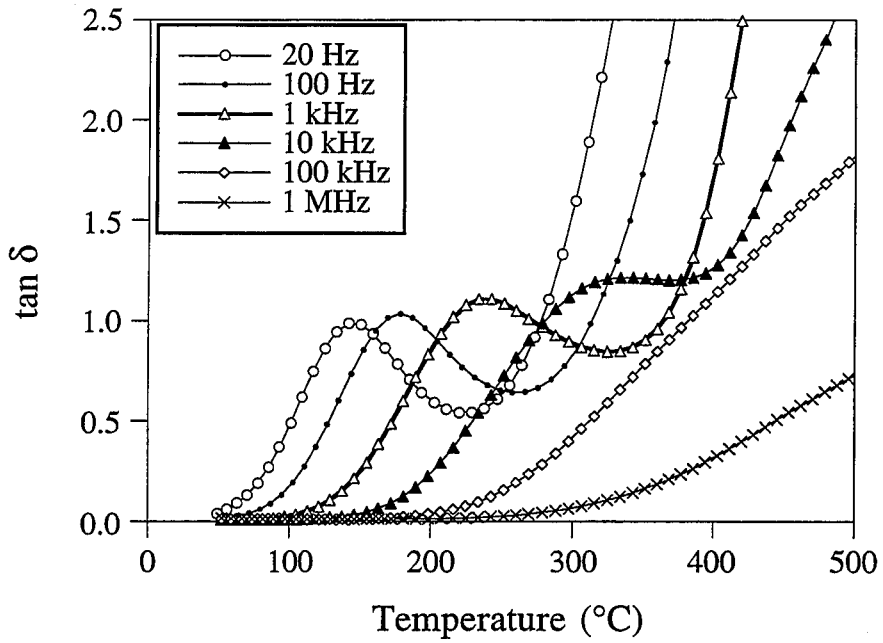

Figure 5.9. Details of the dielectric loss tangent as a function of temperature (from Figure 5.8b).

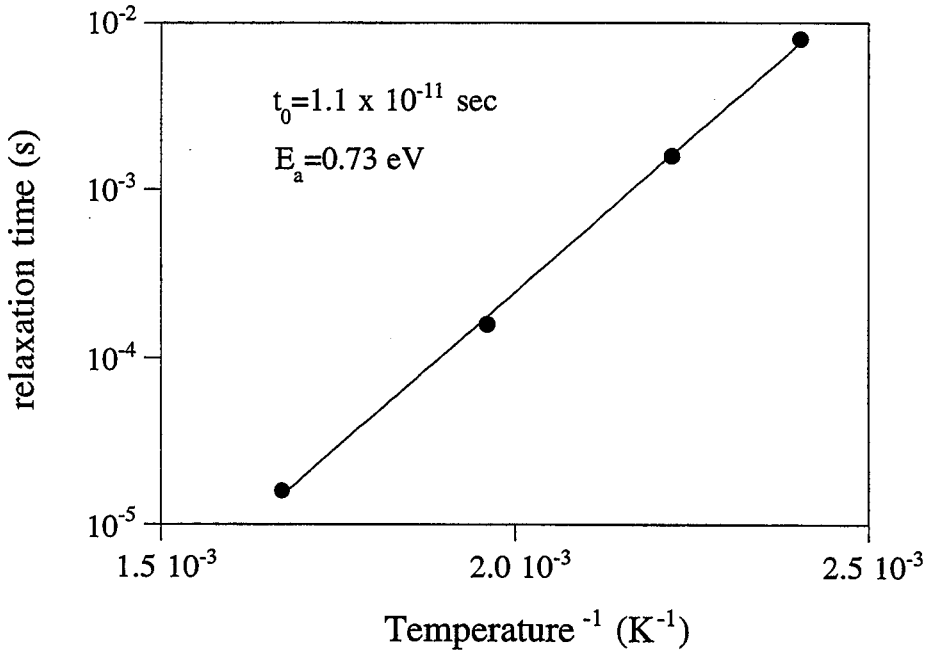

Figure 5.10 Relaxation time for each peak (from Figure 5.9) **versus reciprocal temperature for the peak showing an Arrhenius relationship.**

Seth and Schultz[19,25] observed three relaxations from the complex impedance. They attributed the two relaxations in the intermediate and high temperature regions (II and III) to ionic motion resulting in ionic polarization. The low temperature relaxation (I) was attributed to space charge polarization at the grain boundaries, however, their data was not conclusive in this temperature range.

Evidence given here, shows that the low temperature relaxation (region I) is characteristic of ionic motion. Much lower values of τ_o ($<10^{-14}$ s) than were measured ($\sim10^{-11}$ s), can be expected from space charge polarization.[154] Furthermore, the low temperature relaxation occurs in single crystals which do not contain grain boundaries.[20]

The dielectric properties were not affected by the type of electrode (Au vs. Pt) which suggests that space charge at the electrodes was not responsible for the dielectric anomalies. Relaxation due to space charges at the surface of the electrodes was investigated by Sinyakov, et al.[24] These authors determined that the potential of the high voltage polarization becomes zero at temperatures above 250 °C in single crystal bismuth titanate. They concluded that the dielectric anomaly (region I) cannot be due to space charge polarization.

It appears that the relaxations, two of which (regions I and II) add to the anomaly in the relative permittivity at ~550 °C, are caused by an ion jump mechanism. This ionic motion must be a local phenomenon which does not promote significant DC ionic conduction, since it has been demonstrated that the conductivity is predominantly p-type and electronic.

Further investigation of the relaxation mechanism was conducted on hot forged bismuth titanate in the **c**-direction and **ab**-directions, as shown in Figure 5.11. Representative microstructures of these samples can be found in Chapter 3. The hot forged samples had a Lotgering orientation factor of 0.70 ± 0.02. Since the alignment was not complete, one would expect the **ab**-directions to have some influence on the properties in the hot forged **c**-direction, and visa versa. Distinct peaks were not observed in the dielectric loss tangent in the **c**-direction, but were clearly observed in the **ab**-direction.

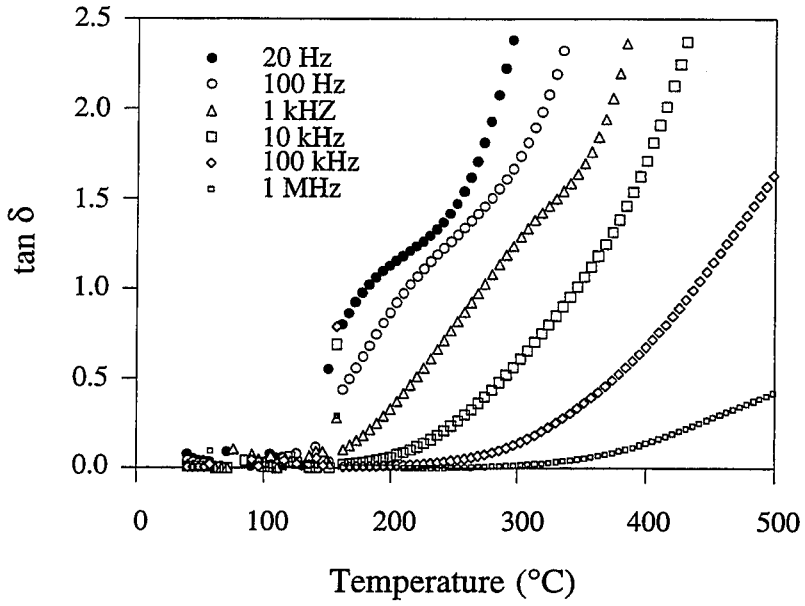

a) Measurement parallel to the hot forging direction which gives the c-direction. Due to the non-perfect alignment, Lotgering factor of 0.7, one would expect the **ab** plane to have some influence on the properties.

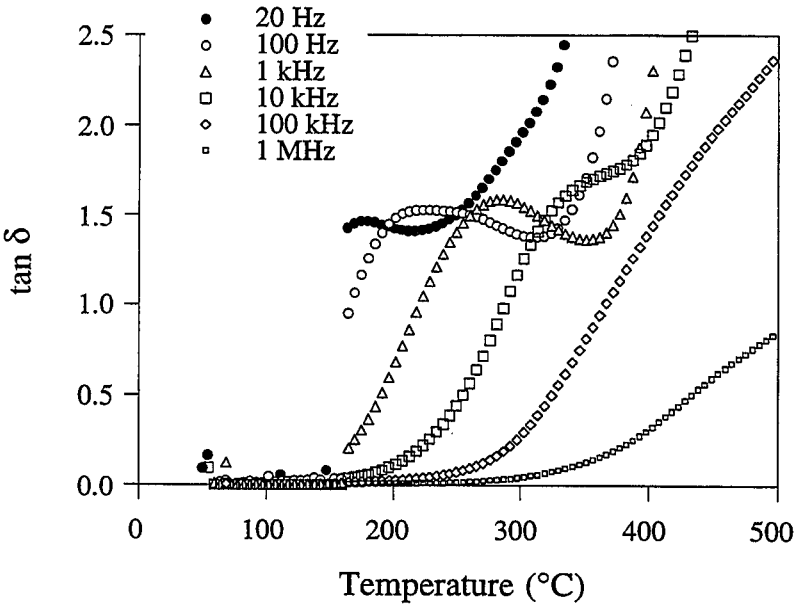

b) This measurement direction represents the ab plane. Relaxation peaks are evident.

Figure 5.11 Dielectric loss tangent versus temperature in hot forged bismuth titanate for six frequencies.

An activation energy of 0.87 eV and a time constant, τ_o, of $1.7x10^{-12}$ sec ($6x10^{11}$ Hz) were calculated from the frequency and temperature dependence of the peaks in dielectric loss tangent in the **ab** plane. (Figure 5.11b). This is in good agreement with parameters attributed to an ionic jump mechanism in the randomly oriented ceramic and strongly suggests that the ionic motion occurs preferentially in the **ab** plane. This agrees with the result of Seth, et al.[19] who studied the directionality of the dielectric properties in bismuth titanate oriented by tapecasting.

Evidence was presented in Chapters 3 and 4 that oxygen is more mobile than the cations in bismuth titanate. It is proposed here that oxygen ions are responsible for the ionic jump mechanism causing the low temperature relaxation. In the following section, oxygen vacancy formation in Nb doped bismuth titanate is shown to increase dielectric loss which supports this premise.

One can examine the positions, between which the oxygen ions may jump, from the bismuth titanate crystal structure. The positions of the ions and their respective valence states were given in Chapter 4, Figure 4.29 and Table 4.1. The activation energy for the relaxation can be viewed as an energy barrier which separates two equivalent ion positions.

There are eight nearly equivalent oxygen positions in the perovskite layer with a valence state of -2.03 ± 0.03. Several possibilities can be envisioned for oxygen ions to switch positions with neighboring vacant sites in the perovskite layer. The direction of many jumps, e.g. O(1)->O(3)->O(1)', would be roughly 45° from the **a**- or **b**-direction. If this motion were responsible for the low temperature relaxation, the relaxation would be observed in the **c**-direction as well as in the **ab** plane, which was not the case. This mechanism may be responsible for one of the higher temperature relaxations. In fact, dielectric data from Sinyakov, et al.[24] indicates a **c**-direction relaxation in single crystal bismuth titanate at higher temperatures. Jumps such as O(1)->O(1)->O(1)', do not have a component in the **c**-direction. This motion represents a reasonable mechanism to explain the observed phenomena in the low temperature regime.

Oxygen motion in the bismuth oxide layer can also be considered. The oxygen ions in this layer are either underbonded (O(2) and O(2)'), or overbonded (O(4) and O(4)'). Taking the O(2) ion as an example, there are three possible positions within the $(Bi_2O_2)^{2+}$ layer into which it can move. These are the O(2)', O(4), and O(4)' positions. The latter two are also part of the perovskite layers. Only the O(2)' position has a nearly equivalent charge, -2.30 compared to -2.36, for O(2). The direction of this jump lies exactly in the **ab** plane.

To summarize, one of the three relaxational processes observed in bismuth titanate was attributed to an ion jump relaxation. This occurred in the low temperature range (50-500 °C) and was observed in the **ab** plane in hot forged samples. It was proposed that this relaxation is due to the jump of oxygen ions. Several possible jump directions were considered.

5.3.3 Niobium doping and dielectric relaxation

In this section, the relationship between Nb doping and the low temperature dielectric relaxation is discussed.

It was shown in Figures 5.3 to 5.6, that Nb doping suppressed a frequency dependent peak in relative permittivity. The dielectric loss tangent for 0.74 at% Nb doped bismuth titanate in the low temperature region (I) in Figure 5.12 can be compared to undoped bismuth titanate in Figure 5.9. The relaxation, which was attributed to an ion jump mechanism, was suppressed with Nb.

To test the premise that oxygen vacancies are responsible for the ion jump relaxation, the effect of oxygen vacancies was studied by reducing a highly Nb doped bismuth titanate sample in a vacuum (10^{-8} atm) for 4 hours at 400 °C. The dielectric loss tangent as a function of temperature before the treatment is given in Figure 5.12 and after the treatment in Figure 5.13. The loss tangent increased drastically with the treatment in vacuum and several peaks can be observed.

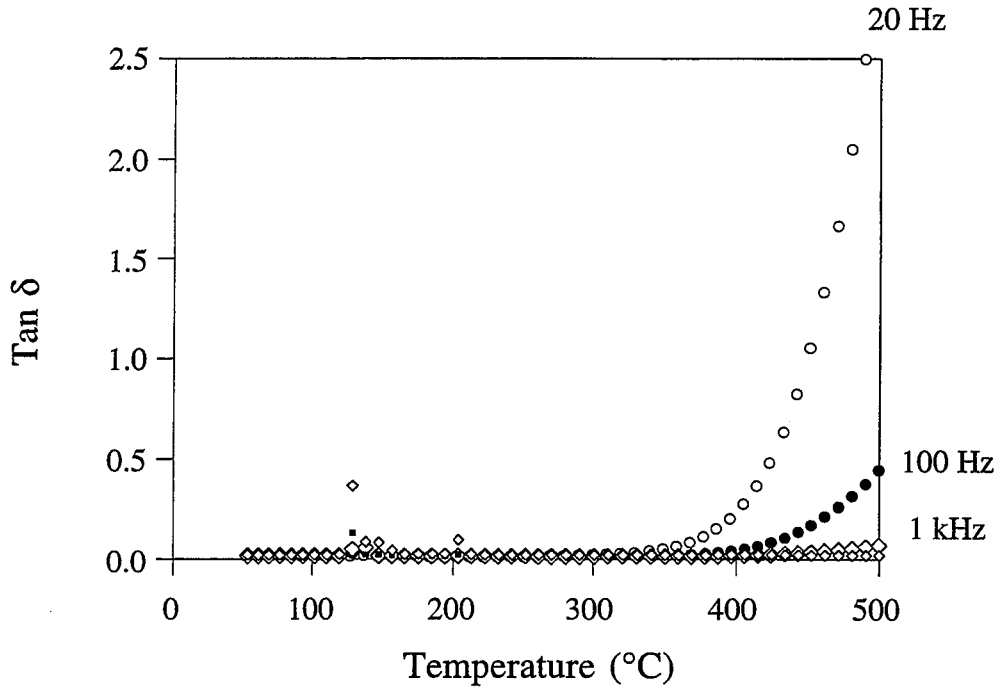

Figure 5.12 Dielectric loss tangent as a function of temperature and frequency in highly Nb doped bismuth titanate showing very low loss.

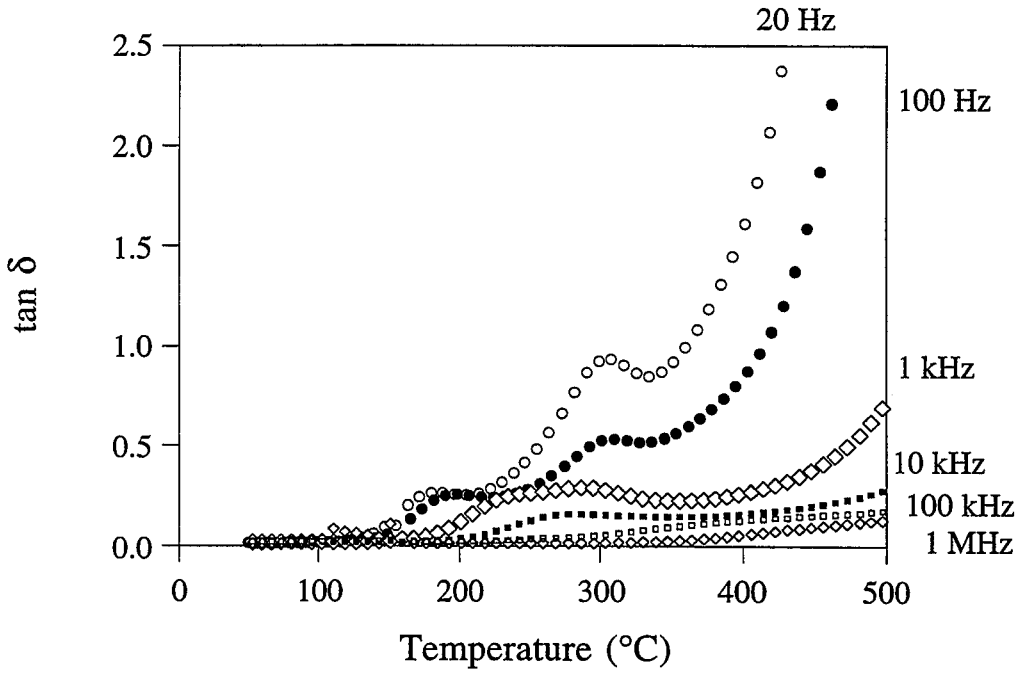

Figure 5.13 Dielectric loss tangent as a function of temperature and frequency for the highly Nb doped bismuth titanate from Figure 5.12 after annealing in a reducing atmosphere. Increased loss and relaxation peaks are evident.

It is clear from Figures 5.12 and 5.13 that the oxygen vacancy concentration has an impact on the dielectric loss, however, the introduction of oxygen vacancies was not sufficient to produce exactly the same phenomena as in undoped bismuth titanate. This suggests that the mobility of oxygen vacancies (as well as the concentration) decreases with Nb doping. In chapter 4, section 4.7, it was indicated that lightly Nb doped bismuth titanate loses oxygen slowly during sintering. Nb also shifts the equilibrium to lower concentrations of oxygen vacancies. This combination may lead to a suppression of the oxygen ion jump relaxation.

In the previous section, the positions of oxygen ions and the possible jump directions was discussed. Niobium replaces Ti in the perovskite layer and also appears to inhibit the motion of oxygen. These observations favor the mechanism of ion jump relaxation in the perovskite layer.

In summary, Nb suppressed the low temperature dielectric relaxation in bismuth titanate. This was attributed to the suppression of oxygen vacancies and a decrease in the mobility of oxygen.

5.4 Poling Conditions for Bismuth Titanate Ceramics

The initial premise in this work was that bismuth titanate could withstand higher poling fields if the conductivity were decreased, and that as a result, dipole alignment would be improved. A distinction is made between the poling regime and the polarization process. The former refers to the time, temperature, and field which the material can withstand before electrical breakdown, while the latter refers to the effect of these conditions on the domain structure. The poling regime is discussed in this section, and the effect of Nb on the piezoelectric response is discussed in section 5.5. The literature can be consulted for a description of electrical breakdown and polarization in ferroelectric ceramics.[38,45,154]

5.4.1 Poling procedure

Electroded samples were poled in a heated silicon oil bath (Haake S F3 Fisons). The field was applied with a Sensor Technologies Hipotronics 9065 Power supply. Electric fields between 5 kV/cm and 80 kV/cm with temperatures from 100 °C to 240 °C were investigated.

Optimum poling conditions were considered to be the temperature and field at which d_{33} was maximized. For undoped bismuth titanate, the poling conditions were determined by electrical breakdown. It was found experimentally that a field of 70 kV/cm at 200 °C was sufficient to pole the Nb doped BIT compositions*. Higher temperatures and fields did not significantly increase d_{33} and often led to electrical breakdown.

5.4.2 Poling regime

The effect of Nb doping on the poling regime is shown schematically in Figure 5.14. With Nb dopant (0.05-0.74 at%) samples could be poled in a field of up to 80 kV/cm and 240 °C without electrical breakdown. In contrast, a maximum field of 20 kV/cm was applied at 125 °C to undoped bismuth titanate, although, in most cases electrical breakdown occurred at much lower fields. In addition, the time before electrical breakdown was usually less than five minutes, even for fields as low as 5 kV/cm. Due to the erratic behavior, no correlation could be found between electrical breakdown and the type of electrodes (Au vs. Pt), sample thickness, grain size, or raw materials in undoped bismuth titanate.

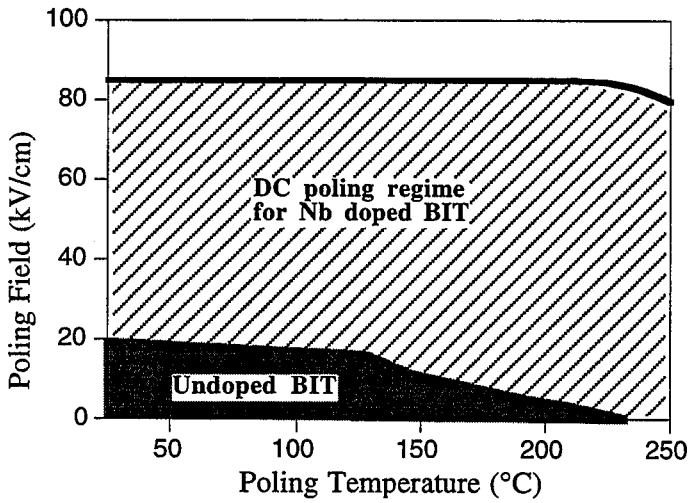

Figure 5.14 Comparison of the poling regime for undoped and Nb doped bismuth titanate.

* One exception to this rule was for Nb doped BIT with high conductivity. This subject is discussed in section 5.5

One might question whether Nb has an effect other than decreasing the conductivity which is significant for establishing the poling regime*. In Chapter 4 (section 4.7), a large grain 0.05 at% Nb doped sample was as conductive as the fine grain undoped bismuth titanate. This Nb doped material could not withstand the typical poling regime. It was found that the conductivity could be decreased by annealing in oxygen. The standard conditions of 70 kV/cm at 200 °C for 30 minutes could then be applied to the sample without electrical breakdown. This demonstrates the importance of the conductivity on the poling regime, however, does not address other possible effects of Nb on the domain configuration and alignment.

To summarize, it was established that Nb doping allowed the application of higher poling fields for longer times and at higher temperatures than was possible in undoped bismuth titanate. It was shown that the decrease in conductivity with Nb was an important factor in the improved poling regime.

5.5 Analysis of the Complex Piezoelectric Coefficient

The piezoelectric coefficients are formally expressed in the Maxwell relations for the thermodynamic equations of state.[32] In the following sections, only the longitudinal piezoelectric coefficient, (d_{33}) is discussed.

The electrical response due to the direct piezoelectric effect is expressed in equation 5.4.

equation 5.4 $$\mathbf{P} = \mathbf{dX}$$

where **P** is the polarization, **X** is the stress, and **d** is a third rank tensor which represents the piezoelectric coefficients.

The converse effect can be expressed as follows:

equation 5.5 $$\mathbf{x} = \mathbf{dE}$$

where **x** is the strain and **E** is the electric field.

---

* The grain size effect is discussed in section 5.5.6.

5.5.1 Description of the complex piezoelectric coefficient

A desired feature for piezoelectric sensors is that a unique level of charge is produced by a given stress. One obtains a linear relationship between the charge and the force for an "ideal" piezoelectric, the slope of which gives the piezoelectric coefficient, d_{33} (see Cady[27]). In real materials, an electro-mechanical hysteresis is often observed, so that, for example, a singular force can be correlated to two different charges.[160]

An example of the hysteretic behavior in the direct piezoelectric effect is given in Figure 5.15 for undoped bismuth titanate. In order to describe this behavior, the piezoelectric coefficient can be treated as a complex quantity, d_{33}^* in the following equations:

equation 5.6 $$\mathbf{d_{33}^* = d_{33}' - id_{33}''}$$

equation 5.7 $$\mathbf{d_{33}^* = d_0 e^{-i\delta_p}}$$

equation 5.8 $$\mathbf{d_0 = \sqrt{\left(d'^2 + d''^2\right)}}$$

where i is $\sqrt{-1}$. The real part of the piezoelectric coefficient, d_{33}' represents the ideal response, which can be taken from the slope of a linear fit to the curve in Figure 5.15. The imaginary part, d_{33}'' reflects an electro-mechanical relaxation.

A phase angle δ_p, can be measured from the difference in the time dependencies of the applied sinusoidal force, F, and the resulting charge, Q:

equation 5.9 $$\mathbf{F = F_0 \exp(i\omega\tau)}$$

equation 5.10 $$\mathbf{Q = Q_0 \exp\left[i\left(\omega\tau - \delta_p\right)\right]}$$

such that:

equation 5.11 $$\mathbf{d_0 = \frac{Q_0}{F_0}}$$

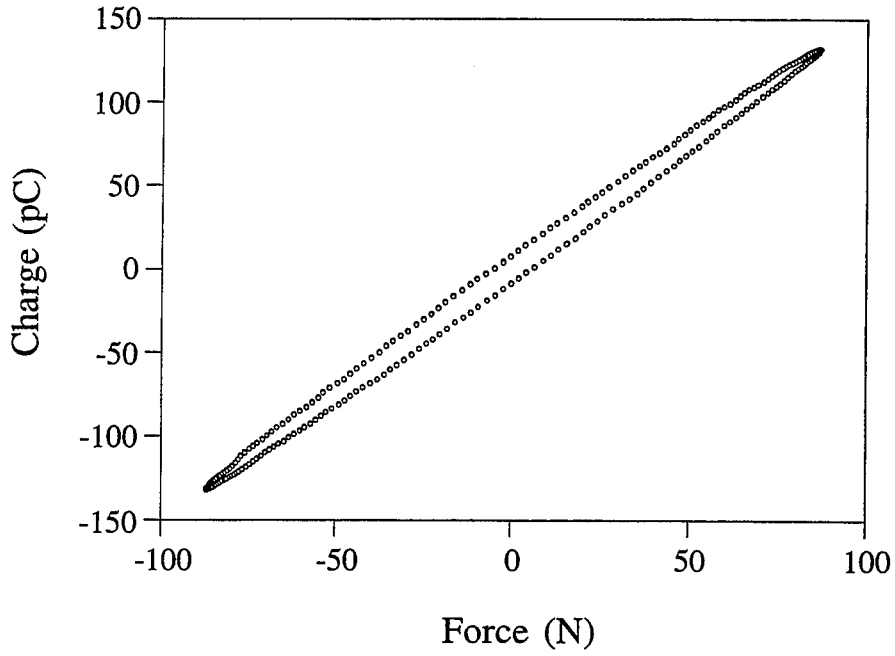

Figure 5.15 An example of the hysteresis between the force and charge in an undoped $Bi_4Ti_3O_{12}$ ceramic.

The hysteresis can be quantified by the piezoelectric phase angle, δ_p, or by the piezoelectric tangent, tan δ_p:

equation 5.12 $$\tan\delta_p = \frac{d_{33}''}{d_{33}'}$$

The superscript denoting the real part (d_{33}') will be dropped. This will be referred to as the piezoelectric coefficient, d_{33}. The phase angle and the tangent are sometimes referred to as "piezoelectric loss" and the "piezoelectric loss tangent" in the literature (e.g.[161]). The term "loss" is used from the analogy with mechanical and dielectric loss, however, it may not represent an accurate description of a physical mechanism. Damjanovic and Demartin[162] and Damjanovic, et al.[163] have demonstrated that for the case of domain wall pinning in weak field conditions, the treatment described above gives a reasonable first approximation of behavior which is better described by the Rayleigh Law.

It has been demonstrated that electrical and mechanical losses in ferroelectric ceramics are linked and originate from the same loss mechanism.[159,164] It is believed that piezoelectric "loss" involves the coupling of the electrical and mechanical relaxations and therefore also originates in the same mechanism.[23] There is now substantial evidence in the literature that the motion of non-180° domain walls contributes to the phase angle observed in the electrical, mechanical, and electro-mechanical response.[159,160,162,164-169] Other mechanisms responsible for relaxation in dielectrics, such as dipolar re-orientation and space charge migration, may also lead to mechanical and piezoelectric relaxation somewhere in the stress/charge regime.

5.5.2 Piezoelectric measurements

The piezoelectric coefficient d_{33} was measured using a configuration which consisted of a dynamic press with two charge amplifiers, a Hewlett Packard 3245A universal source, and a high voltage amplifier from Physik Instrumente. A sinusoidal pressure using an HP universal source for frequencies from 0.1 Hz to 100 Hz and voltages from 1 V to 10 V was applied through a PZT actuator in the dynamic press. The applied pressure was measured via a reference quartz sensor that was placed in between the sample and the source of alternating force. The resulting waveforms from the quartz reference and piezoelectric ceramic (direct piezoelectric effect) were analyzed on a Tektronix TDS 410 Digitizing Oscilloscope. A static pressure of 15 MPa was applied to ensure a good transfer of force between the source, the sample, and the reference sensor. The latteral effects of DC pressure on d_{33} in bismuth titanate may be neglected since d_{31} is small compared to d_{33} ($d_{33}/d_{31}>10$). If this were not the case (e.g. PZT), thick samples would be required to decrease the error with this measurement.

5.5.3 Niobium concentration

It was shown that Nb doping decreased the conductivity so that a higher poling field could be applied to bismuth titanate ceramics. The improved poling regime was expected to produce higher piezoelectric coefficients. This is demonstrated in Figure 5.16a, where the d_{33} increased with Nb doping. The notable sample variation is explored in the next section.

The magnitude of the piezoelectric coefficient saturated at approximately 20 pC/N with 0.53 at% Nb dopant. The maximum d_{33}, ~ 20 pC/N, agrees well with values for pulse poled bismuth titanate[19] and an earlier report on Nb doped bismuth titanate.[15]

In Figure 5.16b, the piezoelectric tangent *increased* with 0.05 at% Nb dopant and then *decreased* to zero with further Nb additions. A high piezoelectric coefficient was achieved with even slight Nb doping, however, at least 0.5 at% Nb was required to suppress the piezoelectric relaxation in bismuth titanate. The origins of this relaxation are explored further in the following sections.

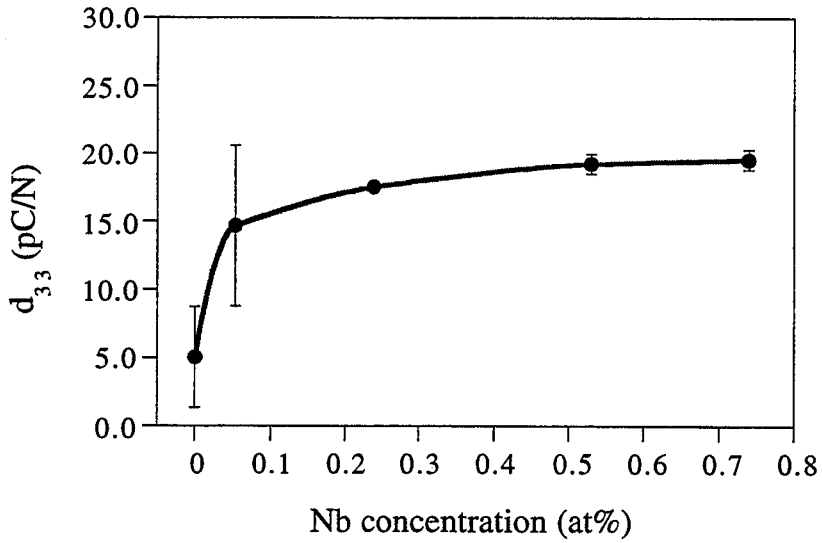

a)

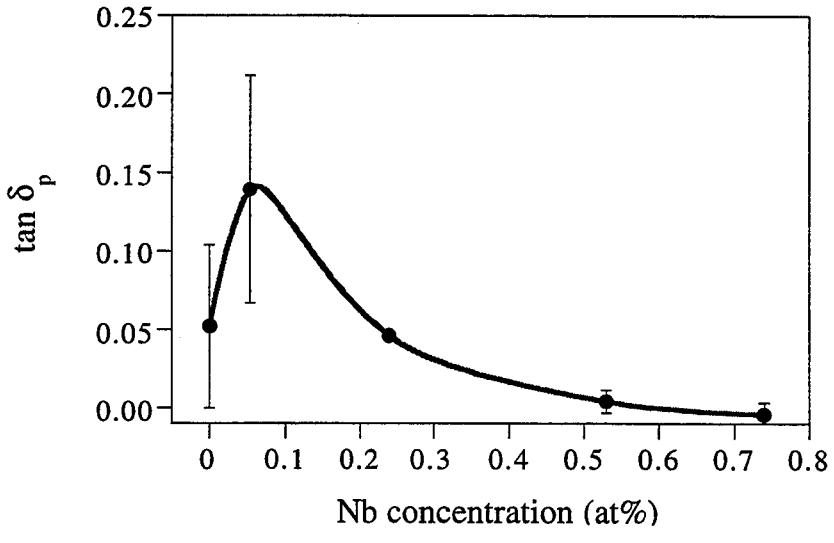

b)

Figure 5.16 a) piezoelectric coefficient and b) piezoelectric tangent as a function of Nb concentration. The error bars represent twice the standard deviation calculated from at least 6 samples with equivalent processing treatments. The 0.24 at% Nb composition was an exception with only two sample measurements. The error indicates sample variation. The measurement error was $< \pm 1$ pC/N for d_{33} and $< \pm 0.003$ for tan δ_p.

In summary, Nb doping was an effective method of producing polarizable bismuth titanate ceramics (in a DC field) with a d_{33} of ~20 pC/N. The addition of at least 0.53 at% Nb was required to obtain a reproducible response without any measurable piezoelectric relaxation. Anomalous effects of Nb (0.05 at%) on the sample variation and piezoelectric tangent were noted.

5.5.4 Sample variation

At this juncture, it is useful to analyze the sample-to-sample variation from the piezoelectric measurements.

The graphs in Figures 5.17 and 5.18 show the measured d_{33} and tan δ_p for 7 samples of 0.05 at% Nb and 6 samples of 0.74 at% Nb doped bismuth titanate. The samples from each composition underwent similar processing, electroding, and poling, and had similar sample dimensions. All of the samples of one composition were prepared from the same batch. All of the 0.05 at% Nb doped samples were sintered at 1100 °C for 1 hour. The 0.74 at% Nb bismuth titanate samples were sintered at 1130 °C for one hour. The piezoelectric measurements were taken with 15 MPa of static pressure and 5 MPa alternating pressure (amplitude) at 1 Hz.

One factor which complicates the reproducibility is the effectiveness of poling. In undoped bismuth titanate, one might expect considerable variation in the d_{33} from the erratic behavior during poling. For 0.05 at% Nb doped samples, the poling was performed with a standard method (70 kV/cm at 200 °C for 30 min) and yet a great deal of variation in d_{33} and tan δ_p was observed.

The piezoelectric coefficient in 0.05 at% Nb doped samples varied from 11 to 20 pC/N. This range of 9 pC/N corresponded to a tangent which ranged from 0.050 to 0.150 with no obvious correlation between tan δ_p and d_{33}. In contrast, for higher concentrations of Nb (0.5-0.7 at%), the sample range for d_{33} was less than 1 pC/N and the tangent varied by less than 0.004.

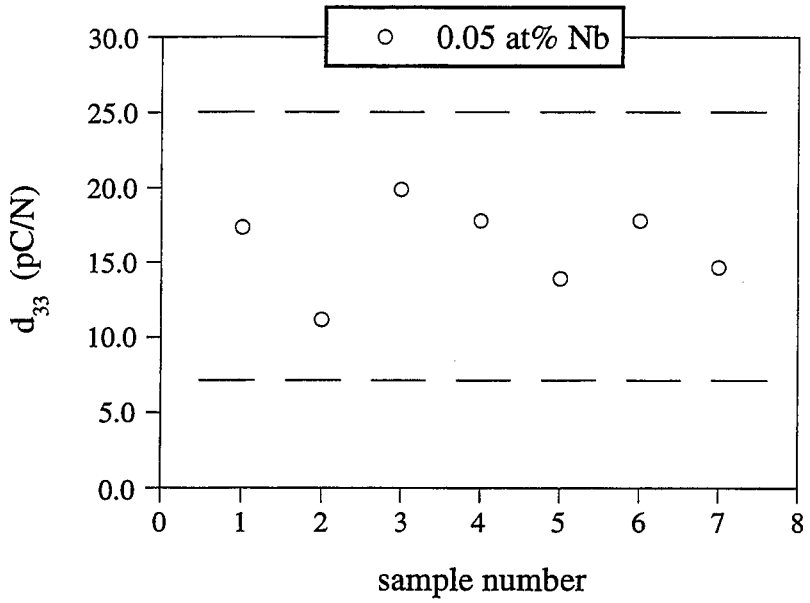

a) d_{33} in 0.05 at% Nb doped bismuth titanate.

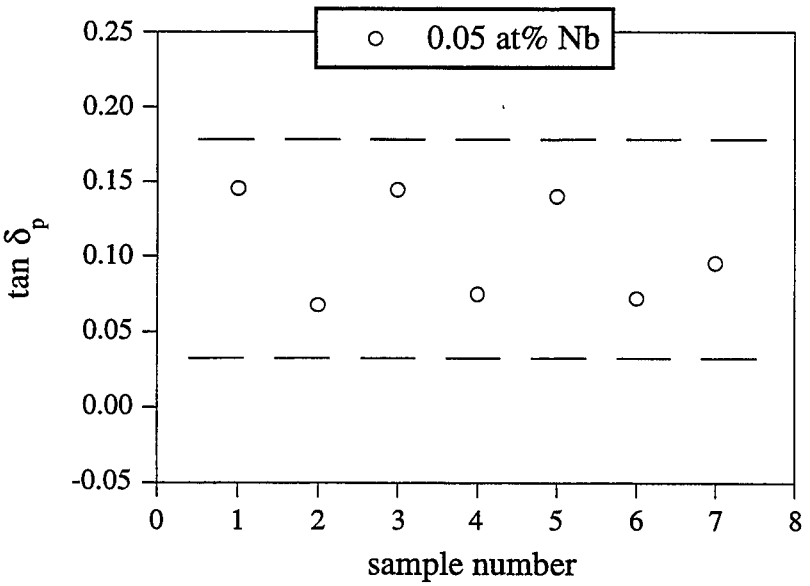

b) tan δ_p in 0.05 at% Nb doped bismuth titanate.

Figure 5.17 Analysis of the sample reproducibility for a low Nb dopant level. The piezoelectric coefficient and piezoelectric tangent show very large confidence intervals ($\pm 2\sigma$) due to sample variation. The measurement error was $< \pm 1$ pC/N for d_{33} and $< \pm 0.003$ for tan δ_p.

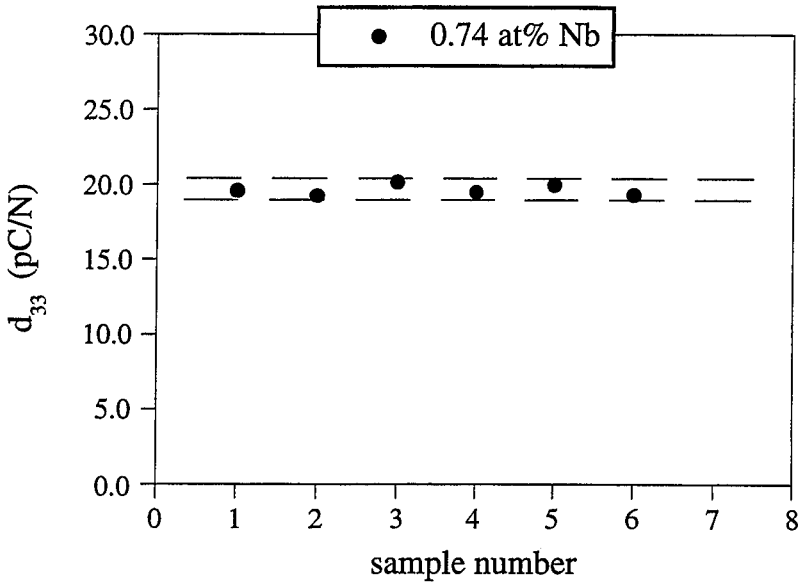

a) d_{33} in 0.74 at% Nb doped bismuth titanate.

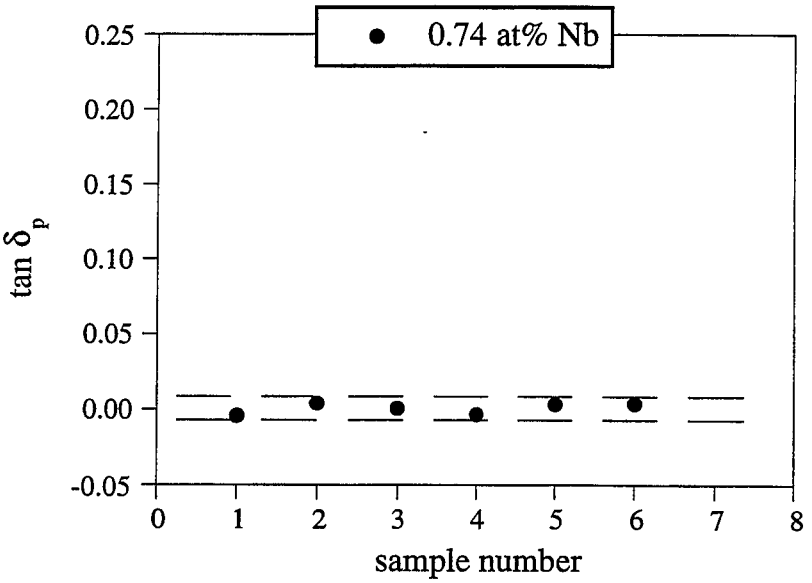

b) tan δ_p in 0.74 at% Nb doped bismuth titanate.

Figure 5.18 Analysis of the sample reproducibility for a high Nb dopant level. The piezoelectric coefficient and piezoelectric tangent show very small confidence intervals ($\pm 2\sigma$) which are on the order of the measurement error.

One possible explanation is that the dopant was not evenly distributed during powder preparation. Samples with slightly less Nb in the 0.05 at% doped composition could behave more like undoped bismuth titanate with a very low d_{33}, hence, a slight difference in composition could cause a large difference in d_{33}. A problem with this argument is that all of the Nb doped samples supported the normal poling conditions while undoped bismuth titanate did not. The original premise was that the conductivity prevented polarization of BIT, not that the d_{33} was inherently low. This does not rule out the possibility that variations in the Nb concentration affect the polarization through some other process, such as domain wall displacement.

Another possible explanation for the observed behavior is that Nb affects the domain structure differently in low or high concentrations. One would expect most 180° domain walls to be eliminated during polarization, while non 180° domains often remain. Variation in the type and amount of non-180° domains may cause a variation in the piezoelectric properties in the lightly Nb doped composition.

Highly doped bismuth titanate (0.74 at% Nb) showed minimal sample variation on the order of the measurement error. This demonstrates the importance of the Nb concentration on the sample reproducibility. Since reproducible properties were observed with high concentrations of Nb, it suggests that a reproducible domain configuration was achieved during poling.

The highly Nb doped BIT was n-type, with an order of magnitude higher conductivity than the lightly doped composition. One possibility for the effect of Nb is that excess free charges stabilize the domain configuration during poling. Another possibility which is supported by the binding energy analysis in Chapter 4, is that a structural change prevents the formation of certain non-180° domain walls. The implications of this mechanism are explored further in the following sections.

5.5.5 Frequency dependence

Although the piezoelectric properties can be affected by sample variation for low levels of Nb doping, the trends shown were consistently obeyed within each composition. In Figure 5.19a, The piezoelectric coefficient measured at four frequencies (2 MPa AC and 15 MPa DC) is given as a function of the Nb concentration. It is clear that the piezoelectric coefficient was frequency dependent for Nb concentrations less than 0.5 at%.

The corresponding piezoelectric tangents are shown in Figure 5.19b, where the effect of Nb on the relaxation is observed. The tangent increased with 0.05 at% Nb and then decreased to essentially zero with 0.74 at% Nb. The frequency dependence of the piezoelectric tangent is also the most pronounced with 0.05 at% Nb. These data are consistent with a piezoelectric relaxation process which is eliminated at high concentrations of Nb.

A more detailed analysis of the frequency dependence of the piezoelectric properties is shown in Figure 5.20. There was no frequency dispersion for the piezoelectric coefficient with Nb dopant levels $\geq$ 0.53 at% and the tangent was nearly zero. The decrease in d_{33} for low Nb dopant levels implies that some piezoelectric contribution becomes less active as the frequency increases. The concurrent decrease in piezoelectric tangent indicates that a relaxing contribution inflates d_{33}. As the frequency increases, this extrinsic contribution cannot follow the field as effectively. In undoped bismuth titanate, the piezoelectric tangent has a different frequency dependence than for the lightly doped compositions which implies that a different mechanism is operative.

In summary, a frequency dispersion in the piezoelectric properties with low Nb dopant levels (0.05-0.21 at%) signifies a piezoelectric relaxation phenomenon which was eliminated with higher dopant levels (0.53-0.74 at% Nb) for these measurement conditions.

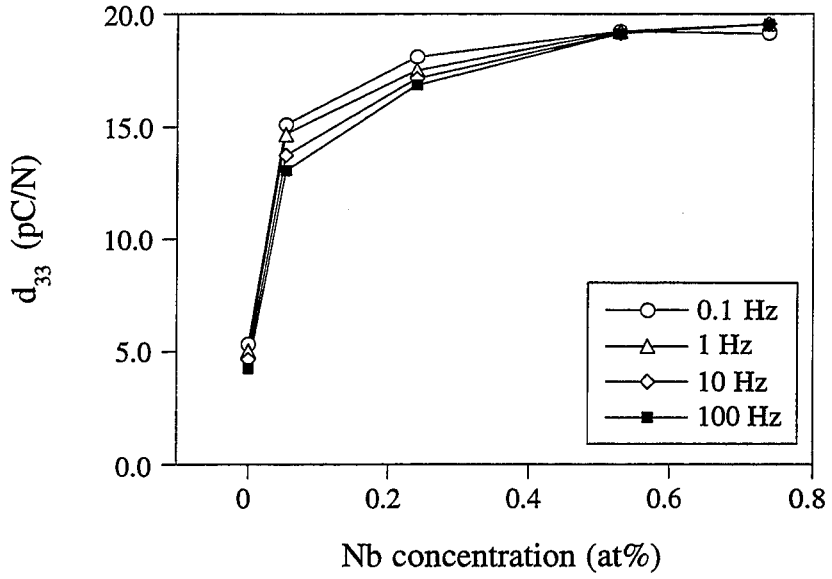

a)

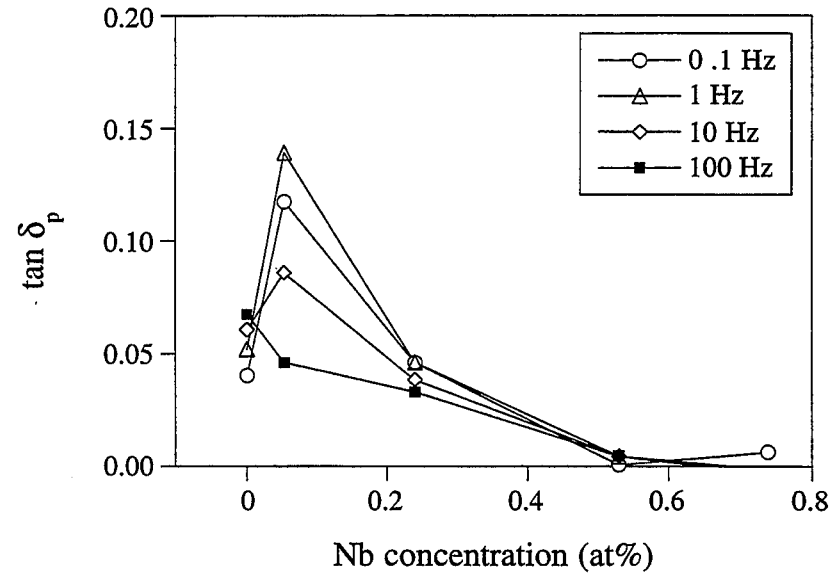

b)

Figure 5.19 a) piezoelectric coefficient and b) piezoelectric tangent in bismuth titanate as a function of Nb dopant at four frequencies
(2 MPa AC and 15 MPa DC).

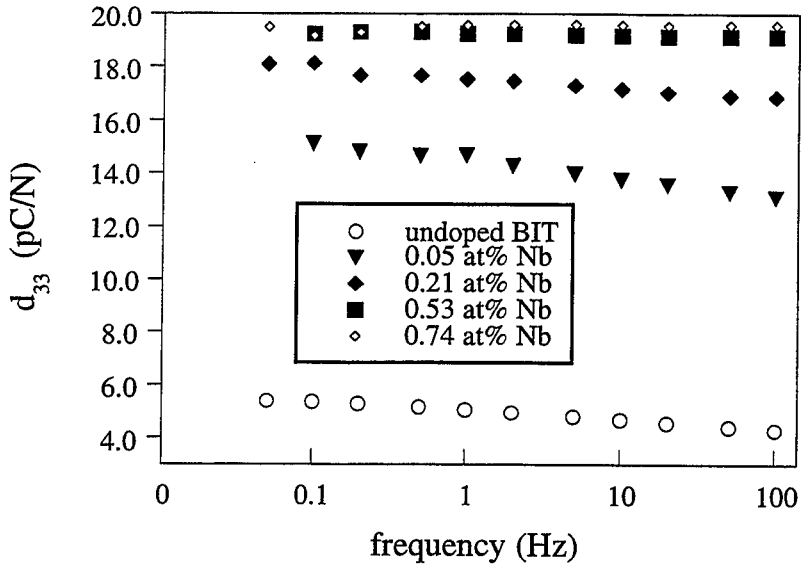

a) d_{33} diminishes with increasing frequency for Nb doping < 0.5 at%, but is frequency independent for Nb doping ≥ 0.53 at%.

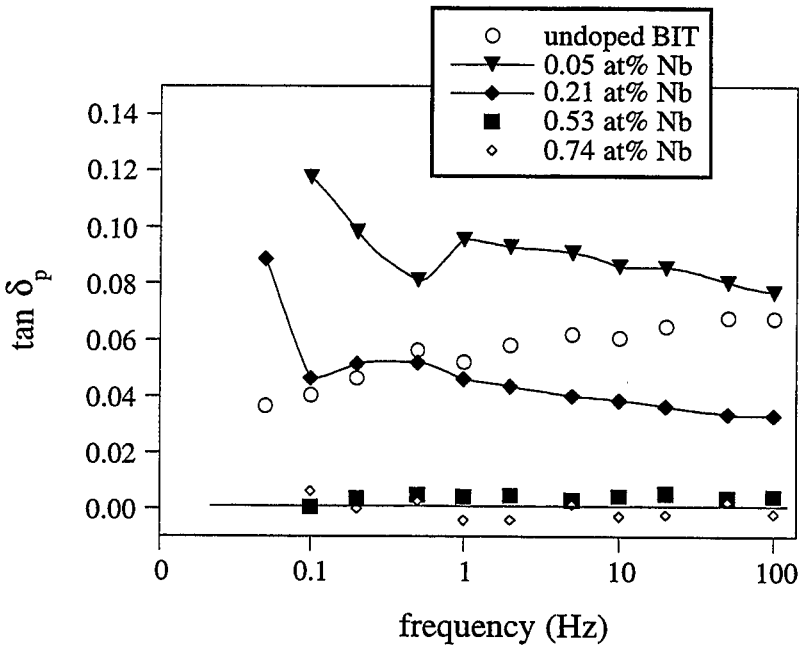

b) tan δ_p is independent of frequency for highly Nb doped compositions.

Figure 5.20 Frequency dependence of a) piezoelectric coefficient and b) piezoelectric tangent for undoped and Nb doped bismuth titanate (2 MPa AC and 15 MPa DC).

5.5.6 Alternating pressure

Another variable which is important for characterizing the piezoelectric properties is the amplitude of the alternating pressure. Ideally, the piezoelectric coefficient should be constant over a broad pressure range. One might expect, however, elastic contributions to be pressure sensitive.

In Figure 5.21 the piezoelectric coefficient and tangent are shown as a function of the amplitude of the alternating pressure, measured at 1 Hz with a static stress of 15 MPa, for undoped and Nb doped bismuth titanate. An increase in d_{33} was observed for bismuth titanate with low Nb dopant levels (0.05-0.21 at%). This is in contrast with the high dopant levels (0.53-0.74 at%) which were stable over the same pressure range. The piezoelectric properties of undoped bismuth titanate were fairly insensitive to the magnitude of the alternating pressure for these measurement conditions.

It is interesting to note that tan δ_p approaches zero rapidly as the pressure approaches zero for 0.05 and 0.21 at% Nb doping, while their is a slow rate of change for tan δ_p in undoped bismuth titanate (Figure 5.21b). This again suggests that different mechanisms control the relaxation.

In summary, a pressure dependence was demonstrated for the complex piezoelectric coefficient in bismuth titanate with low Nb dopant levels (0.05-0.21 at%). This is in sharp contrast with the properties of highly doped compositions (0.53-0.74 at%) which were independent of the amplitude of the alternating pressure. The piezoelectric response in undoped bismuth titanate was relatively insensitive to the AC pressure, however, a non-zero piezoelectric tangent was observed.

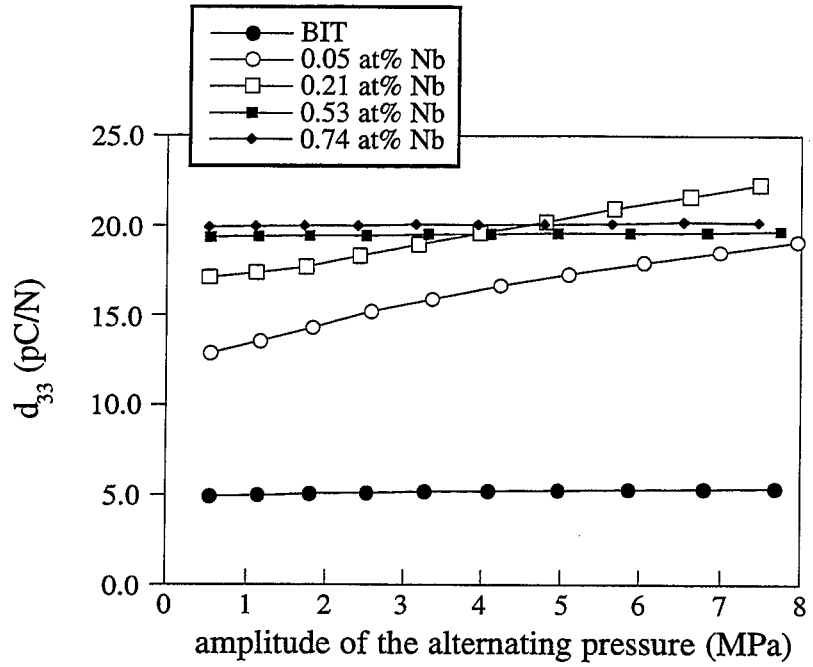

a)

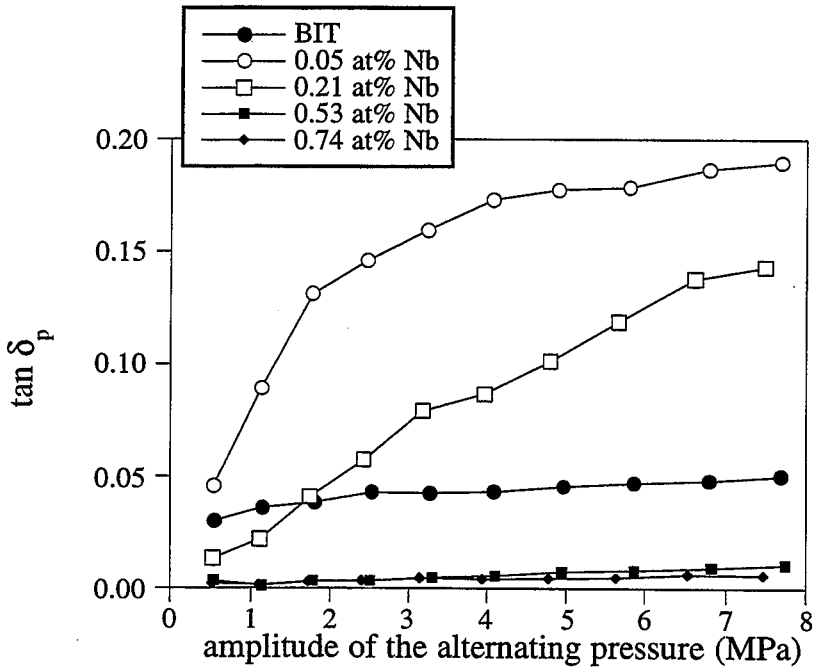

b)

Figure 5.21 Dependence of the a) piezoelectric coefficient and b) piezoelectric tangent on the amplitude of the alternating pressure for undoped and Nb doped bismuth titanate (15 MPa DC, 1 Hz).

5.5.7 The effect of grain size, conductivity, and partial polarization

It is well known that grain size plays an important role in domain configuration and can affect the dielectric and piezoelectric properties. In concentrations > 0.2 at%, Nb was a grain growth inhibitor, therefore, large grain ceramics could not be obtained for these compositions. A further complication exists since the conductivity of lightly doped compositions increased with grain growth. This is most significant in the composition with 0.05 at% Nb. The large grain samples could not be poled under the standard conditions. The effect of grain size on the polarization and complex piezoelectric coefficient is addressed in this section.

In Figure 5.22 the piezoelectric coefficient and tangent are shown as a function of sintering time. Increased sintering time represents an increase in grain size as discussed in Chapter 3. The piezoelectric coefficient increased with sintering time for undoped bismuth titanate, even though the conductivity also increased. The same trend was found in the other bismuth titanate compositions, TC and AC BIT. Samples with large grains poled more readily, (i.e. have improved domain wall motion).

It is interesting to note that for the samples sintered 10 hours, undoped bismuth titanate had a higher d_{33} (10.9 pC/N) than the 0.05 at% Nb doped BIT (4.8 pC/N) in spite of the order of magnitude higher conductivity. It appears that the alignment of dipoles, (i.e. domain wall motion) was more efficient in bismuth titanate. This suggests that the conductivity is not the only parameter which controls the polarization. Incomplete alignment of domains may contribute to the lack of reproducibility in lightly Nb doped bismuth titanate and the resulting low d_{33} values (< 20 pC/N).

The decrease in d_{33} after 10 hours of sintering for 0.05 at% Nb doped BIT corresponds to a poorly poled sample with high conductivity. The other samples were poled with the standard conditions and show sample variation typical of the composition. When the large grain sample (10 hour sintering) was annealed in oxygen, the conductivity decreased, and the sample was poled under the standard conditions. In Figure 5.22, it is shown that the d_{33} returned to a typical value of ~18 pC/N. There is no trend in this data which indicates a grain size effect on d_{33} in the 0.05 at% Nb doped bismuth titanate. When one considers the well poled oxygen

annealed sample, the piezoelectric tangent was also within the normal sample variation for this composition.

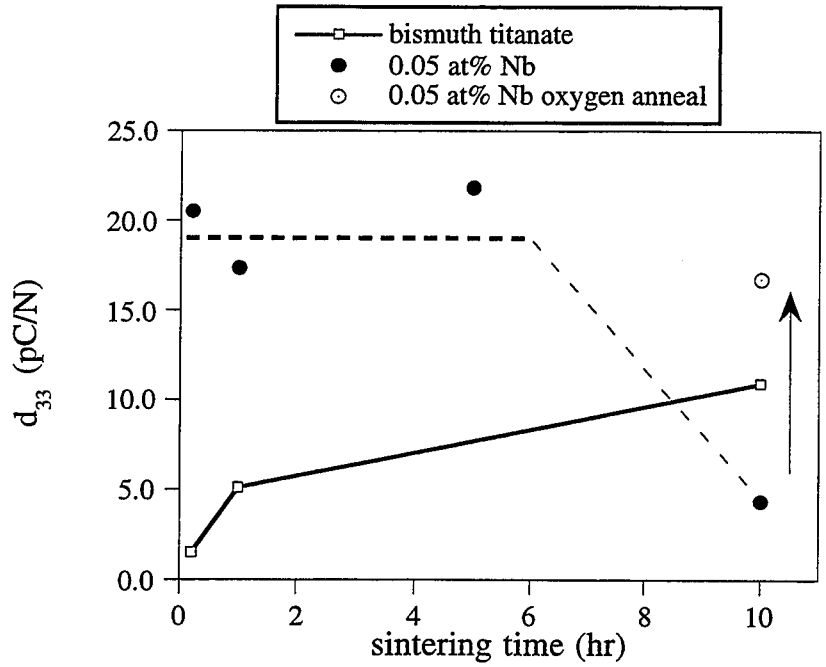

a)

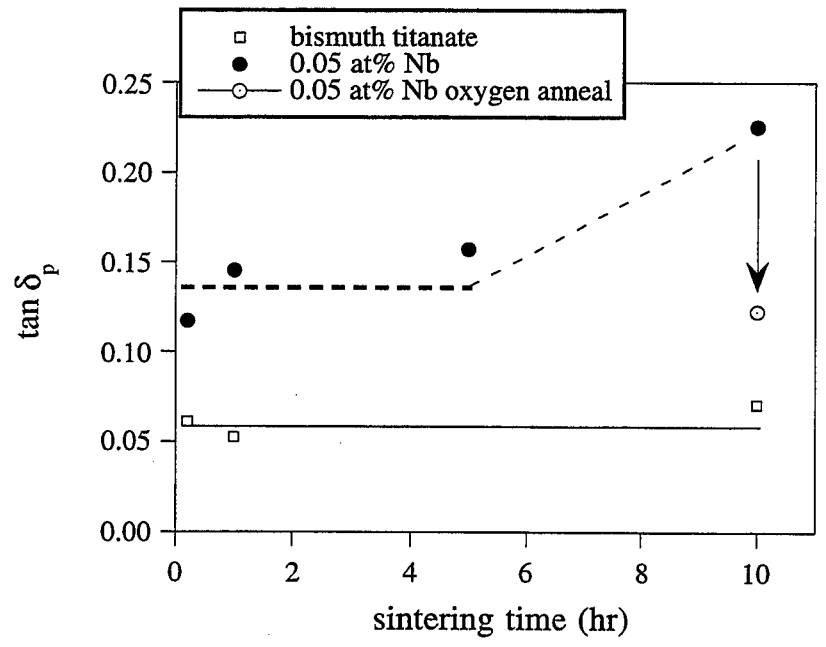

b)

Figure 5.22 Comparison of a) piezoelectric coefficient and b) piezoelectric tangent as a function of sintering time for undoped and 0.05 at% Nb doped bismuth titanate. (Representative microstructures for undoped BIT after 1 hour and 10 hours of sintering are found in Chapter 3, Figures 3.9c and f, respectively. The microstructure of 0.05 at% Nb doped BIT sintered 1 hour is shown in Figure 3.12b.)

There is no evidence of a grain size effect on the piezoelectric tangent, however, there was a significantly higher tangent for large grain 0.05 at% Nb doped bismuth titanate which was not well poled. This suggests that the high piezoelectric tangent is related to partial polarization, although the excess free charge may also be significant.

In Figure 5.23 the effect of partial polarization on the piezoelectric properties is observed. The piezoelectric coefficient increased with the poling temperature accompanied by a decrease in the piezoelectric tangent. This may explain why the partially poled sample showed an abnormally high tan δ_p, however, it was noted previously (Figure 5.17) that no correlation could be found between the d_{33} and tan δ_p for the sample variation. A contribution to the piezoelectric tangent from poor polarization may be most significant for very low poling levels (i.e. $d_{33} < 10$ pC/N).

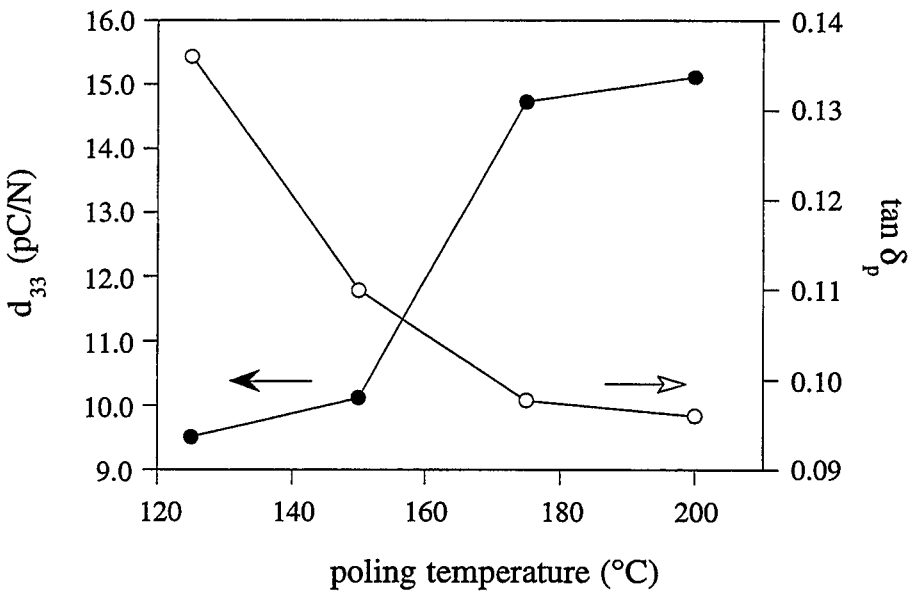

Figure 5.23. Bismuth titanate doped with 0.05 at% Nb showing an inverse relationship between the piezoelectric coefficient and piezoelectric tangent with poling temperature. The problem of large sample variation was avoided by progressively poling and measuring the same sample.

In summary, the piezoelectric coefficient increased with grain size for undoped bismuth titanate without a measurable effect on the piezoelectric tangent. This increase reflects improved domain wall motion for large grains in spite of a higher conductivity. There was no correlation between the grain size and the piezoelectric coefficient or piezoelectric tangent in 'fully' poled 0.05 at% Nb doped bismuth titanate. An inverse relationship was shown between d_{33} and tan δ_p with poling temperature for this composition. It was suggested that the partial polarization promotes a high piezoelectric phase angle, however the excess free charge may also be significant.

5.5.8 Discussion of possible piezoelectric relaxation mechanisms

Any explanation of the effect of Nb on the piezoelectric properties must take into account the following observations:

1) Undoped and lightly doped (0.05-0.24 at% Nb) BIT ceramics display a hysteresis between the force and charge which is described in terms of a complex piezoelectric coefficient. The imaginary term describes a piezoelectric relaxation. This relaxation did not occur with ≥ 0.53 at% Nb dopant for the defined measurement conditions.

2) The d_{33} and tan δ_p were frequency dependent in undoped and lightly doped BIT, but tan δ_p showed different trends. No frequency dependence occurred with high concentrations of dopant.

3) The d_{33} and tan δ_p were pressure dependent in lightly Nb doped compositions, but pressure independent with high concentrations of dopant. Only a slight pressure dependence was observed in undoped BIT.

4) Notable sample variation occurred in lightly Nb doped BIT, which did not occur with high dopant levels.

5) Piezoelectric tangent decreased with improved polarization (increased d_{33}) in 0.05 at% Nb doped BIT. The tangent was not effected by an increase in d_{33} in undoped BIT.

The frequency and pressure dependence of the properties in lightly Nb doped BIT suggest a mechanism of non-180° domain wall motion. It is known that non-180° domain walls can vibrate under certain frequencies[165] and pressures.[163] An increase in pressure causes a larger displacement of the domain wall resulting in a higher piezoelectric coefficient. An example of 90° domains in a large grain of 0.05 at% Nb doped bismuth titanate is found in Figure 5.24.

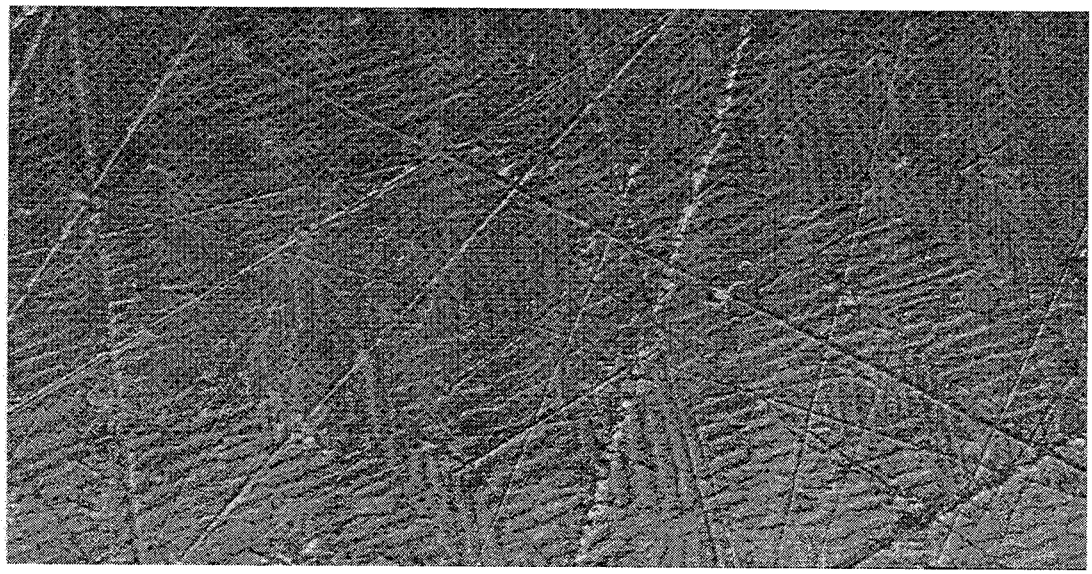

Figure 5.24 Optical micrograph showing regions of 90° domains in a large grain 0.05 at% Nb doped bismuth titanate sample. (sample sintered at 1130 °C for 10 hours, polished, and chemically etched).

A mechanism which can be proposed for the relaxation in lightly doped bismuth titanate is that of pinning and unpinning of domain walls from the trapped position. Recent work [163]

has shown that the piezoelectric response in lightly Nb doped bismuth titanate (~0.2 at%) follows the Rayleigh law for weak field conditions. This law is based on a model of irreversible displacement of domain walls by a mechanism of pinning and unpinning. The applicability of this model to the piezoelectric response in lightly Nb doped bismuth titanate is a strong indication that this mechanism is operative.

One would expect a similar behavior in undoped bismuth titanate, since non-180° domains also exist. Unlike the lightly Nb doped compositions, the piezoelectric tangent in BIT was not greatly affected by the AC pressure and increased rather than decreased with frequency. This suggests that a different mechanism is responsible for the dominant contribution to the piezoelectric relaxation in bismuth titanate.

A possible mechanism for piezoelectric relaxation in undoped bismuth titanate which should be fairly pressure independent is related to ionic motion. The dielectric properties indicate a relaxational process due to ionic jump. A mechanism of ionic motion in the polymer phase of piezoelectric polymer composites has been sited as the cause of a Maxwell-Wagner type effect which produces a piezoelectric relaxation.[161]

The equation derived from the experimental data in Figure 5.10 [($\tau=\tau_0 exp(E_a/kT)$ where $\tau_0=1.1x10^{-11}$ sec and $E_a=0.73$ eV] was used to calculate the frequency ($1/\tau$) at which ionic relaxation would occur at room temperature in bismuth titanate. A peak in the piezoelectric tangent due to this relaxation should appear at ~0.03 Hz which is at too low a frequency to explain the piezoelectric relaxation in terms of ionic motion. In other words, oxygen vacancy defects are frozen in for the measured frequencies.

One explanation for the behavior of the piezoelectric response in bismuth titanate which is consistent with the observations above, is that domain walls oscillate reversibly about fixed trapping sites. A wall trap is a region where the domain wall has a lower energy.[165] This condition may exist when a wall intersects regions which differ from the regular lattice, such as point defects, (e.g. oxygen vacancies), dislocations, stacking faults, etc. One would not expect a significant pressure dependence of the piezoelectric effect for symmetric oscillations. As the frequency increases, the piezoelectric coefficient decreases due to the smaller displacement of

the domain wall. It can be envisioned that the loss will depend on the restoring force and the damping of the oscillation as a function of frequency.

It can be recalled from Chapter 4, that bismuth titanate is p-type while the lightly Nb doped compositions have a low conductivity which corresponds to near complete compensation of free holes. The concentration of charged defects and free charges may play a role in the pinning of charged domain walls. For example, a charged defect, such as $V_O^{\bullet\bullet}$, may behave as a strong trap in bismuth titanate, but may be a weak pinning site if less free charge were available, as in 0.05 at% Nb doped BIT. Warren, et al.[170] present evidence that the amount of switchable polarization can be suppressed by electronic and ionic trapping of domain walls in $BaTiO_3$. They suggest that charges become trapped at domain walls with a polarization discontinuity (i.e. 90° walls or head to head configurations) and thus inhibit the domain wall motion.

Alternatively, a model can be envisioned where a charged defect contributes to the piezoelectric effect without involving domain wall motion. Piezoelectric relaxation in single domain single crystal Rochelle salt has been attributed to this mechanism. In this case the relaxation may be activated by pressure and not be field dependent if a lattice distortion is involved. In $BaTiO_3$ doped with Fe, it has been shown that Fe ions are displaced towards oxygen vacancies in Fe^{3+}-$V_O^{\bullet\bullet}$ complexes.[171] The p-type conductivity in undoped bismuth titanate is likely to be governed by acceptor impurities which may form similar complexes.

With higher Nb dopant levels, where there is no pressure or frequency dependence, the domain wall oscillations may be completely damped for the measurement conditions or oscillate freely with zero loss at the investigated frequency range. Different trapping sites would be expected in this material due to the different defects promoted by Nb doping (e.g. decreased oxygen vacancy concentration, possible Nb second phase, and increased stacking faults[172]). The free charges in this material are electrons rather than holes which may also affect the stability of the trapping site.

Alternatively, high enough concentrations of Nb may suppress the *formation* of certain non-180° domains. There are several types of non-180° domains in bismuth titanate which result from the lowering of symmetry from orthorhombic to monoclinic.[73,173] The monoclinic

distortion is very slight and occurs in order to satisfy the bonding requirements of the Ti which is severely overbonded in the parent Fmmm structure.[152] A structural effect of Nb is supported by the binding energy analysis in Chapter 4. Adding sufficient Nb may satisfy the bonding requirements and eliminate the need for a symmetry lowering operation, hence, domains associated with the monoclinic structure would not be present. There was no affect on the binding energies with low concentrations of Nb. This is consistent with the suggestion that this composition (0.05 at% Nb doped BIT) maintains the monoclinic structure. The piezoelectric response of highly Nb doped bismuth titanate can be compared to the Aurivillius phase $SrBi_4Ti_4TO_{15}$. This composition is orthorhombic in the ferroelectric phase and shows no hysteresis under similar measurement conditions.[160]

5.6 Chapter Summary

The Curie temperature in bismuth titanate was taken to be the same as the transition temperature and was measured from the peak in the relative permittivity. Niobium decreased the Curie temperature from 689 to 665 °C for the highest dopant level (0.74 at%).

An anomaly appears in the relative permittivity at ~550 °C in undoped bismuth titanate, which was shown to be a combination of two frequency dependent peaks. One of the sets of frequency dependent peaks was described by a Debye type relaxation which was characteristic of an ion jump/dipole re-orientation process. It was shown by studying hot forged samples that the relaxation occurred preferentially in the **ab** plane. It was suggested that the relaxation is caused by oxygen vacancies jumping between oxygen sites. The addition of Nb to bismuth titanate, drastically inhibited the relaxation process and eliminated the anomalous peak. It was proposed that Nb decreased the mobility and the concentration of oxygen vacancies.

Undoped bismuth titanate could not be well poled due to the high conductivity which led to electrical breakdown. It was noted that a higher d_{33} was obtained for large grain bismuth titanate which had a higher conductivity than fine grain samples. This indicates that although the conductivity interfered with the application of a suitable poling field, it was not the only factor involved in domain alignment. It was established that Nb doping allowed the application of higher poling fields at higher temperatures which resulted in higher piezoelectric coefficients.

Given the same poling conditions, the reproducibility of the piezoelectric properties improved with high concentrations (0.53-0.74 at%) of Nb doping.

A study of the frequency and pressure dependence of the piezoelectric response as a function of Nb doping suggests the following mechanisms:

1) In undoped bismuth titanate, piezoelectric relaxation may be related to reversible domain wall displacements from strong pinning sites and/or defect couples which cause a lattice distortion.

2) Lightly Nb doped bismuth titanate (0.05-0.21 at%) contains non-180° domain walls which undergo irreversible pinning between different trapping sites as described by the Rayleigh law.

3) Highly Nb doped compositions (0.53-0.74 at%) did not display a piezoelectric hysteresis for the measurement conditions. Three mechanisms can be suggested. i) The non-180° domains associated with a Rayleigh type loss were not present due to a suppression of the monoclinic distortion, ii) the domain walls become trapped by charged defects, or iii) non-180° domain walls are trapped in deep potential wells and move without loss in the examined frequency and field regime.

Chapter 6. Summary

6.1 Conclusions

Piezoelectric bismuth titanate ceramics were prepared using standard ceramic processing methods. The problem of high conductivity in bismuth titanate was overcome by adding niobium, a donor dopant. It was found that stable and reproducible piezoelectric properties were achieved with Nb concentration near the solubility limit (0.53-0.74 at%) of Nb in bismuth titanate.

The study of bismuth titanate ceramics has led to an understanding of the combined effects of raw materials, sintering conditions, and dopants on the conductivity. It was discovered that acceptor impurities in the raw materials and possibly cation vacancies produce electronic p-type conduction in bismuth titanate. A donor dopant was effective at compensating the free holes. The Nb doped composition corresponding to complete compensation of ionized holes did not provide the optimum piezoelectric properties.

Although decreasing the conductivity was a prerequisite to achieving well poled bismuth titanate ceramics, an isolated study of the conduction process was not sufficient to optimize the piezoelectric behavior. High levels of Nb doping, which promote n-type conductivity, were required to decrease the domain wall contribution to the piezoelectric effect.

In the course of this thesis, a deeper understanding of the relationship between the defect structure, microstructure and electrical properties than was previously available in bismuth titanate has been achieved. The important results are outlined as follows:

1) Oxygen vacancies are mobile in bismuth titanate at relatively low temperatures. This leads to a dielectric relaxation in the temperature range of 50 to 500 °C and is partially responsible for an anomalous peak in the permittivity.

2) In bismuth titanate, the defect $Nb_{Ti}^{\bullet}$, impedes diffusion of O^{2-} and either Ti^{4+} or Bi^{3+}. One consequence of this function, is a suppression of the dielectric relaxation in 1). Other effects include a decrease in the reaction rate during the mixed oxide process and suppression of grain growth during sintering.

3) A conductivity minimum in bismuth titanate was achieved by doping with Nb. The concentration of Nb required to fully compensate the free holes, depends on the impurities in the raw materials.

4) The conductivity as a function of temperature for fully compensated bismuth titanate was fit with three Arrhenius equations. The activation energies (E_a) from these relationships suggest the following

i) thermally activated hole mobility at low temperatures (20 to 200 °C, E_a~0.3 eV) attributed to hopping through the Bi^{3+} ion.

ii) combined activated hole mobility and enthalpy of ionization in the intermediate temperature range (200-400 °C, E_a~1.0 eV). This places the acceptor levels ~0.7 eV above the valence band.

iii) intrinsic conduction in the high temperature range (400-650 °C, E_a~1.7 eV). Intrinsic conduction is not observed in undoped bismuth titanate up to 950 °C. The compensation of free holes shifts the intrinsic regime to lower temperatures.

5) Analysis of the piezoelectric response as a function of Nb doping suggests the following mechanisms for the extrinsic contribution to the complex piezoelectric coefficient in the longitudinal mode.

i) In undoped bismuth titanate, piezoelectric loss was attributed to reversible domain wall displacements from strong pinning sites and/or defect couples which cause a lattice distortion.

ii) The piezoelectric phase angle in lightly Nb doped bismuth titanate (0.05-0.21 at %) was attributed to irreversible displacement of non-180° domain walls. The potential energy of these walls varies randomly with the position.

iii) Highly Nb doped compositions (0.53-0.74 at%) did not display any frequency or pressure dependence of the piezoelectric response under the measurement conditions. It was proposed that for high enough concentrations of Nb doping (into the n-type region), the monoclinic distortion was suppressed. As a result, certain non-180° domains are not favored. The elimination of these domain walls may impart the stable reproducible piezoelectric response to this material, however, the possibility that walls are pinned in deep potential wells and vibrate without measurable dissipation has not been ruled out. Another possible pinning mechanism may be related to the excess electrons introduced at high levels of Nb.

6.2 Suggestions for Future Work

From this work, several interesting avenues of investigation can be suggested.

1. Further investigation of the defect structure

Although it was shown that undoped bismuth titanate is p-type, it is not known which defects are the major contributors of ionized holes. Conductivity data must be collected from bismuth titanate samples in equilibrium with well defined partial pressures of oxygen to construct a Brouwer diagram. Using this method, the dominant defect responsible for p-type conduction (in pO_2~0.2 atm) may be revealed. Evidence of a thermally activated hole mobility can also be obtained by measuring the conductivity versus pO_2 as a function of temperature.

2. Diffusion in bismuth titanate

Evidence has been presented which indicates that oxygen diffuses more readily than the cations in bismuth titanate. It would be of interest to determine which cation, Bi^{3+} or Ti^{4+}, is the rate limiting ion for diffusion during the mixed oxide reaction and for grain growth during

sintering. Observing the progress of diffusion in couples of $Bi_{12}TiO_{20}$ and TiO_2 may help to determine the relative diffusion of Bi^{3+} and Ti^{4+} through the $Bi_4Ti_3O_{12}$ reaction layer.

Through the course of this work it has become apparent that oxygen vacancies have an impact on the conductivity and dielectric properties. It is also likely that oxygen vacancies are mobile during the poling process and may have some influence on the piezoelectric response, for example, as pinning sites or as polar defects. The concentration of oxygen vacancies in bismuth titanate is affected by the impurities in the raw materials, the sintering temperature, grain size, and cooling rate. It is therefore of interest to study the kinetics of oxygen diffusion in bismuth titanate as well as understanding the equilibrium conditions.

A quantitative measurement method for oxygen self-diffusion is with O^{18} tracers. This can be done in undoped, acceptor doped, and Nb doped bismuth titanate. It is expected that this will reveal a higher diffusion coefficient in acceptor doped than undoped, and a much lower diffusion coefficient in Nb doped bismuth titanate. Another method of measuring oxygen diffusion is to abruptly change the pO_2 after equilibration and measure the change in the conductivity as the oxygen vacancy concentration re-adjusts. Comparing the oxygen diffusion from these two methods gives an idea if there is an enhancement or suppression due to ambipolar diffusion.[112]

It is also important to confirm that the diffusion coefficient for oxygen through the grain boundary is smaller than self-diffusion in undoped bismuth titanate, but higher than in Nb doped bismuth titanate. This condition was necessary to explain the unusual effect of "grain size" on the conductivity.

3. Investigation of the crystal structure of highly Nb doped bismuth titanate

It was suggested that Nb may prevent the monoclinic distortion in bismuth titanate which would effect the possible domain wall orientations. In order to confirm or eliminate this possibility, the crystal structure can be evaluated using high resolution XRD and TEM with electron diffraction.

An attempt was made to compare undoped and Nb doped bismuth titanate by high resolution XRD. A difference was observed, but the measurements were not reproducible. This

is partly due to slight inhomogeneities from the mixed oxide method. Instead samples should be prepared from a method such as sol-gel.

4. Investigate mechanisms of domain wall pinning.

Recently, it has been demonstrated that the Rayleigh law can be used to quantify the contribution of irreversible domain wall pinning to the relaxation of the piezoelectric response.[162] This method can be applied to the lightly doped Nb bismuth titanate.

Following the method of Warren, et al.[170] (EPR coupled with polarization-voltage measurement) it may be possible to explore electronic and ionic trapping at domain walls for single crystals of undoped and Nb doped bismuth titanate.

Since grain growth is inhibited by Nb doping, large grain samples could not be obtained. It would be interesting to dope a large grain sample of bismuth titanate with Nb by annealing in a Nb rich powder. The domain structure can be compared optically or by SEM. It may be possible to determine the relative significance of the grain size on the piezoelectric response in highly Nb doped bismuth titanate.

It would be of interest to co-dope with acceptors and ~0.7 at% Nb such that the conductivity is p-type and at a level similar to the 0.53-0.74 at% Nb doped compositions. It may be possible to determine if excess electrons are important to the stable piezoelectric properties of the highly Nb doped bismuth titanate.

References

1. Turner, R.C., P.A. Fuierer, R.E. Newnham and T.R. Shrout (1994). *Appl. Acoustics* **41** p. 299.
2. Aurivillius, B. (1949). *Ark. Kemi.* **1** p. 466, 499.
3. Aurivillius, B. (1950). *Ark. Kemi.* **1** p. 499.
4. Cummins, S.E. and L.E. Cross (1968). *J. Appl. Phys.* **39** (5) p. 2268.
5. Herbert, J.M. (1982). Electrocomponent Science Monographs, Vol. 3: **Ferroelectric Transducers and Sensors.** New York: Gordon and Breach.
6. Taylor, G.W. and A. Miller (1970). *Proceedings of the IEEE* **58** (8) p. 1220.
7. Linqing, M.A., C.M. Beck and D.A. Payne (1994) in **Electroceramics: Production, Properties and Microstructures**, Editors: W.E. Lee and A. Bell. London: The Institute of Materials, p. 45.
8. Takenaka, T. and K. Sakata (1980). *Jpn. J. Appl. Phys.* **19** (1) p. 31.
9. Ferroperm Catalogue Piezoceramics Division, 1992: Kvistgård, Denmark.
10. Keramos Inc. Catalogue Advanced Piezoelectrics, 1993: Indianapolis, IN, USA.
11. Hopkins, M.M. and A. Miller (1970). *Ferroelectrics* **1** p. 37.
12. Luke, T.E. (1974). *J. Appl. Phys.* **45** p. 1605.
13. Déverin, J.A. (1980). *Ferroelectrics* **23** p. 51.
14. Takenaka, T. and K. Sakata (1986) in *Proceedings of the Sixth IEEE International Symposium on Applications of Ferroelectrics (June 8-11 1986)*, Bethlehem, PA, USA. p. 414.
15. Lopatin, S.S., T.G. Lupeiko, T.L. Vasil'tsova, N.I. Basenko, and I.M. Berlizev (1988). *Inorg. Mater.* **24** p. 1328.
16. Pask, L.A. (1975) in *The U.S.-Japan Seminar on Basic Science of Ceramics (June 23-27 1975)*, Hakone, Japan, Editor: W. Komatzu, *et al.* p. 73.
17. Brook, R.J., W.H. Tuan and L.A. Xue (1988) in Ceramic Transactions Vol. 1: **Ceramic Powder Science II**, Editors: G. L. Messing, J. Fuller, E.R. and H. Hausner. Westerville, OH, USA: The American Ceramic Society, p. 811.
18. Brooks, H.S. and D. Damjanovic (1993) in *Third Euro-Ceramics,* Madrid, Spain, Editor: P. Duran and J.F. Fernandez, p. 199.
19. Seth, V.K. and W.A. Schulze (1986) in *Proceedings of the Sixth IEEE International Symposium on Applications of Ferroelectrics (June 8-11 1986)*, Bethleham, PA, USA. p. 338.
20. Fouskova, A. and L.E. Cross (1970). *J. Appl. Phys.* **41** (7) p. 2834.
21. Shulman, H.S., M. Testorf, D. Damjanovic and N. Setter (1996). *J. Am. Ceram. Soc.* **79** (12), 3124 .
22. Damjanovic, D. (1994) in *Proc. Electroceramics IV (Sept. 5-7 1994)*, Aachen, Germany, p. 239.
23. Arlt, G. (1982). *Ferroelectrics* **40** p. 149.
24. Sinyakov, E.V., E.F. Dudnik, V.M. Duda, V.A. Podol'skii, and M.A. Gorfunkel' (1974). *Sov. Phys. Solid State* **16** (5) p. 979.
25. Ehara, S., K. Muramatsu, M. Shimazu, J. Tanaka, M. Tsukioka, Y. Mori, T. Hattori, and H. Tamura (1981). *Jpn. J. Appl. Phys.* **20** (5) p. 877.
26. von Hippel, A.R. (1962). **Dielectrics and Waves**. New York: John Wiley & Sons.
27. Cady, W.G. (1946). **Piezoelectricity**. New York: McGraw-Hill.
28. Cady, W.G. (1949). *Scientific American* p. 46.
29. Mason, W.P. (1950). **Piezoelectric Crystals and Their Application to Ultrasonics**. New York: D. Van Nostrand.
30. Curie, J. and P. Curie (1880). *Compi. rend.* **91** p. 294.
31. Lippman, M.G. (1881). *Ann. Chim.* **24** p. 145.
32. Nye, J.F. (1972). **Physical Properties of Crystals**. Oxford: Clarendon Press.
33. Lang, S.B. (1981). *Ferroelectrics* **33** (1-4).
34. Lang, S.B. (1981). *Ferroelectrics* **34** (1-2).
35. Lang, S.B. (1974). **Sourcebook of Pyroelectricity**. London: Gordon and Breach.
36. Whatmore, R.W. (1986). *Rep. Prog. Phys.* **49** p. 1335.

37. Valasek, J. (1921). *Phys. Rev.* **17** p. 475.
38. Jaffe, B., W.R. Cook and H. Jaffe (1971). **Piezoelectric Ceramics**. London: Academic Press.
39. Subbarao, E.C. (1961). *Phys. Rev.* **122** p. 804.
40. Subbarao, E.C. (1961). *J. Chem. Phys.* **34** p. 695.
41. Subbarao, E.C. (1962). *J. Phys. Chem. Solids* **23** p. 665.
42. Newnham, R.E., R.W. Wolfe and J.F. Dorrian (1971). *Mat. Res. Bull.* **6** p. 1029.
43. Frit, B. and J.P. Mercurio (1992). *J. Alloys and Compounds* **188** p. 27.
44. Déri, M. (1969). **Ferroelectric Ceramics**. New York: Gordon and Breach.
45. Moulson, A.J. and J.M. Herbert (1990). **Electroceramics**. London: Chapman and Hall.
46. Nanamatsu, S., M. Kimura and T. Kawamura (1974). *Ferroelectrics* **8** p. 511.
47. Nanamatsu, S., M. Kimura, K. Doi and M. Takahashi (1971). *J. Phys. Soc. Jpn.* **30** p. 300.
48. Smith, R.T. and F.S. Welsh (1971). *J. Appl. Phys.* **42** (6) p. 2219.
49. Takenaka, T. and K. Sakata (1985). *Jpn. J. Appl. Phys.* **24** (Suppl. 24-2) p. 730.
50. Takenaka, T. and K. Sakata (1989). *Ferroelectrics* **94** p. 175.
51. Shulman, H.S. (1992-1995). *Unpublished work*.
52. Ismailzade, I.G. and V.I. Nesterenko (1968). *Sov. Phys. Cryst.* **12** (4) p. 625.
53. Takenaka, T. and K. Sakata (1984). *J. Appl. Phys.* **55** (4) p. 1092.
54. Korzunova, L.V., I.V. Brante, D.K. Petersone and E.Z. Freidenfeld (1987). *I.A.N. S.S.S.R. Neorganicheskie Materialy* **23** (9) p. 1509.
55. Ikegami, S., I. Ueda and T. Nagata (1971). *J. Am. Acoust. Soc.* **50** p. 1060.
56. Fuierer, P.A., (1991). **Grain-Oriented Perovskite Layer Ceramics for High Temperature Applications**. Ph.D Thesis, The Pennsylvania State University: State College, PA, USA.
57. Goldschmidt, V.M. (1926). *Mat. Naturv. Kl.* **1** (2) p. 8.
58. Shannon, R.D. and C.T. Prewitt (1969). *Acta. Cryst. B* **25,26** p. 925.
59. Evans, H.T. (1964). **An Introduction to Chrystal Chemistry**. London: Cambridge University Press.
60. CRC (1995). **Handbook of Chemistry and Physics**. Boca Raton, FL, USA: CRC Press.
61. Brandon, J.K. and H.D. Megaw (1970). *Phil. Mag.* **21** (8) p. 189.
62. Hutchinson, J.L., J.S. Anderson and C.N.R. Rao (1977). *Proc. R. Soc. Lond.* **A** p. 301.
63. Kikuchi, T., A. Watanabe and K. Uchida (1977). *Mat. Res. Bull.* **12** p. 299.
64. Armstrong, R.A. and R.E. Newnham (1972). *Mat. Res. Bull.* **7** p. 1025.
65. Rae, A.D., J. G. Thompson, R. L. Withers and A.C. Willis (1990). *Acta Cryst. B* **46** p. 474.
66. Rae, A.D., J.G. Thompson and T.L. Withers (1991). *Acta Cryst. B* **47** p. 870.
67. Thompson, J.G., A.D. Rae, R.L. Withers and D.C. Craig (1991). *Acta Cryst. B* **47** p. 174.
68. Cross, L.E. and R.C. Pohanka (1971). *Mat. Res. Bull.* **6** p. 939.
69. Tambovtsev, D.A., V.M. Skorokov and I.S. Zheludev (1964). *Sov. Phys. Cryst.* **8** p. 713.
70. Luke, T.E. (1974). *Ferroelectrics* **6** p. 307.
71. Ismailzade, I.G. (1961). *Azerb. Khim. Zh.* **5** p. 91.
72. Reaney, I.M., M. Roulin, H.S. Shulman and N. Setter (1995). *Ferroelectrics* **165** p. 295.
73. Fousek, J. and V. Janovek (1967). *Am. Phys. Soc. Bull.* **12** p. 902.
74. Härdtl, K.H. (1982). *Ceramics International* **8** (4) p. 121.
75. Noblanc, O. and P. Gaucher (1994). *Ferroelectrics* p. 145.
76. Zhang, Q.M., W.Y. Pan, S.J. Lang and L.E. Cross (1988). *J. Appl. Phys.* **64** p. 6645.
77. Jovalekic, C., L. Atanasoska, V. Petrovic and M.M. Ristic (1991). *J. Mat. Sci.* **26** p. 3553.
78. Holmes, M., R.E. Newnham and L.E. Cross (1979). *Am. Ceram. Soc. Bull.* p. 872.
79. Kimura, T., T. Kanazawa and T. Yamaguchi (1983). *J. Am. Ceram. Soc.* **66** (8) p. 597.
80. Jovalekic, C. and S. Stevic (1992). *Ferroelectrics* **132** p. 185.
81. Shrout, T.R. (1991). *Chem. Electron. Ceram. Mater.* **804** p. 105.

82. Dayalan, E., C.H. Peng and S.B. Desu (1991) in Ceramic Transactions Vol. 25: **Ferroelectric Films**, Editor: A. S. Bhalla. Westerville, OH, USA: The American Ceramic Society, p.279.
83. Yamaguchi, O., N. Maruyama and K. Hirota (1991). *Brit. Ceram. Trans. J.* **90** p. 111.
84. Powder Diffraction File, card no. 42-0186. Newton Sq., PA, USA: JCPDS International Center for Diffraction Data.
85. Kato, T. (1983). *Jpn. J. Appl. Phys.* **22-2** p. 47.
86. Shoji, K. and Y. Uehara (1983). *Jpn. J. Appl. Phys.* **22** (Supplement 22-2) p. 50.
87. Galasso, F.S. (1973). *Inorg. Syntheses* **14** p. 144.
88. Levin, E.M. and R.S. Roth (1964). *J. Research Natl. Bur. Standards* **68A** (2) p. 197.
89. Jovalekic, C., L. Atanasoska, V. Petrovic and M.M. Ristic (1989) in **Science of Sintering**, Editors: D.P. Uskokovic, H. Palmour III and R.M. Spriggs. New York: Plenum Press, p. 537.
90. Ikegami, S. and I. Ueda (1974). *Jpn. J. Appl. Phys.* **13** (10) p. 1572.
91. Gurevich, V.M. (1971). **Electrical Conductivity of Ferroelectrics**. Jerusalem: Israel Program for Scientific Translations.
92. Swartz, S., W.A. Schulze and J.V. Biggers (1983). *Transactions of the Bismuth Institute* , 2nd Quarter, **40** p. 1.
93. Briggs, D. and M.P. Seah, eds. (1983). **Practical Surface Analysis by Auger and X-Ray Photoelectron Spectroscopy**. New York: John Wiley & Sons.
94. Tilley, R.J.D. (1987). **Defect Crystal Chemistry**. New York: Blackie & Son.
95. Brook, R.J. (1974) in **Electrical Conductivity in Ceramics and Glass Part A**, Editor: N. M. Tallan. New York: Marcel Dekker, p. 179.
96. Kroger, F.A. (1973). **The Chemistry of Imperfect Crystals**. New York: American Elsevier.
97. Kingery, W.D., H.K. Bowen and D.R. Uhlmann (1976). **Introduction to Ceramics**. New York: John Wiley & Sons.
98. Dorrian, J.F., R.E. Newnham, D.K. Smith and M.I. Kay (1971). *Ferroelectrics* **3** p. 17.
99. Vusevker, Y.A., L.G. Epremyan, Y.V. Gurvich, O.P. Kramarov, and D.E. Fainrider (1975). *Byull. Izobret.* **48** .
100. Vusevker, Y.A., V.I. Rivkin, O.P. Kramarov and D.E. Fainrider (1980). *Byull. Izobret.* **18** .
101. Lotgering, F.K. (1959). *J. Inorg. Nucl. Chem.* **9** p. 113.
102. Okazaki, K. and H. Igarashi (1976) in **Ceramic Microstructures '76**, Editors: R.M. Fulrath and J.A. Pask. Boulder, CO, USA: Westview Press, p. 564.
103. Reed, J.S. (1988). **Introduction to the Principles of Ceramic Processing**. New York: John Wiley & Sons.
104. Galasso, F.S. (1969). **Structure, Properties, and Preparation of Perovskite-type Compounds**. New York: Pergamon Press.
105. Speranskaya, E.I., I.S. Rez, L.V. Kozlova, V.M. Skorikov, and V.I. Slavov (1965). *J. Inorg. Materials (English Translation)* p. 213.
106. Shimada, S. (1977). *J. Cryst. Growth* **41** p. 317.
107. Powder Diffraction File, card no. 34-0097, Newton Sq., PA, USA: JCPDS International Center for Diffraction Data.
108. Bruton (1974). *J. Sol. State Chem.* **9** p. 173.
109. Jander, W. (1927). *Z. Anorg. Allg. Chem.* **1** p. 163.
110. Freer, R. (1980). *J. Mat. Sci.* **15** p. 803.
111. Daniels, J., K. H. Härdtl, D. Hennings and R. Wernicke (1976). *Philips Research Reports* **31** p. 487.
112. Müller, A. and K.H. Härdtl (1989). *Appl. Phys. A* **49** p. 75.
113. Waser, R. (1991). *J. Am. Ceram. Soc.* **74** (8) p. 1934.
114. Cohn, J.G. (1967) in Materials Science Research Vol. 4: **Kinetics of Reactions in Ionic Systems**, Editors: T.J. Gray and V. D. Fréchette. New York: Plenum Press, p. 1.
115. Lapshin, V.I. and V.K. Yarmarkin (1989) in **Science of Sintering**, Editors: D. P. Uskokovic, H. Palmour III and R. M. Spriggs, New York: Plenum Press.
116. Eppler, R.A. (1967) in **Kinetics of Reactions in Ionic Systems**, Editors: T.J. Gray and V.D. Fréchette, New York: Plenum Press, p. 501.

117. Anderson, H.U. (1965). *J. Am. Ceram. Soc.* **48** p. 118.
118. Seuter, A.M.J.H. (1974). *Philips Research Reports Supplements* **3** p.1.
119. Kuczynski, G.C., ed. (1979). Materials Science Research Vol. 13: **Sintering Processes**. New York: Plenum Press.
120. Uskokovic, D.P., H. Palmour and R.M. Spriggs, eds. (1989). **Science of Sintering.** New York: Plenum Press.
121. Kuczynski, G.C., ed. (1975). Materials Science Research Vol. 10: **Sintering and Catalysis**. New York: Plenum Press.
122. Burke, J.E. and J.H. Rosolowski (1976). in Treatise on Solid State Chemistry, Vol. 4: **Reactivity of Solids**, Editor: N.B. Hannay. New York: Plenum Press, p.621.
123. German, R.M. (1985). **Liquid Phase Sintering**. New York: Plenum Press.
124. Kibbel, B.W. and A. Heuer (1989). *J. Am. Ceram. Soc.* **72** (3) p. 517.
125. Exner, H.E. (1987). *Acta Stereol.* **6** p. 1023.
126. Rollett, A.D., D.J. Srolovitz, and M.P. Anderson, (1989). *Acta Metall.*. **37** (4) p.1227.
127. Kunaver, U. and D. Kolar, (1993). *Acta Metall. Mater.* **41** (8) p. 2255.
128. Brook, R.J. (1976) in Treatise on Material Science and Technology Vol. 9: **Ceramic Fabrication Processes**, Editor: F. F. Wang. New York: Academic Press, p. 331.
129. Jonscher, A.K. (1983). **Dielectric Relaxation in Solids**. London: Chelsea Dielectrics Press.
130. Blumenthal, R.N. and M.A. Seitz (1974) in **Electrical Conductivity in Ceramics and Glass Part A**, Editor: N. M. Tallan. New York: Marcel Dekker, p. 35.
131. Ching, W.Y. (1990). *J. Am. Ceram. Soc.* **73** (11) p. 3135.
132. Chan, N.-H., R.K. Sharma and D.M. Smyth (1981). *J. Am. Ceram. Soc.* **64** (9) p. 556.
133. Cox, P.A. (1987). **The Electronic Structure and Chemistry of Solids**. Oxford: Oxford University Press.
134. Duffy, J.A. (1990). **Bonding, Energy Levels, and Bands in Inorganic Solids**. New York: John Wiley & Sons.
135. Adler, D. (1971) in **Physics of Electronic Ceramics Part A**, Editors: L.L. Hench and D.B. Dove, New York: Marcel Dekker, p. 29.
136. Smyth, D.M. (1993) in **Properties and Applications of Perovskite-Type Oxides**, Editors: L.G. Tejuca and J.L.G. Fierro. Basel: Marcel Dekker, p. 47.
137. Robertson, J., W.L. Warren, B.A. Tuttle, D. Dimos, and D.M. Smyth (1993). *Appl. Phys. Lett.* **63** (11) p. 1519.
138. Adler, D. (1974) in **Electrical Conductivity in Ceramics and Glass Part A**, Editor: N. M. Tallan. New York: Marcel Dekker, p. 1.
139. Raymond, M.V. and D.M. Smyth (1995) in **Science and Technology of Electroceramic Thin Films**, Editors: O. Aucrello and R. Waser. Dordrecht, DE: Kluwer Academic Publishers, p. 315.
140. Tagansev, A., private communication, 1995.
141. Warren, W.L., J. Robertson, D.B. Dimos, B.A. Tuttle, and D.M. Smyth (1994). *Ferroelectrics* **153** p. 303.
142. Badwal, S.P.S. (1994) in Material Science Technology: **Structure and Properties of Ceramics**, Editors: R.W. Cahn, P. Haasen and E.J. Kramer. Weinheim, DE: VCH, p. 567.
143. Mansfield, R. (1949). *Proceedings of the Physical Society of London* **62** p. 476.
144. Brooks, H.S., M. Testorf, D. Damjanovic, and N. Setter, (1994). *Proceedings of the Assemblée générale de la SVMT, 1994* p. 77.
145. Sugano, S., T. Yoshimoto and A. Nagai (1991). in *Proceedings of the Seventh IEEE International Symposium on Applicatons of Ferroelectrics, 1990* , p. 584.
146. Huanosta, A., O. Alvarez-Fregoso, E. Amano, C. Tabarez-Munoz, M.E. Mendoza-Alvarez, and J.G. Mendoza-Alvarez (1990). *J. Appl. Phys.* **69** (1) p. 404.
147. Goodenough, J.B., A. Manthiram and J.F. Kuo (1993). *Mat. Chem. Phys.* **35** p. 221.
148. Prisedsky, V.V., V.I. Shishkovsky and V.V. Klimov (1978). *Ferroelectrics* **17** p. 465.
149. Haneda, H., I. Sakagychi, A. Watanabe and J. Tanaka (1992). in *The US-Japan Seminar on. Electronic Structure and Fermiology of High T_c Superconductors , Sendai, Japan, 1992.* p. 351.

150. Chan, N.-H. and D.M. Smyth (1976). *J. Electrochem. Soc.: Solid State Science and Technology* **123** (10) p. 1584.
151. Wagner, C.D., W.M. Riggs, L.E. Davis and J.F. Moulder (1979). **Handbook of X-Ray Photoelectron Spectroscopy,** Editor: G. E. Muilenberg. Eden Prairie, MI, USA: Perkin Elmer Corp.
152. Withers, R.L., J.G. Thompson and A.D. Rae (1991). *J. Solid State Chem.* **94** p. 404.
153. Van Oeffelen, D.A.G. (1985). *J. Catal.* **95** p. 84.
154. Hench, L.L. and J.K. West (1990). **Principles of Electronic Ceramics**. New York: John Wiley & Sons.
155. Hisano, K. and K. Toda (1976). *Solid State Communications* **18** p. 585.
156. Lines, M.E. and A.M. Glass (1977). **Principles and Applications of Ferroelectric and Related Materials**. Oxford: Clarendon Press.
157. Jona, F. and G. Shirane (1962). **Ferroelectric Crystals**. London: Pergamon Press.
158. Ehara, S., T. Hattori and J. Tanaka (1986). *Jpn. J. Appl. Phys.* **25** (11) p. 1749.
159. Härdtl, K.H. (1982). *Ceramics International* **8** (4) p. 121.
160. Damjanovic, D., M. Demartin, H.S. Shulman, M. Testorf, and N. Setter (1996). *Sensor. Actuat.* **A53** p. 353.
161. Furukawa and Fukada (1977). *Jpn. J. Appl. Phys.* **16** p. 453.
162. Damjanovic, D. and M. Demartin (1996). *J. Phys. D: Appl. Phys.* **29** p. 2057.
163. Damjanovic, D., F. Chu, H.S. Shulman, and N. Setter (in press). in *The Tenth Symposium on the Applications of Ferroelectrics (Aug. 18-21 1996)*, Rutgers University, NJ, USA.
164. Gerthsen, P., K.H. Hardtl and N.A. Schmidt (1980). *J. Appl. Phys.* **51** (2) p. 1131.
165. Burfoot, J.C. (1967). **Ferroelectrics: An Introduction to the Physical Principles**. Toronto: D. Van Nostrand Co. Ltd.
166. Arlt, G., H. Dedrichs and R. Herbiet (1987). *Ferroelectrics* **74** p. 37.
167. Damjanovic, D., M. Demartin, H.S. Shulman and N. Setter (1995). in *Transducers '95-Eurosensors IX*, Stockholm, Sweden. p. 218.
168. Demartin, M. and D. Damjanovic (1996). *Appl. Phys. Lett.* **68** p. 3046.
169. Li, S., W. Cao and L.E. Cross (1991). *J. Appl. Phys.* **64** p. 7219.
170. Warren, W.L., D. Dimos and B.A. Tuttle (1994). *J. Am. Ceram. Soc.* **77** (10) p. 2753.
171. Siegel, E. and K.A. Müller (1979). *Phys. Rev. B: Condens. Matter.* **19** p. 109.
172. Sagalowicz, L., private communication, TEM observations, 1995.
173. Reaney, I.M. and D. Damjanovic (1996). *J. Appl. Phys.* **80** p. 4223 .

Curriculum Vitae

Holly Sue Shulman born the 18th of October 1961, Ridgewood, New Jersey, USA

EDUCATION

1967-1974	Elementary school in North Plainfield, New Jersey, USA
1974-1980	Secondary school Teaneck High School, New Jersey, USA
1983-1987	Bachelor of Science in Ceramic Engineering at Alfred University The State University of New York, College of Ceramics, New York, USA
1990-1992	Masters of Science in Material Science and Engineering at the University of Pittsburgh, Pennsylvania, USA
1992-1997	Ph.D. student within the group of Prof. N. Setter at the Laboratory of Ceramics of the Swiss Federal Institute of Technology of Lausanne

PROFESSIONAL EXPERIENCE

1987-1989	Research Engineer, Material and Electrochemical Research, Tucson, AZ, USA
1989-1991	Research Engineer, Kennametal Inc., Latrobe, PA, USA
1996-present	Research Scientist, Industrial Research Ltd., Lower Hutt, New Zealand

PUBLICATIONS

H. S. Brooks, D. Damjanovic, (1993). *Microstructural Control of Bismuth Titanate Based Ceramics*, Third Euro-Ceramics, Vol. 2, pp. 199-204. P. Duran and J. F. Fernandez, ed.

H. S. Brooks, M. Testorf, D. Damjanovic, N. Setter, (1994). *Effects of Processing and Dopants on the Electrical Conductivity of Bismuth Titanate Layer Structure Perovskites*, Proceedings of the Assemblée générale de la SVMT, p. 77-80.

H. S. Shulman, M. Testorf, D. Damjanovic, N. Setter, (1996). *Microstructure, Electrical Conductivity, and Piezoelectric Properties of Bismuth Titanate*, J. Amer. Ceram. Soc. **79** (12) p. 3124-3129.

I. M. Reaney, M. Roulin, H. S. Shulman, D. Damjanovic, (1994). *Characterization of the Perovskite Layer Structure $SrBi_8Ti_7O_{27}$*, Electroceramics IV Conference, p. 11-16.

D. Damjanovic, M. Demartin, H. Shulman, N. Setter, (1995). *Instabilities in the Piezoelectric Properties of Ceramic Sensors and Actuators under Extreme Conditions*, Transducers '95-Eurosensors IX, Stockholm Sweden, p. 218-221.

I. M. Reaney, M. Roulin, H. S. Shulman, N. Setter, (1995). *In Situ Observations of Octahedral Tilt Transitions in Strontium Bismuth Titanate Layered Perovskites*, Ferroelectrics, **165**, p. 295-305.

D. Damjanovic, M. Demartin, H. S. Shulman, M. Testorf, N. Setter, (1996). *Instabilities in Piezoelectric Properties of Ferroelectric Ceramics*, Sensors and Actuators A 53, p. 353-360.

D. Damjanovic, F. Chu, H. S. Shulman, N. Setter (in press) in *The Tenth Symposium on the Applications of Ferroelectrics (Aug. 18-21 1996)* Rutgers University, NJ, USA.

Holly Sue Shulman **Wainuiomata, New Zealand, the 9th of March, 1997**